Damage identification in skeletal structures: A dynamic stiffness approach

A thesis submitted in fulfilment
of the requirements for the degree
of
Doctor of Philosophy in
Mechanical Engineering
at
The University of Waikato
by

Julian Octavio De Los Rios Giraldo

The University of Waikato
2017

THE UNIVERSITY OF
WAIKATO
Te Whare Wānanga o Waikato

Dedication

I want to dedicate this thesis to my mother and my daughter.

Thanks to you both; every day, I want to be a better man surpassing every challenge and looking forward for solutions to unsolved problems.

Nellyto, you are my inspiration and the glue who has kept our family close together. Your tenacity and constant push to make us be the best are embedded on me.

PaulAndrea, you thought me what loves means. Your innocence and unconditional love for me are my motor and motivation to be the best for you.

Abstract

The present work is devoted to investigate ways of identifying cracks in skeletal structures by frequency monitoring. This is a challenging problem as the number of cracks, their severity and location all need to be found. It has been shown that roving bodies with rotary inertia could be used to find the total number of cracks and their locations without any knowledge of their severity. The Dynamic Stiffness Method was chosen due to its capabilities in enabling an exact solution while facilitating addition of new elements such as springs and masses to the structure in the same way as in the approximate Finite Element Method (FEM). Using the Dynamic Stiffness Matrices (DSM), it was possible to derive an interesting and useful relationship between the determinants of the DSM of the following: the original undamaged structure, the cracked structure and the structure with a hinge at the potential crack location. This relationship is a simple equation which gives the determinant of the cracked structure as the sum of the determinant of the undamaged structure multiplied by the rotational stiffness of the beam at the crack and the determinant of a structure with a hinge at the same crack location.

Experimental results from literature are used to validate the application of the found features in beam structures and frameworks to identify damages or dynamic properties. A semi-experimental methodology is proposed to treat multi-cracked structures where, as a first step, the roving inertia method is used to identify the number and location of the cracks in a simple way without the need to perform any calculations or theoretical analysis. The theoretical basis of this method is explained using the DSM. Experimental work was carried out on a cantilever beam to verify the applicability of the roving inertia method but no conclusive results were obtained. Further experimental investigations are needed to study the practical feasibility of the method. It is hoped that once the locations of all cracks are identified, the severity of the cracks can be found using the frequency measurements as the determinants of the DSM are linear functions of crack severity.

Acknowledgements

I want to thank my supervisory panel, your unconditional guidance and advice challenged me to devise a new solution to an old problem. In addition, I want to thank my companions in this research journey: Nicoloy, Ken and Kaveth. You did not only help me through the research process itself, but you also gave me advice and support dealing with a new culture in a foreign land away from family and friends.

Last but not least, I want to thank my family: parents, siblings, nieces, nephews, brothers and sisters in-laws. You all trusted me and gave me your unconditional support. Your unconditional support and unparalleled example motivated me to complete this journey.

Table of Contents

List of Figures

List of Tables

List of Symbols

$\mathbf{A}$	Frequency dependent matrix
$\mathbf{a}$	Nodal actions vector
$\mathbf{B}_i$, $\mathbf{B}_i^*$	Initial and updated frequency dependent DSM submatrices
β	Non-dimensional frequency parameter
$\mathbf{C}$	Vector of constants
$\mathbf{D}$	Frequency dependent displacements matrix
D_c, D_0, D_h	Determinants of damaged, undamaged and hinged structure
$\overline{D}_c$, $\overline{D}_0$, $\overline{D}_h$	Numerators of determinants of damaged, undamaged and hinged structure
D_{cm}	Determinant of damaged structure with added point mass
D_{cmr}, D_{cr}	Determinant of rotary inertia effects for damaged structure
D_m	Determinant of structure with a point mass added
$\overline{D}_m$	Numerator of determinant of structure with a point mass added
D_{mc}	Determinant of hinged structure at crack and point mass position
D_{mr}, D_r	Determinant of rotary inertia effects for undamaged structure
$\mathbf{d}$	Nodal displacements vector
d/h	Crack depth over sectional height
δ	Transverse displacement
EI	Flexural rigidity
e	Effective eccentricity of concentrated mass
f	Rotational spring flexibility
f_1, f_2, f_3	Measured natural frequencies
f_I	Inertial force
$\boldsymbol{\phi}$	Amplitude of displacements vector, mode shape
ϕ_1, ϕ_2	Frequency-load dependent parameters
$\mathbf{G}$	Vector of constants
I_0	Dynamic effect of rotary inertia for added mass
$\mathbf{K}_u$, $\mathbf{K}_u^*$	Initial and updated DSM for undamaged structure
$\mathbf{K}_c$, $\mathbf{K}_c^*$	Initial and updated DSM for cracked structure
$\mathbf{K}_{um}$, $\mathbf{K}_{um}^*$	Initial and updated DSM for undamaged structure
$\mathbf{K}_{cm}$, $\mathbf{K}_{cm}^*$	Initial and updated DSM for cracked structure with added mass
$\mathbf{K}_m$	DSM for a beam with appended mass

$\mathbf{K}_i$, $\mathbf{K_0}$	Sub matrix
K_i	Matrix elements
k ,$\bar{k}$	Non-dimensional and accommodated rotational spring stiffness
k_{ij}, k_{ij}^*	Initial and updated frequency dependent DSM scalar elements
L	Beam element length
λ	Frequency parameter
M	Bending moment
m, $\bar{m}$, m^*	Non-dimensional and dimensional masses
μ	Linear density
N	Axial force
Q	Dynamic stability parameter in DSM
Qq	Dynamic stability parameter in DSM
S	Dynamic stability parameter in DSM
SC	Dynamic stability parameter in DSM
σ	Axial load parameter
T	Dynamic stability parameter in DSM
Tt	Dynamic stability parameter in DSM
t	Time
τ	Harmonic function in time
$\mathbf{\Psi}_0$, $\mathbf{\Psi}_d$	System parameter, undamaged and damaged cases
θ	Nodal rotation
$\mathbf{U}$	Modal displacements vector
u	Continuous displacement
V	Transverse force
v	Transverse displacement response
ω	Circular frequency
x	Spatial coordinate
Y	Amplitude of transverse displacement
y_o	Signal output for a reference system
y_d	Signal output from a damaged system

Chapter 1

Introduction

Structural integrity of engineering constructions and structures is affected by the normal process of deterioration which can compromise their safety and serviceability. In the past few decades many efforts have been undertaken by engineers to detect and localize damage in its early stage using vibrational measurements as is implicit in the comprehensive literature review on structural health monitoring and damage identification made by Doebling, et al. [1], Sohn, et al. [2] , Sinou [3] and An, et al. [4] the latest in 2015.

In the words of Doebling, et al. [5] “The vibration based identification methods rely on the fact that damage generates singularities in the modal parameters”. Therefore to characterise the dynamics of the structure, most of the vibration measurements came from acceleration data processed through the Fourier Transform [6] in order to extract modal parameters such as natural frequencies.

Recently, considerable amount of research is focused on other signal processing techniques to overcome limitations of fixed resolution in the Fourier transform windowing, which include techniques like wavelet transform [7] using longer windows for low frequencies and shorter windows for higher frequencies. Other methods coined as data-driven methods are focused on statistical feature extraction to create statistics-based models that can be continuously monitored in order to indicate whether or not the structure has deviated from its normal condition [8]. There is another approach to check structural deviation by means of residual errors and optimization techniques such as genetic algorithms [9] or artificial neural networks [10]. It is also possible to find some published works [11, 12] which combine techniques, and reviews for particular methodologies such as Reda Taha, et al. [13] for wavelet transform, Hao and Xia [14] for genetic algorithms, Stache, et al. [15] for model updating, Hossain, et al. [16] for artificial neural networks and Tibaduiza, et al. [17] for principal components analysis.

1.1 Background and Motivation

Damage identification on the basis of dynamic measurements is usually conducted by means of numerical procedures in view of the difficulty in obtaining explicit solutions to both the direct and inverse analysis problems. However, analytical studies of simple structural systems, such as straight beams subject to concentrated damages have been conducted by several authors. Caddemi and Caliò [18] presented a list of the most representative works in this regard, and indicated that only a few authors have successfully addressed aspects regarding the identification of single cracks; leading to explicit expressions for the solution of the inverse problem. Greater attention has been devoted in recent years to the solution of the direct analysis problem of vibrating beams in the presence of multiple concentrated cracks, in order to gain a deeper insight and better understanding of the problem with the ultimate aim of addressing the inverse formulation. However, several characteristics, particularly concerning the case of identification of damage and positions of multiple cracks by means of dynamic tests, remain unsolved [19].

Several studies introduced concentrated damages on beams by considering a local reduction of the flexural stiffness. According to the latter model, and following the fracture mechanics principles [20-23], a crack can be macroscopically represented as an elastic link connecting the two adjacent beam segments [24]. More precisely, a model in which an internal hinge enclosed in a rotational spring, whose stiffness is dependent on the extent of damage, proved to be accurate and is often used [25-29].

There is an increasing concern regarding the breathing mechanism on cracks. As a crack breathes when in an oscillatory movement, its originally separated surfaces enter in contact, closing an initial open crack [30]. Under the action of the excitation force, crack opening and closing will alternate as a function of time making the equations of motion non-linear. There is no exact solution to these equations, and therefore a numerical method must be adopted [31].

1.2 Damage identification and the inverse problem

The purpose of damage identification is to define the variables that characterise the occurrence of potentially risky changes in a built structure. Initial technologies developed a model of the structure to define as baseline for detection [32]. The

extracted modal parameters of this baseline are compared with those obtained from the structure in operation. An error function is introduced that is to be minimised when updating the initial model and analysing its sensitivities. The technology is known as the direct problem as opposed to the inverse problem which can be used to find the parameters that cause the change in the structural response using the baseline model and the measured parameters [33].

Fritzen [29] explained the difference between direct and inverse methodologies in the following way. An undamaged system with a set of parameters $\boldsymbol{\Psi}_0$ has an output signal y_0 as its signature. A damage generates a new set of parameters $\boldsymbol{\Psi}_d$. The forward problem finds the output signal y_d from a reference signal using the system parameters,

$$y_d = f(\boldsymbol{\Psi}_0, \boldsymbol{\Psi}_d, y_0),$$

while the inverse problem finds the damage parameters using the inverse of the function evaluating both signal outputs and the reference parameters

$$\boldsymbol{\Psi}_d = f^{-1}(\boldsymbol{\Psi}_0, y_0, y_d).$$

Using vibration measurements, the parameters of the physical system are to be determined from the knowledge of its dynamical behaviour, implying that spectral information has to be extracted from the measured data, and therefore the correctness of the obtained model is highly dependent on the signal processing and noise treatment. Regarding the function that modelled the structure, it is important to develop a very accurate mathematical model, so that it correctly captures the actual structural dynamic behaviour in some predetermined frequency range to be sure that the changes in the measured quantities are only caused by structural damage.

1.3 Aims and objectives

The last section implies that models are valid in certain frequency ranges, for example, when the crack is simulated by the addition of a rotational spring the dynamic response in low-frequency vibration measurements, will have similar effect because the damage is treated as a local stiffness reduction. A significant advantage in using low-frequency vibration measurements is that the low-frequency modes are generally global and therefore the vibration sensors may be mounted remotely from the damage site [33]. However, the changes in the frequency are usually very small at lower modes and one needs to bear in mind that the solution of the inverse problem has two sets of unknowns,

the locations and severity. These initial attempts to solve relatively simpler inverse problems of identifying idealised artificial cracks lead to the main objectives of this research with the following questions:

- Is it possible to separate the crack stiffness and location effects in the determination of the natural frequencies?
- Is it possible to identify more than one crack?

1.4 Methodology and scope

As mentioned previously, the field of damage identification in engineering problems is very broad. However, this thesis will be limited to methods that are used to infer damage from changes in vibration characteristics of skeletal structures.

1.5 Thesis layout

Including the present introduction, there are seven chapters in this thesis. Chapter 2 introduces the Dynamic Stiffness Matrix (DSM) presenting a general formulation from the idea of Banerjee [34] applied to axial loaded beams.

In Chapter 3 it was decided to use the DSM to find the natural frequencies of single beam units with symbolic manipulation tools in Matlab® to see how the crack stiffness (severity) affected the determinantal equation. From this an interesting linear determinantal relationship emerged: it was found that the determinants of the dynamic stiffness matrices of undamaged, damaged structures and a structure with a hinge at the crack location were linearly related, and the rotational stiffness at the crack also appeared as a constant in this equation. This relationship is expressed in Equation (3.6) and its derivation is proved for frame structures in Section 3.2; this development is the main contribution of this thesis and some implications are explained in Chapter 6.

Section 3.3 deals with the closed-form solution for four common boundary conditions on beams, addressing the effect of crack location in the analysis on the normalised determinant for the hinged structure evaluated at the natural frequency for the undamaged case. This normalised plot provides the exact frequency variation with the important benefit of eliminating the dependency on the crack severity for beams.

Section 3.5 presents a by-product of the research with another interesting relationship between the determinant of a cracked structure and the square of the bending moment in an undamaged beam at the would-be crack location - a relationship that can also be inferred from previous publications [27, 35]. The knowledge of this relationship is not necessarily required or useful in the damage identification process, but it is a property that leads to a better understanding of the effect of the crack position in specific vibration modes for skeletal structures.

In Chapter 4 the DSM was used to understand the effect of a point mass on a cracked structure, and assess an interesting idea that appeared to hold some promise in the identification of cracks proposed in an earlier work [36]. Zhong and Oyadiji [36] use a probe mass roving along the length of the beam knowing that a crack will produce a discontinuity in the otherwise continuous graph of mass locations versus measured frequencies. The assessment shows that while some changes in the slope of the frequency vs mass location plot was observed, the changes were found to be small and if one did not know the location of the crack they could be missed.

Chapter 5 introduces the use a roving body possessing rotary inertia and explains, through the DSM, the parameters that can make observable a sudden change in the frequency at the crack location.

Chapter 6 uses experimental results in an attempt to validate the application of the found features to damage identification in frameworks and dynamic properties identification in beam structures.

A summary of the conclusions is presented in Chapter 7 as well as some questions to be addressed in future.

Chapter 2

Continuous Elements Method

The term "continuous" is used to clarify that no a priori spatial discretization is introduced and the discretisation of the structure into elements is determined by its geometric properties rather than a priori knowledge of the result to be obtained. Therefore geometrically simple structures need not to be cut down to pieces in order to get reasonable precision [37].

2.1 Continuous versus Finite

The Finite Element Method (FEM) is a method in which a system is discretised into a finite number of elements and is based on the principle that the smaller the element the more precise the result will be. The expected behaviour of the field variable such as the displacement of a structure or the temperature of a body is approximately modelled within each element using polynomial expressions. When faced with vibrational problems, each element is described by two matrices, the mass matrix which account for the inertial effects and the stiffness matrix that accounts for the elastic and geometric resistance and the degrees of freedom at the interconnecting nodes form the eigenvector.

On the other hand Continuous Element Methods avoid discretization by using the analytical solution of the underlying differential equations to define the exact shape functions of the expected behaviour. In dynamic problems, each element is described by a matrix that accounts at the same time the elastic and inertial effects with frequency dependent components. This matrix is called the Dynamic Stiffness Matrix (DSM) and provides the analyst with much better model accuracy when compared to finite element or other approximate methods and it is independent of the number of elements used in the analysis [38]. As no approximations concerning the displacement are made, the method is exact and the results can be obtained to any degree of accuracy that is only limited by machine precision.

The application of the dynamic stiffness matrix to solve free vibration problems of structures (or structural elements) is quite simple. First, the DSM of all the individual

elements in a structure are assembled in the usual way as it is done in the FEM (except that there is only one matrix for each element to assemble, i.e. there are no separate mass and stiffness matrices). Then a suitable eigensolution procedure can be adopted to obtain the natural frequencies.

The direct treatment of continuous systems, though historically older (it is reported Koloušek worked in the subject since 1940 [37]), has never reached the degree of popularity of the FEM mainly because of the limited set of structural elements for which the DSM is currently available and the versatility of the FEM which can be used for irregular boundaries and varying loading and material properties. In addition, the solution procedure using the DSM leads to what is perceived as a non-linear eigenvalue problem, and the elements of the dynamic stiffness matrix are generally highly irregular (transcendental) functions of the frequency (going through zeros and infinities).

Another cause for the lack of popularity of the DSM, is that at present it has been developed predominantly for one-dimensional elements such as rods, shafts, and beams or beam-columns. The main sources of understanding to initial readers are the book by Koloušek and McLean [39] and the article by Williams and Banerjee [40] who covered already several aspects of the continuous solution of both prismatic and non-prismatic members. The latter formulations have also been applied to more rigorous member theories including coupling effects due to torsion. In recent years there has been an important effort to expand the solutions for plate and shell problems subject to various boundary conditions [41] shapes [42] and materials [43].

2.2 Dynamic Stiffness General Formulation

The general formulation for the DSM is given in a comprehensive work by Banerjee [34] where the derivation of the governing differential equation of motion of the structural element is the first step in the procedure.
For a structural element undergoing free undamped vibration its governing differential equation of motion can be symbolically written as

$$\mathcal{L}(\mathbf{u}) = 0 \tag{2-1}$$

Equation (2.1) is a set of partial differential equations (PDEs) where $\mathcal{L}$ is a differential operator and $\mathbf{u}$ is the corresponding displacement vector which is a function of two independent variables, namely time t and position x. This equation could be derived by applying one of many techniques available in the literature such as Newton's laws, D'Alembert's principle, Lagrange's equations, principle of virtual work or Hamilton's principle.

An analytical solution of the above differential equation could be obtained using separation of variables method assuming harmonically varying displacements with the general solution of the PDE is expressed in the form

$$\mathbf{u}(x,t) = \boldsymbol{\phi}(x)\mathrm{e}^{i\omega t} \tag{2-2}$$

where $\boldsymbol{\phi}(x)$ represents amplitudes of displacements vector, usually known as modal shape for a specific frequency and $i = \sqrt{-1}$.

The time dependent terms in the PDE disappears but the variable ω, the circular frequency becomes a parameter of the modal shape

$$\boldsymbol{\phi}(x) = \mathbf{U}(x,\omega)\mathbf{C} \tag{2-3}$$

with $\mathbf{C}$ a constant vector and a frequency dependent vector $\mathbf{U}(x,\omega)$, which relates the modal displacements.

In the next two steps the end conditions for displacements and actions are applied to Eq. (2.3) in order to obtain the nodal displacement and action vectors

$$\mathbf{d} = \mathbf{D}(x,\omega)\mathbf{C} \tag{2-4}$$

$$\mathbf{a} = \mathbf{A}(x,\omega)\mathbf{C} \tag{2-5}$$

where $\mathbf{d}$ and $\mathbf{a}$ are the displacement and action vectors which correspond to the nodal displacements (translation and rotation) and actions (force and moment). $\mathbf{D}(x,\omega)$ and $\mathbf{A}(x,\omega)$ are frequency dependent square matrices.

The constant vector $\mathbf{C} = \mathbf{D}^{-1}(x,\omega)\mathbf{d}$ can now be eliminated from Eqns. (2.4) and (2.5) to give

$$\mathbf{a} = \mathbf{K}(x,\omega)\mathbf{d} = \mathbf{A}(x,\omega)\mathbf{D}^{-1}(x,\omega)\mathbf{d} \tag{2-6}$$

where

$$\mathbf{K}(x,\omega) = \mathbf{A}(x,\omega)\mathbf{D}^{-1}(x,\omega) \tag{2-7}$$

is the required dynamic stiffness matrix.

In Eq. (2.7) the two steps needed to obtain the dynamic stiffness matrix are: (i) to invert the $\mathbf{D}(x,\omega)$ matrix to give $\mathbf{D}^{-1}(x,\omega)$; and then (ii) to pre-multiply the inverted matrix (i.e. $\mathbf{D}^{-1}(x,\omega)$) by the $\mathbf{A}(x,\omega)$ matrix to give $\mathbf{K}(x,\omega)$. Computer implementation of these steps can be accomplished either numerically or algebraically. Figure 2.1 explains in a flowchart, the symbolic computation of the exact dynamic stiffness matrix [38].

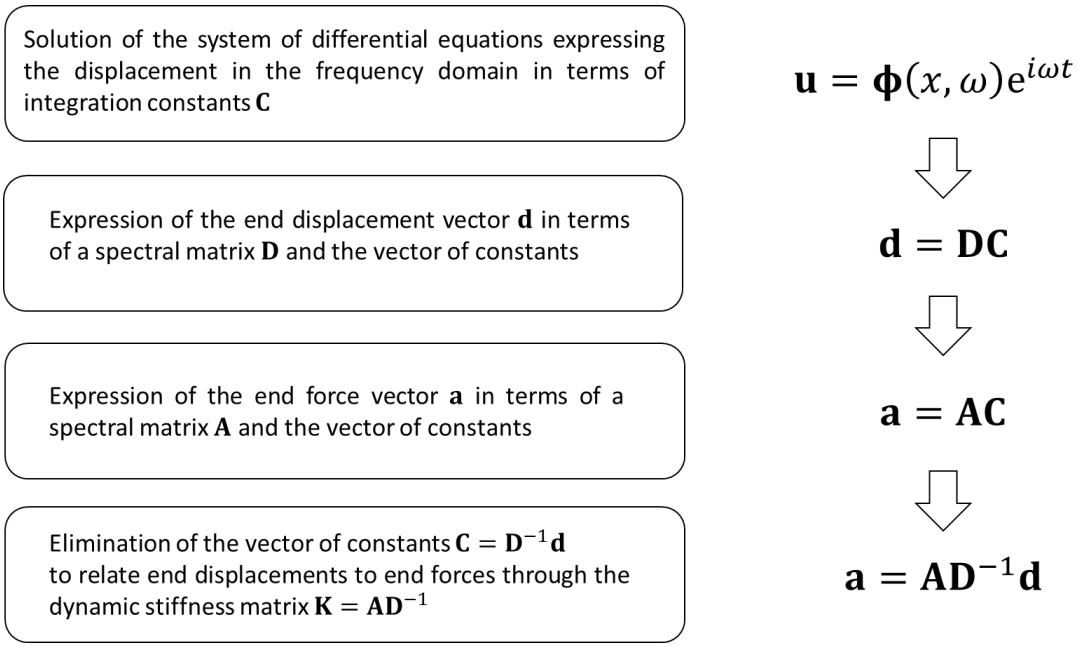

Figure 2.1. Flowchart to create dynamic stiffness matrix

2.3 Formulation of Dynamic Stiffness for an axially loaded beam

For the Euler-Bernoulli beam theory there are already well explained procedures to obtain the governing partial differential equation of motion, for example as explained by Clough and Penzien [44] using D'Alambert's principle or Rebecchi [45] using Hamilton's principle.

To use D'Alambert's principle, we start from the infinitesimal beam element of length δx depicted in Figure 2.2 located between axial coordinates x and $x + \delta x$. Following

the Euler-Bernoulli beam theory assumptions, shear deformations are neglected and beam cross section remains plane and perpendicular to the beam axes after deformation.

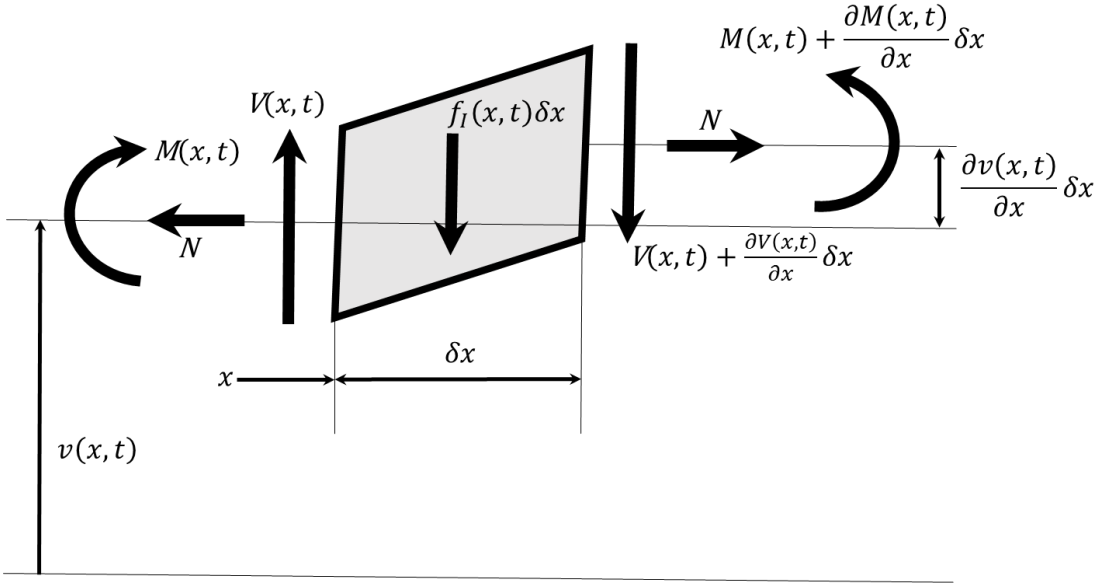

Figure 2.2. Infinitesimal Euler-Bernoulli beam element

Figure 2.2 is a free body diagram and shows the response $v(x,t)$ of the infinitesimal element affected not only by the bending moment $M(x,t)$ and the transverse force $V(x,t)$ acting on both sides of the element but also by the element inertial effect $f_I(x,t)$ and the internal axial force N. Summing all forces acting transversely gives

$$V(x,t)-\left[V(x,t)+\frac{\partial V(x,t)}{\partial x}\delta x\right]-f_I(x,t)\delta x=0 \tag{2-8}$$

which reduces to

$$\frac{\partial V(x,t)}{\partial x}=-f_I(x,t) \tag{2-9}$$

From D'Alambert's principle the intensity of inertial equivalent static force, using μ as the linear density, is given by

$$f_I(x,t)=\mu\frac{\partial^2 v(x,t)}{\partial t^2} \tag{2-10}$$

Therefore Eq.(2.9) becomes

$$\frac{\partial V(x,t)}{\partial x}=-\mu\frac{\partial^2 v(x,t)}{\partial t^2} \tag{2-11}$$

It may be noted that the same result would be obtained by applying Newton's second law to the free-body shown in Fig.2.2.

The second equilibrium relationship, Eq. (2.12) is obtained by summing moments about a point located in the centre of the right surface of the element.

$$M(x,t) + V(x,t)\delta x + N\frac{\partial v(x,t)}{\partial x}\delta x - \left[M(x,t) + \frac{\partial M(x,t)}{\partial x}\delta x\right] = 0$$

$$V(x,t) = \frac{\partial M(x,t)}{\partial x} - N\frac{\partial v(x,t)}{\partial x} \quad (2\text{-}12)$$

Note that because the direction of the axial force does not change with the beam deflection, there is no effect on the transverse equilibrium equation, but due to the changes in the line of action of the axial force, a moment has to be included in the moment-equilibrium equation.

Differentiating Eq. (2.12) with respect to x and assuming the axial force constant gives

$$\frac{\partial V(x,t)}{\partial x} = \frac{\partial^2 M(x,t)}{\partial x^2} - N\frac{\partial^2 v(x,t)}{\partial x^2} \quad (2\text{-}13)$$

The moment-curvature relationship is

$$M(x,t) = EI\frac{\partial^2 v(x,t)}{\partial x^2} \quad (2\text{-}14)$$

Then substituting Eq. (2.11) and Eq.(2.14) into Eq.(2.13) gives

$$\frac{\partial^2}{\partial x^2}\left[EI\frac{\partial^2 v(x,t)}{\partial x^2}\right] - N\frac{\partial^2 v(x,t)}{\partial x^2} + \mu\frac{\partial^2 v(x,t)}{\partial t^2} = 0 \quad (2\text{-}15)$$

where EI is the flexural rigidity.

To obtain the solution to the governing beam vibration equation stated in Eq. (2.15), the separation of variables technique is applied. Using this technique it is assumed $v(x,t) = Y(x)\,\tau(t)$, a product of $\tau(t)$ a harmonic function in time $e^{\omega t}$ and $Y(x)$ a function in space. Differentiating with respect to x and denoting it with prime gives,

$$\frac{\partial v(x,t)}{\partial x} = Y'(x)\,\tau(t) \quad (2\text{-}16)$$

$$\frac{\partial^2 v(x,t)}{\partial x^2} = Y''(x)\,\tau(t) \quad (2\text{-}17)$$

differentiating now with respect to t and denoting it with dots leads to Eq. (2.18) with ω, the circular frequency as the most relevant parameter.

$$\frac{\partial^2 v(x,t)}{\partial t^2} = Y(x)\,\ddot{\tau}(t) = -\omega^2 Y(x)\,\tau(t) \quad (2\text{-}18)$$

Substituting Eqns. (2.17) and (2.18) into Eq. (2.15) gives a fourth order spatial Ordinary Differential Equation (ODE) with constant coefficients as given in Eq. (2.19),

$$EI\frac{\partial^2}{\partial x^2}[Y''(x)] - N\frac{\partial}{\partial x}[Y'(x)] - \mu\,\omega^2 Y(x) = 0$$
$$Y'^{v}(x) - \frac{N}{EI}Y''(x) - \frac{\mu}{EI}\omega^2 Y(x) = 0 \qquad (2\text{-}19)$$

Introducing the parameters λ for the frequency defined in Eq. (2.20) and the axial parameter σ defined in Eq. (2.21), Eq. (2.19) is rewritten as Eq. (2.22)

$$\lambda^4 = \frac{\mu}{EI}\omega^2 \qquad (2\text{-}20)$$

$$2\sigma^2 = \frac{N}{EI} \qquad (2\text{-}21)$$

$$Y'^{v}(x) - 2\sigma^2 Y''(x) - \lambda^4 Y(x) = 0 \qquad (2\text{-}22)$$

The exponential form e^{rx} is assumed for the solution of the above differential equation. Substituting this into Eq. (2.22) leads to the characteristic equation given in Eq. (2.23).

$$r^4 - 2\sigma^2 r^2 - \lambda^4 = 0 \qquad (2\text{-}23)$$

Equations (2.24) and (2.25) define the four roots for the characteristic equation as well as two frequency-load parameters ϕ_1 and ϕ_2.

$$r_{1,2} = \pm\sqrt{(\lambda^4 + \sigma^4)^{1/2} + \sigma^2} = \pm\phi_1 \qquad (2\text{-}24)$$

$$r_{3,4} = \pm i\sqrt{(\lambda^4 + \sigma^4)^{1/2} - \sigma^2} = \pm i\phi_2 \qquad (2\text{-}25)$$

The analytical solution of Eq. (2.22) using the four roots is then expressed in the exponential form as,

$$Y(x) = C_1 e^{r_1 x} + C_2 e^{r_2 x} + C_3 e^{r_3 x} + C_4 e^{r_4 x} \qquad (2\text{-}26)$$

or in terms of trigonometric and hyperbolic functions,

$$Y(x) = G_1\cosh(\phi_1 x) + G_2\sinh(\phi_1 x) + G_3\cos(\phi_2 x) + G_4\sin(\phi_2 x) \qquad (2\text{-}27)$$

In order to obtain the assembly capabilities used in the FEM, the spectral element of length L_e will use two nodes with two degrees of freedom (DOF), transverse displacement and rotation at each node that have to be related with the nodal actions (forces and moments) following the sign convention shown in Figure 2.3.

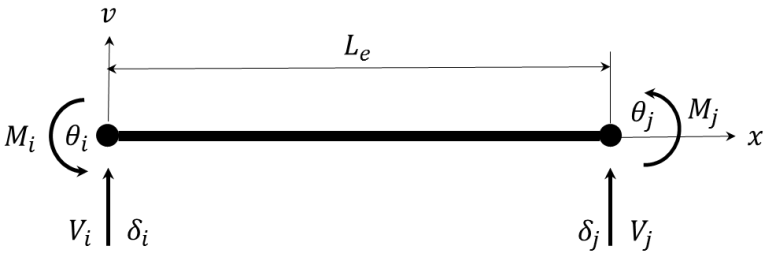

Figure 2.3. Nodal sign convention

Following the sign convention described for the spectral element and adjusting it for the differential element depicted in Figure 2.2, the displacement and force vectors at the boundaries used in Eqns. (2.4) and (2.5) must be defined as

$$\mathbf{d} = \begin{bmatrix} v'(0,t) \\ v(0,t) \\ v'(L_e,t) \\ v(L_e,t) \end{bmatrix} = \begin{bmatrix} \theta_i \\ \delta_i \\ \theta_j \\ \delta_j \end{bmatrix} e^{i\omega t} = \mathbf{D} \begin{bmatrix} G_1 \\ G_2 \\ G_3 \\ G_4 \end{bmatrix} e^{i\omega t} \tag{2-28}$$

$$\mathbf{a} = \begin{bmatrix} -M(0,t) \\ V(0,t) \\ M(L_e,t) \\ -V(L_e,t) \end{bmatrix} = \begin{bmatrix} M_i \\ V_i \\ M_j \\ V_j \end{bmatrix} e^{i\omega t} = \mathbf{A} \begin{bmatrix} G_1 \\ G_2 \\ G_3 \\ G_4 \end{bmatrix} e^{i\omega t} \tag{2-29}$$

Substituting Eqns. (2.28) and (2.29) into Eq. (2.7), the DSM for an uniform beam element can be obtained, leading to an equation of the form Eq. (2.6) as follows

$$\begin{bmatrix} M_i \\ F_i \\ M_j \\ F_j \end{bmatrix} = EI \begin{bmatrix} S_e & Q_e & SC_e & -Qq_e \\ Q_e & T_e & Qq_e & -Tt_e \\ SC_e & Qq_e & S_e & -Q_e \\ -Qq_e & -Tt_e & -Q_e & T_e \end{bmatrix} \begin{bmatrix} \theta_i \\ \delta_i \\ \theta_j \\ \delta_j \end{bmatrix} \tag{2-30}$$

Here the elements of the matrix are called dynamic stability functions [46] and are listed in the following table,

Table 2.1. Dynamic stability functions for an axially loaded Euler-Bernoulli beam

S_e	$\frac{(\phi_1{}^2+\phi_2{}^2)[\phi_1\cosh(\phi_1 L_e)\sin(\phi_2 L_e)-\phi_2\sinh(\phi_1 L_e)\cos(\phi_2 L_e)]}{(\phi_1{}^2-\phi_2{}^2)\sinh(\phi_1 L_e)\sin(\phi_2 L_e)+2\,\phi_1\phi_2[1-\cosh(\phi_1 L_e)\cos(\phi_2 L_e)]}$
T_e	$\frac{\phi_1\phi_2(\phi_1{}^2+\phi_2{}^2)[\phi_2\cosh(\phi_1 L_e)\sin(\phi_2 L_e)+\phi_1\sinh(\phi_1 L_e)\cos(\phi_2 L_e)]}{(\phi_1{}^2-\phi_2{}^2)\sinh(\phi_1 L_e)\sin(\phi_2 L_e)+2\,\phi_1\phi_2[1-\cosh(\phi_1 L_e)\cos(\phi_2 L_e)]}$
Q_e	$\frac{\phi_1\phi_2(2\phi_1\phi_2\sinh(\phi_1 L_e)\sin(\phi_2 L_e)+(\phi_1{}^2-\phi_2{}^2)[1-\cosh(\phi_1 L_e)\cos(\phi_2 L_e)])}{(\phi_1{}^2-\phi_2{}^2)\sinh(\phi_1 L_e)\sin(\phi_2 L_e)+2\,\phi_1\phi_2[1-\cosh(\phi_1 L_e)\cos(\phi_2 L_e)]}$
SC_e	$\frac{(\phi_1{}^2+\phi_2{}^2)[\phi_2\sinh(\phi_1 L_e)-\phi_1\sin(\phi_2 L_e)]}{(\phi_1{}^2-\phi_2{}^2)\sinh(\phi_1 L_e)\sin(\phi_2 L_e)+2\,\phi_1\phi_2[1-\cosh(\phi_1 L_e)\cos(\phi_2 L_e)]}$
Qq_e	$\frac{\phi_1\phi_2(\phi_1{}^2+\phi_2{}^2)[\cosh(\phi_1 L_e)-\cos(\phi_2 L_e)]}{(\phi_1{}^2-\phi_2{}^2)\sinh(\phi_1 L_e)\sin(\phi_2 L_e)+2\,\phi_1\phi_2[1-\cosh(\phi_1 L_e)\cos(\phi_2 L_e)]}$
Tt_e	$\frac{\phi_1\phi_2(\phi_1{}^2+\phi_2{}^2)[\phi_2\sin(\phi_2 L_e)+\phi_1\sinh(\phi_1 L_e)]}{(\phi_1{}^2-\phi_2{}^2)\sinh(\phi_1 L_e)\sin(\phi_2 L_e)+2\,\phi_1\phi_2[1-\cosh(\phi_1 L_e)\cos(\phi_2 L_e)]}$

The equation presented in Eq. (2.30) may be presented in the form

$$\mathbf{a} = \mathbf{K}\mathbf{d} \tag{2-31}$$

where **a** is the action vector, **K** is the Dynamic Stiffness Matrix and **d** is the nodal displacements (or degrees of freedom).

2.4 Summary

This chapter was devoted to explain the conceptual development of the continuous element method and application to derive the DSM components of beam elements through the analytical solution of their governing differential equations of motion in free vibration. The DSM for beam elements will be used to understand the effects of elements of local flexibility or/and inertia in structural systems, such as portal frames, whose discretization is performed using beam elements.

Chapter 3

Crack Effect

As all materials contain imperfections or defects, the difficulty is to decide when a structure is 'damaged' and to do so, definition of fault has to be made. Worden and Dulieu-Barton [47] explain the differences in the following way: "*A fault is when the structure can no longer operate satisfactorily. If one defines the quality of a structure or system as its fitness for purpose or its ability to meet customer or user requirements, it suffices to define a* ***fault*** *as a change in the system that produces an unacceptable reduction in quality.* ***Damage*** *is when the structure is no longer operating in its ideal condition, but it can still function satisfactorily, but in a suboptimal manner. A* ***defect*** *is inherent in the material and statistically all materials will contain a known amount of defects. This means that the structure will operate at its optimum if the constituent materials contain defects*". With this definitions in mind, faults and defects are not considered in this work, which is devoted to the analysis of damaged structures where the structural discontinuity does not affect an adequate operation.

3.1 Vibration of damaged structures

In the context of structural health monitoring, damage is defined as changes to the material and/or geometric properties of a system which adversely affect its current or future performance [48]. It can be appreciated from the literature mentioned in the introduction that crack is one type of structural damage that has received considerable attention in many publications. Cracks are treated in the form of small slots that generate changes in the cross sectional areas breaking the structural continuity.

A state of the art review for the vibration of cracked structures was presented by Dimarogonas [49], in which Kirmser [50] and Thomson [51] are credited as the earliest researchers on vibrational characteristics of a beam with local discontinuities. A recent review paper by Shirazizadeh, et al. [52] gives a wide range of crack spring models.

In view of obtaining a closed-form solution for the effect of a crack in a structural system, a concentrated crack and its reduction in the sectional area has to be modelled as a set of massless springs connecting undamaged components. These springs possess

translational, rotational and axial stiffness whose values are defined according to the properties of the connecting sections and the crack severity [53, 54]. Among them, the rotational spring model has been an acceptable approach towards an exact solution, as can be seen from for recent works in beams [55] frames [56] and plates [57, 58].

3.1.1 Rotational spring model

Even in the early studies, structural discontinuity is treated in the form of a small slot that generates a beam with different cross sectional areas to replace the notched section of the beam. Dimarogonas [49] states that using the results from fracture mechanics Irwin [24] represents intensities of the concentrated cracks by the rotational stiffness of springs using the local compliance computed from the strain energy density function. An important difference is remarked between a crack and a notch. The former, as is treated in the fracture mechanics theory, generates a singularity at the crack tip and the latter produces an area reduction such as that produced by a saw cut. With this difference taken into in account, when speaking of continuous cracked beam theory, Christides and Barr [59] are credited as the pioneers to develop a cracked Euler-Bernoulli beam theory by deriving the differential equation and associated boundary conditions for a uniform Euler-Bernoulli beam containing one or more pairs of symmetric discontinuities. However, because the crack function proposed avoids the singularity at the crack tip, it treats the crack as a notch.

Nowadays the word notch is no longer used. Instead the term ‘open crack’ is mentioned and mathematically treated as the former since the paper presented by Chondros, et al. [20] based on the model of Christides and Barr [59] which considers the crack as a local flexibility and assumes that the effect of the crack is apparent in its neighbourhood only. Chondros, et al. [20] treat the cracked beam as two uniform beams connected by a rotational spring at the crack location and to validate the assumption, compare the results obtained by the open-crack model with those measured for a simply supported beam with fatigue propagated cracks reporting consistent measurements for crack depths up-to half the beam height. Neither the nonlinearity effects generated by crack closure during the bending [60] nor crack growth (fatigue cracks) are considered in these researches and these assumptions are kept throughout the present work. Due to the fact that natural frequency reduction for

a breathing crack is much smaller than the one for an open crack [61] it is difficult to recognize their effects by frequency monitoring only as is intended in this work.

3.1.2 Beams with multiple cracks

A paper by Ruotolo and Surace [62] is one of the early articles considering beams with several cracks along the length, formulating additionally the inverse problem of damage assessment for cantilever beams using genetic algorithms in the optimization of a finite element model. Since then several authors investigated this phenomenon applying different approaches. Shifrin and Ruotolo [63] proposed a method in which the entire beam is dived into $(n+1)$ beam elements connected by massless springs representing the n cracks. The discontinuity is converted into a function by means of Dirac's deltas and Heaviside step functions. When the integration is performed, a system of $n+2$ linear equations with $n+2$ unknowns is obtained. Zheng and Fan [64] used a modified Fourier series to compute the natural frequencies of Euler–Bernoulli and Timoshenko beams with standard linear eigenvalue equations. In the same year Khiem and Lien [65] used a transfer matrix approach; the method built a 4x4 global matrix multiplying orderly, according with the compatibility conditions, the transfer matrices for beams and cracks. A system of four linear equations is obtained from the product of the global matrix and the boundary conditions vector whose solution leads to a nonlinear eigenvalue problem of finding the frequency that nulls the determinant of the global matrix.

Caddemi and Caliò [18] presented an exact closed-form solution that could be used for either damaged or undamaged beams. The work gives a good description of the mathematical process to arrive at the exact closed-form expression for the vibration of the Euler-Bernoulli beam with multiple concentrated cracks without requiring the enforcement of continuity conditions just by enforcing the standard boundary conditions. This method even works for the general case of rotational and translational spring supports. The concept adopted is modelled via generalised functions (Dirac's delta based) on the Euler-Bernoulli partial differential governing equation for beams but taking into consideration the local effect in the flexural stiffness of concentrated cracks. The novelty of their approach is the integration of these generalised functions by means of distribution theory. The general solution for multi-cracked beams is assumed as a combination of the standard trigonometric and hyperbolic functions

where the coefficients are generalised functions, but when the inverse problem has to be faced, its applicability is unknown.

Section 3.2 will present a novel form of see the frequency equation of a cracked structure that stands not only for beams but also to frames that could be easily accommodated in order to solve the inverse problem of a single cracked structure and could be iterative applied to solve the direct problem of multiple damaged structures.

3.2 Uncoupling severity and location

Although the methodology being discussed is applicable to any structure with a DSM, for illustrative purposes let us consider the vibration of a beam section with a crack at the coordinate x_c, represented by a spring limiting the relative rotation of the beam segments at the hinge which connects the structure parts at the crack location (Figure 3.1).

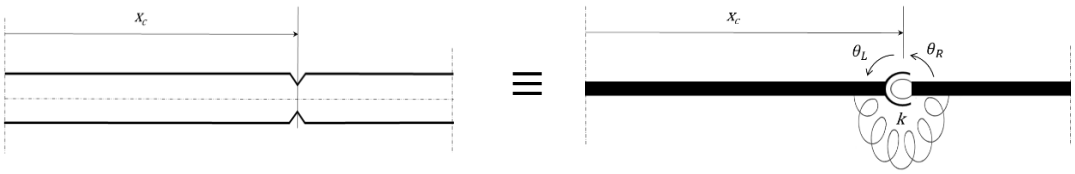

Figure 3.1. Equivalent representation of cracked section

The nodal actions $\mathbf{a}_c$ are related to the nodal displacements $\mathbf{d}_c$ (or the degrees of freedom) in the damaged structure through $\mathbf{K}_c$ the global stiffness matrix. The degrees of freedom of the damaged structure consist of the rotations at the crack and all other degrees of freedom in the structure ($\mathbf{d}_0$) which are no shown in Fig. 3.1. The actions corresponding to these displacements are $\mathbf{a}_0$. The rotations at each end of the spring are the two extra degrees of freedom that account for the rotational discontinuity generated by the stiffness reduction; for this demonstration let us allocate these extra degrees of freedom in the final two rows and columns of the global matrices.

$$\mathbf{a}_c = \mathbf{K}_c(x_c, \omega, k)\mathbf{d}_c,\ \mathbf{a}_c = \begin{bmatrix} \mathbf{a}_0 \\ M_L \\ M_R \end{bmatrix},\ \mathbf{d}_c = \begin{bmatrix} \mathbf{d}_0 \\ \theta_L \\ \theta_R \end{bmatrix}$$

Following the above mentioned steps, the dynamic stiffness matrix for the cracked structure is presented in the form

$$\mathbf{K}_c = \begin{bmatrix} \mathbf{K}_0(x_c,\omega) & \mathbf{B}_1(x_c,\omega) & \mathbf{B}_2(x_c,\omega) \\ \mathbf{B}_1^{\mathrm{T}}(x_c,\omega) & k_{11}(x_c,\omega)+k & -k \\ \mathbf{B}_2^{\mathrm{T}}(x_c,\omega) & -k & k_{22}(x_c,\omega)+k \end{bmatrix} \tag{3-1}$$

where the last two rows and columns relate to the rotational degrees of freedom on either side of the crack, and the first row and column contain the sub-matrices for all other degrees of freedom of the structure. Thus $\mathbf{K}_0(x_c,\omega)$ is a square submatrix; $\mathbf{B}_1(x_c,\omega)$ and $\mathbf{B}_2(x_c,\omega)$ are column vectors, $k_{11}(x_c,\omega)$ and $k_{22}(x_c,\omega)$ are scalars and k is the stiffness of the rotational spring representing the crack severity. A Gaussian elimination will offer a more manageable expression for the determinant of the cracked structure, maintaining focus on the last two rows that contain the crack related elements. After eliminating the elements below $\mathbf{K}_0(x_c,\omega)$ in Eq. (3.1), $\mathbf{K}_c$ becomes,

$$\mathbf{K}_c^* = \begin{bmatrix} \mathbf{K}_0^{\Delta}(x_c,\omega) & \mathbf{B}_1^*(x_c,\omega) & \mathbf{B}_2^*(x_c,\omega) \\ 0 & k_{11}^*(x_c,\omega)+k & k_{12}^*(x_c,\omega)-k \\ 0 & k_{21}^*(x_c,\omega)-k & k_{22}^*(x_c,\omega)+k \end{bmatrix},$$

where $\mathbf{K_0^{\Delta}}(x_c,\omega)$ is an upper triangular square matrix, $\mathbf{B}_1^*(x_c,\omega)$ and $\mathbf{B}_2^*(x_c,\omega)$ are updated column vectors and $k_{ij}^*(x_c,\omega)$ updated scalars defined as follows,

$$k_{11}^*(\omega) = k_{11}(x_c,\omega) - \mathbf{B}_1^{\mathrm{T}}(x_c,\omega)\mathbf{K}_0^{-1}(x_c,\omega)\mathbf{B}_1(x_c,\omega)$$
$$k_{12}^*(\omega) = k_{21}^*(x_c,\omega) = -\mathbf{B}_1^{\mathrm{T}}(x_c,\omega)\mathbf{K}_0^{-1}(x_c,\omega)\mathbf{B}_2(x_c,\omega)$$
$$k_{22}^*(\omega) = k_{22}(x_c,\omega) - \mathbf{B}_2^{\mathrm{T}}(x_c,\omega)\mathbf{K}_0^{-1}(x_c,\omega)\mathbf{B}_2(x_c,\omega)$$

Thus the determinant of the dynamic stiffness matrix of the cracked structure is

$$\begin{aligned} D_c(x_c,\omega) &= \left|\mathbf{K}_0^{\Delta}(x_c,\omega)\right|\left[(k_{11}^*(\omega)+k)(k_{22}^*(\omega)+k)-(k_{12}^*(\omega)-k)^2\right] \\ &= \left|\mathbf{K}_0^{\Delta}(x_c,\omega)\right|\left[\left(k_{11}^*(\omega)k_{22}^*(\omega)-\left(k_{12}^*(\omega)\right)^2\right)+k\left(k_{11}^*(\omega)+k_{22}^*(\omega)+2k_{12}^*(\omega)\right)\right] \end{aligned} \quad (3\text{-}2)$$

The above analysis can be applied to the structure with a hinge at the position x_c by setting $k=0$, i.e.

$$D_h(x_c,\omega) = \left|\mathbf{K}_0^{\Delta}(x_c,\omega)\right|\left[\left(k_{11}^*(\omega)k_{22}^*(\omega)-\left(k_{12}^*(\omega)\right)^2\right)\right] \quad (3\text{-}3)$$

It could also be applied to the uncracked structure by setting $k=\infty$. However knowing that the continuity of the slope does not change, it can be stated $\theta_L = \theta_R = \theta$. Therefore it is more appropriate to equate the two rotations at the location of the crack by a single degree of freedom, adding the corresponding matrix elements so that the dynamic stiffness matrix of the undamaged structure $\mathbf{K}_u$ becomes

$$\mathbf{K}_u\begin{bmatrix}\mathbf{d}_0\\ \theta\end{bmatrix} = \begin{bmatrix}\mathbf{K}_0(x_c,\omega) & \mathbf{B}_1(x_c,\omega)+\mathbf{B}_2(x_c,\omega)\\ \mathbf{B}_1^{\mathrm{T}}(x_c,\omega)+\mathbf{B}_2^{\mathrm{T}}(x_c,\omega) & k_{11}(x_c,\omega)+k_{22}(x_c,\omega)\end{bmatrix}\begin{bmatrix}\mathbf{d}_0\\ \theta\end{bmatrix} \quad (3\text{-}4)$$

Performing partial Gaussian elimination to $\mathbf{K}_u$ gives

$$\mathbf{K}_u^* = \begin{bmatrix}\mathbf{K}_0^{\Delta}(x_c,\omega) & \mathbf{B}_1^*(x_c,\omega)+\mathbf{B}_2^*(x_c,\omega)\\ 0 & k^*(x_c,\omega)\end{bmatrix}$$

where,

$$k^*(x_c,\omega) = k_{11}(x_c,\omega) + k_{22}(x_c,\omega) - \left(\mathbf{B}_1^{\mathrm{T}}(x_c,\omega) + \mathbf{B}_2^{\mathrm{T}}(x_c,\omega)\right)\mathbf{K}_0^{-1}(x_c,\omega)\left(\mathbf{B}_1(x_c,\omega) + \mathbf{B}_2(x_c,\omega)\right)$$

$$k^*(x_c,\omega) = \left(k_{11}^*(x_c,\omega) + k_{22}^*(x_c,\omega) + 2k_{12}^*(x_c,\omega)\right)$$

Thus the determinant of the dynamic stiffness matrix of the uncracked structure $D_0(x_c,\omega)$ is

$$D_0(x_c,\omega) = \left|\mathbf{K}_0^{\Delta}(x_c,\omega)\right|\left[\left(k_{11}^*(x_c,\omega) + k_{22}^*(x_c,\omega) + 2k_{12}^*(x_c,\omega)\right)\right] \quad (3\text{-}5)$$

Rearranging Eq. (3.2) using the obtained expressions in Eqns. (3.3) and (3.5) the determinant of the dynamic stiffness matrix of the cracked structure $D_c(x_c,\omega)$ will be seen as

$$D_c(x_c,\omega) = kD_0(x_c,\omega) + D_h(x_c,\omega) \quad (3\text{-}6)$$

The right hand side is the sum of the determinant of the dynamic stiffness matrix of the structure with a hinge at the location x_c denoted by $D_h(x_c,\omega)$ and the determinant of the dynamic stiffness matrix of the uncracked structure multiplied by the stiffness of the rotational spring. Equation (3.6) could be rearranged in terms of the spring flexibility, in Eq. (3.7) with $f = 1/k$ to provide a physical interpretation on the effect of a local flexibility in an otherwise healthy structure in which $f = 0$, means no crack is present.

$$fD_c(x_c,\omega) = D_0(x_c,\omega) + fD_h(x_c,\omega) \quad (3\text{-}7)$$

It should be noted that a closed-form solution similar to Eq. (3.6) was previously presented by Khaji, et al. [66] for simple beams but until now it has not been proven to hold for frames. At this stage it is appropriate to stress that the main achievement of this work is summarized with Eq. (3.6). Its potential implications include a means to separate the location effect and the severity effect in a cracked structure which are explained later.

3.3 Closed-form solutions for beams using the DSM

In this section for the very first time in literature is explained how to reach closed-form solutions for cracked and undamaged Euler-Bernoulli beams expanding the DSM determinant. This close-form solutions for beams with common boundary conditions are sought as a simplified form of Eq. (3.6) and analysed in Section 3.4 to offer a clear demonstration of the of the significance of each term presented on Eq. (3.6).

A beam of length *L* containing an open crack concentrated at a specific axial location $x_c = L_a$ is depicted in Fig. 3.2.a, and modelled by connecting two elements one

between nodes i-c of length $L_a = x_c$ and the other between nodes c-j of length $L_b = L - L_a$ as shown in Fig. 3.2.b.

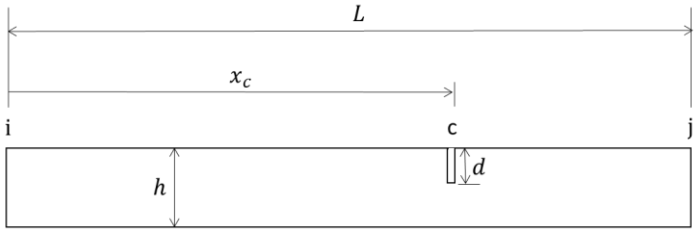

(a) Beam of height *h* with an open crack of depth *d* within its length *L*.

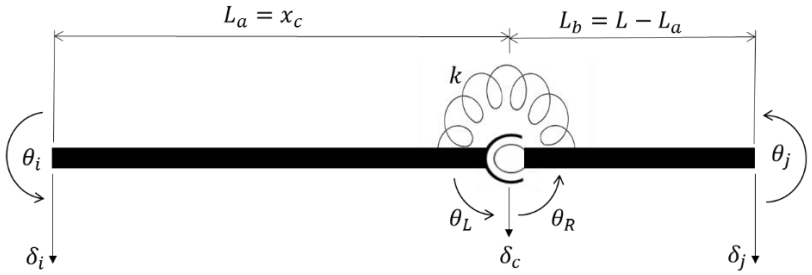

(b) Rotational spring model of a crack connecting two beam segments.

Figure 3.2. Cracked beam representation

Such a crack is represented by a rotational spring of stiffness k, which is assumed to be related to the crack-depth ratio (d/h) by a suitable empirical formula [52, 67]. The presence of the rotational spring results in separate moments and rotations at the intermediate node *c* (θ_L at the left side of the crack and θ_R at the right side of the crack) defining the spring DSM by Eq. (3.8) which relates moments at each side of the spring with the rotations,

$$\begin{bmatrix} M_L \\ M_R \end{bmatrix} = \begin{bmatrix} k & -k \\ -k & k \end{bmatrix} \begin{bmatrix} \theta_L \\ \theta_R \end{bmatrix} \tag{3-8}$$

The overall DSM of the combined system Eq. (3.9) is assembled connecting independent DSM Eq. (2.30) of beam elements L_a and L_b through spring DSM resulting from the expression

$$\mathbf{a}_c = \mathbf{K}_c(x_c, \omega, k)\mathbf{d}_c,\ \mathbf{a}_c = \begin{bmatrix} F_i \\ M_i \\ M_L \\ F_c \\ M_R \\ M_j \\ F_j \end{bmatrix},\ \mathbf{d}_c = \begin{bmatrix} \delta_i \\ \theta_i \\ \theta_L \\ \delta_c \\ \theta_R \\ \theta_j \\ \delta_j \end{bmatrix}$$

$$\mathbf{K}_c = EI\begin{bmatrix} T_a & Q_a & Qq_a & -Tt_a & 0 & 0 & 0 \\ Q_a & S_a & SC_a & -Qq_a & 0 & 0 & 0 \\ Qq_a & SC_a & S_a+\bar{k} & -Q_a & -\bar{k} & 0 & 0 \\ -Tt_a & -Qq_a & -Q_a & T_a+T_b & Q_b & Qq_b & -Tt_b \\ 0 & 0 & -\bar{k} & Q_b & S_b+\bar{k} & SC_b & -Qq_b \\ 0 & 0 & 0 & Qq_b & SC_b & S_b & -Q_b \\ 0 & 0 & 0 & -Tt_b & -Qq_b & -Q_b & T_b \end{bmatrix} \quad (3\text{-}9)$$

It may be noted that a new stiffness parameter $\bar{k} = k/EI$ is used to account for the EI which multiplies all dynamic stability functions to form the stiffness terms. The next step will be to define the boundary conditions for the cracked beam. When working with dynamic stiffness method, the beam fixed at both ends has the simplest determinant. In addition we analyse the case when there are no axial load, then from Eq. (2.21) $\alpha = 0$, and from Eqns. (2.24) and (2.25) the frequency parameter ϕ_1 and ϕ_2 are equal to λ making elements for the DSM of Table 2.1 acquire forms shown in Table 3.1.

Table 3.1. Stability functions for an unloaded Euler-Bernoulli beam

S_e	$\frac{\lambda[\cosh(\lambda L_e)\sin(\lambda L_e) - \sinh(\lambda L_e)\cos(\lambda L_e)]}{1-\cosh(\lambda L_e)\cos(\lambda L_e)}$	SC_e	$\frac{\lambda[\sinh(\lambda L_e) - \sin(\lambda L_e)]}{1-\cosh(\lambda L_e)\cos(\lambda L_e)}$
T_e	$\frac{\lambda^3[\cosh(\lambda L_e)\sin(\lambda L_e) + \sinh(\lambda L_e)\cos(\lambda L_e)]}{1-\cosh(\lambda L_e)\cos(\lambda L_e)}$	Tt_e	$\frac{\lambda^3[\sinh(\lambda L_e) + \sin(\lambda L_e)]}{1-\cosh(\lambda L_e)\cos(\lambda L_e)}$
Q_e	$\frac{\lambda^2[\sin(\lambda L_e)\sinh(\lambda L_e)]}{1-\cosh(\lambda L_e)\cos(\lambda L_e)}$	Qq_e	$\frac{\lambda^2[\cosh(\lambda L_e) - \cos(\lambda L_e)]}{1-\cosh(\lambda L_e)\cos(\lambda L_e)}$

Before the determinant terms are expanded, simplification of common collected terms has to be made to gain better manageability of the expansions. The terms to expand contain some DSM elements which are abbreviated for convenience. These are s_e, c_e, SH_e, CH_e and Δ_e which stand for $\sin(\lambda L_e)$, $\cos(\lambda L_e)$, $\sinh(\lambda L_e)$, $\cosh(\lambda L_e)$ and $(1-\cosh(\lambda L_e)\cos(\lambda L_e))$ respectively. Most of the simplifications are reached by applying the trigonometric identity between squared sine and cosine functions ($c_e^2 + s_e^2 = 1$), and hyperbolic sine and hyperbolic cosine functions ($CH_e^2 - SH_e^2 = 1$)

$$T_eS_e - Q_e^2 = \left(\frac{\lambda^3(s_e\,CH_e + c_e\,SH_e)}{\Delta_e}\right)\left(\frac{\lambda\big((s_e\,CH_e - c_e\,SH_e)\big)}{\Delta_e}\right) - \left(\frac{\lambda^2 s_e\,SH_e}{\Delta_e}\right)^2 \quad (3\text{-}10)$$

$$\frac{\lambda^4(1+c_eCH_e)(1-c_eCH_e)}{\Delta_e^2} = \frac{\lambda^4(2-\Delta_e)}{\Delta_e}$$

$$S_e^2 - SC_e^2 = \begin{matrix} \frac{\lambda^2(s_e^2 CH_e^2 + c_e^2 SH_e^2 - c_e SH_e s_e CH_e)}{\Delta_e^2} - \frac{\lambda^2(s_e^2 + SH_e^2 - 2s_e SH_e)}{\Delta_e^2} \\ \frac{2\lambda^2 s_e SH_e(1 - c_e CH_e)}{\Delta_e^2} = \frac{2\lambda^2 s_e SH_e}{\Delta_e} = 2Q_e \end{matrix} \quad (3\text{-}11)$$

$$(S_e Qq_e^2 + T_e SC_e^2 - 2Q_e SC_e Qq_e = \begin{matrix} \frac{2\lambda^5(s_e CH_e(1 - c_e CH_e)^2 - c_e SH_e(1 - c_e CH_e)^2)}{\Delta_e^3} \\ \frac{2\lambda^5(s_e CH_e - c_e SH_e)}{\Delta_e^2} = \frac{2\lambda^4 S_e}{\Delta_e} \end{matrix} \quad (3\text{-}12)$$

$$Q_e^2 - Qq_e^2 = \begin{matrix} \left(\frac{\lambda^2 s_e\, SH_e}{\Delta_e}\right)^2 - \left(\frac{\lambda^2(CH_e - c_e)}{\Delta_e}\right)^2 \\ -\frac{\lambda^4(1 - c_e CH_e)^2}{\Delta_e^2} = -\lambda^4 \Delta_e \end{matrix} \quad (3\text{-}13)$$

These simplifications will be used in the next sections for a set of boundary conditions to give a demonstration of the linear relationship presented in Eq. (3.6).

3.3.1 Clamped-clamped beam

The 7x7 global matrix Eq. (3.9) for a fixed beam with a crack is reduced to a 3x3 matrix because the clamped ends eliminate the columns 1, 2, 6 and 7 relative to the end displacements and the rows 3, 4 and 5 of the intermediate actions are the remaining ones, leading to the matrix

$$\mathbf{K}_c = EI \begin{bmatrix} S_a + \bar{k} & -Q_a & -\bar{k} \\ -Q_a & T_a + T_b & Q_b \\ -\bar{k} & Q_b & S_b + \bar{k} \end{bmatrix} \quad (3\text{-}14)$$

and its determinant after the grouping of terms with the rotational stiffness yields:

$$D_c = S_a(T_b S_b - Q_b^2) + S_b(T_a S_a - Q_a^2) + \bar{k}((T_a + T_b)(S_a + S_b) - (Q_b - Q_a)^2) \quad (3\text{-}15)$$

when performing the process of collecting terms for the expansion of those multiplied by $\bar{k}$ and using the simplification presented in Eq. (3.10) the expression gain an elegant form as follows

$$\begin{aligned} (T_a + T_b)(S_a + S_b) - (Q_b - Q_a)^2 &= T_a S_a - Q_a^2 + T_b S_b - Q_b^2 + T_a S_b + T_b S_a + 2Q_b Q_a \\ &= \frac{\lambda^4(2 - \Delta_a)}{\Delta_a} + \frac{\lambda^4(2 - \Delta_b)}{\Delta_b} + T_a S_b + T_b S_a + 2Q_b Q_a \\ &= \frac{2\lambda^4\big((s_a s_b - c_a c_b)CH_a CH_b + (s_a s_b - c_a c_b)SH_a SH_b}{(1 - CH_a c_a)(1 - CH_b c_b)} \\ &= \frac{2\lambda^4\big(1 + (s_a s_b - c_a c_b)(SH_a SH_b + CH_a CH_b)\big)}{(1 - CH_a c_a)(1 - CH_b c_b)} \end{aligned}$$

Additionally and thanks to the fact that the sum of each segment length is equal to the total length and we can replace the trigonometric terms with the angle sum formulas

$$\cos(L\lambda) = \; c_a c_b - s_a s_b$$
$$\cosh(L\lambda) = \; SH_a SH_b + CH_a CH_b$$

Leading to the well-known characteristic equation for a clamped-clamped beam of length L on the numerator.

$$(T_a + T_b)(S_a + S_b) - (Q_b - Q_a)^2 = \frac{2\lambda^4(1 - \cos(L\lambda)\cosh(L\lambda))}{(1 - CH_a c_a)(1 - CH_b c_b)}$$

The expansion of the sum of terms $S_a(T_b S_b - Q_b^2)$ and $S_b(T_a S_a - Q_a^2)$ unaffected by k in Eq. (3.15) lead us to the expression

$$\frac{\lambda^5(\sin(L\lambda)\, CH_a CH_b + \sinh(L\lambda)\, c_a c_b + s_a CH_a + s_b CH_b \; - c_a SH_a - c_b SH_b)}{(1 - CH_a c_a)(1 - CH_b c_b)}$$

In view of the Eq. (3.6) the determinant for the cracked structure at a natural frequency ω_{0c} for a beam fixed at both ends has the form

$$D_c(x_c, \omega_{0c}) = kD_0(x_c, \omega_{0c}) + D_h(x_c, \omega_{0c}) = 0 \qquad (3\text{-}16)$$

with

$$D_0(x_c, \omega_{0c}) = \frac{2\lambda^4(1 - \cos(L\lambda)\cosh(L\lambda))}{(1 - CH_a c_a)(1 - CH_b c_b)} \qquad (3\text{-}17)$$

and

$$D_h(x_c, \omega_{0c}) = \frac{\lambda^5(\sin(L\lambda)\, CH_a CH_b + \sinh(L\lambda)\, c_a c_b + s_a CH_a + s_b CH_b \; - c_a SH_a - c_b SH_b)}{(1 - CH_a c_a)(1 - CH_b c_b)} \qquad (3\text{-}18)$$

An important remark must be mentioned; the common denominator for the expressions in Equations (3.17) and (3.18) is the product of the characteristic equations of the two fixed beams segments which could be eliminated when multiplying both sides of the determinantal equation by them. The obtained characteristic equation has the same form as those presented by Caddemi and Caliò [18] and Khaji, et al. [66] with a factor equal to 2/λ which comes out after simplification of the λ factors.

$$\overline{D}_c(x_c, \omega_{0c}) = 2k\overline{D}_0(x_c, \omega_{0c}) + \lambda\overline{D}_h(x, \omega_{0c}) = 0 \qquad (3\text{-}19)$$
$$\overline{D}_0(x_c, \omega_{0c}) = 1 - \cos(L\lambda)\cosh(L\lambda) \qquad (3\text{-}20)$$
$$\overline{D}_h(x_c, \omega_{0c}) = \sin(L\lambda)\, CH_a CH_b + \sinh(L\lambda)\, c_a c_b + s_a CH_a + s_b CH_b \; - c_a SH_a - c_b SH_b \qquad (3\text{-}21)$$

3.3.2 Clamped-pinned beam

The 7x7 global matrix Eq. (3.9) for a beam with a crack fixed at the left end and pinned at the right end is reduced to a 4x4 matrix because the clamped end eliminates the columns 1 and 2 relative to the left end displacements, the pinned end eliminates the column 7 relative to the end translational displacement. Additionally there are four

zero actions, rows 3, 4 and 5 for the intermediate actions and row 6 for the right end moment, bringing the matrix;

$$\mathbf{K}_c = EI\begin{bmatrix} S_a+\bar{k} & -Q_a & -\bar{k} & 0 \\ -Q_a & T_a+T_b & Q_b & Qq_b \\ -\bar{k} & Q_b & S_b+\bar{k} & SC_b \\ 0 & Qq_b & SC_b & S_b \end{bmatrix} \tag{3-22}$$

From Eq. (3.6) it may be seen that the terms in the DSM of a cracked structure that give rise to the determinant of the original uncracked structure are the ones that would have $\bar{k}$ as a factor in the expansion of its determinant. Therefore, by collecting the terms from the determinant $\mathbf{K}_c$ in Eq. (3.2) that would be associated with $\bar{k}$ gives the DSM of the original beam $\mathbf{K}_u$ as given in Eq. (3.23)

$$\mathbf{K}_u = EI\begin{bmatrix} S_a+S_b & Q_b-Q_a & SC_b \\ Q_b-Q_a & T_a+T_b & Qq_b \\ SC_b & Qq_b & S_b \end{bmatrix} \tag{3-23}$$

whose expansion can be simplified using Equations (3.10), (3.11) and (3.12) to the form

$$D_0(x_c,\omega_{0c}) = \frac{2\lambda^5\big(\sin(L\lambda)\cosh(L\lambda)-\sinh(L\lambda)\cos(L\lambda)\big)}{(1-CH_ac_a)(1-CH_bc_b)} \tag{3-24}$$

The remaining terms from the determinant of the matrix Eq. (3.22), could be collected in the following way

$$D_h(x_c,\omega_{0c}) = (S_b^2-SC_b^2)S_b(T_bS_b-Q_b^2) - S_a(S_bQq_b^2+T_bSC_b^2-2Q_bSC_bQq_b) + S_aS_b(T_bS_b-Q_b^2)$$

This is simplified with Equations (3.10), (3.11) and (3.12) as

$$D_h(x_c,\omega_{0c}) = Q_b\frac{2\lambda^4(2-\Delta_a)}{\Delta_a} - \frac{2\lambda^4S_aS_b}{\Delta_b} + \frac{\lambda^4S_aS_b(2-\Delta_b)}{\Delta_b} = \lambda^4\left(2Q_b\frac{(2-\Delta_a)}{\Delta_a} - S_aS_b\right)$$

leading to the expression

$$D_h(x_c,\omega_{0c}) = \frac{\lambda^6(\sin(L\lambda)\,CH_aSH_b+\sinh(L\lambda)\,c_as_b+2s_bSH_b-SH_aSH_bc_ac_b-CH_aCH_bs_as_b)}{(1-CH_ac_a)(1-CH_bc_b)} \tag{3-25}$$

The form expressed by Eq. (3.19) after simplification of the λ factors and multiplying both sides by the common denominator $(1-CH_ac_a)(1-CH_bc_b)$. $\overline{D_0}(x_c,\omega_{0c})$ takes the well-known form of the characteristic equation for a clamped-pinned beam

$$\overline{D}_0(x_c,\omega_{0c}) = \sin(L\lambda)\cosh(L\lambda)-\sinh(L\lambda)\cos(L\lambda)$$

and

$$\overline{D}_h(x_c,\omega_{0c}) = \sin(L\lambda)\,CH_aSH_b+\sinh(L\lambda)\,c_as_b+2s_bSH_b-SH_aSH_bc_ac_b-CH_aCH_bs_as_b$$

3.3.3 Pinned-pinned beam

The 7x7 global matrix Eq. (3.9) for a beam with a crack pinned at the ends is reduced to a 5x5 matrix after eliminating columns 1 and 7 relative to the transversal

displacements. The actions from rows 1 and 7 are not considered in the final matrix (3.26)

$$\mathbf{K}_c = EI\begin{bmatrix} S_a & SC_a & -Qq_a & 0 & 0 \\ SC_a & S_a+\bar{k} & -Q_a & -\bar{k} & 0 \\ -Qq_a & -Q_a & T_a+T_b & Q_b & Qq_b \\ 0 & -\bar{k} & Q_b & S_b+\bar{k} & SC_b \\ 0 & 0 & Qq_b & SC_b & S_b \end{bmatrix} \tag{3-26}$$

The terms multiplied by $\bar{k}$ in the resultant determinant are obtained from the determinant of the matrix in (3.27) when the intermediate rotations are treated as only one degree of freedom

$$\mathbf{K}_u = EI\begin{bmatrix} S_a & SC_a & -Qq_a & 0 \\ SC_a & S_a+S_b & -Q_a+Q_b & SC_b \\ -Qq_a & -Q_a+Q_b & T_a+T_b & Qq_b \\ 0 & SC_b & Qq_b & S_b \end{bmatrix} \tag{3-27}$$

and could be simplified as

$$D_0(x_c,\omega_{0c}) = \frac{4\lambda^6\big(\sin(L\lambda)\sinh(L\lambda)\big)}{(1-CH_ac_a)(1-CH_bc_b)} \tag{3-28}$$

the remaining terms in the determinant of (3.26) are accommodated as

$$\left.\begin{aligned} &+(S_b^2-SC_b^2)\big\{S_a\big(T_aS_a-Q_a^2\big)-\big(S_aQq_a^2+T_aSC_a^2-2Q_aSC_aQq_a\big)\big\}\big) \\ &+(S_a^2-SC_a^2)\big\{S_b\big(T_bS_b-Q_b^2\big)-\big(S_bQq_b^2+T_bSC_b^2-2Q_bSC_bQq_b\big)\big\}\big) \end{aligned}\right\}$$

and simplified from the expressions given in Equations (3.10) to (3.13) to reach the final form gives in Eq. (3.29)

$$2Q_b\left\{S_a\frac{\lambda^4(2-\Delta_a)}{\Delta_a}-\frac{2\lambda^4S_a}{\Delta_a}\right\}+2Q_a\left\{S_b\frac{\lambda^4(2-\Delta_b)}{\Delta_b}-\frac{2\lambda^4S_b}{\Delta_b}\right\}=-2\lambda^4(Q_bS_a+Q_aS_b)$$

$$D_h(x_c,\omega_{0c}) = \frac{2\lambda^7(\sin(L\lambda)\,SH_aSH_b-\sinh(L\lambda)\,s_as_b)}{(1-CH_ac_a)(1-CH_bc_b)} \tag{3-29}$$

The form expressed by Eq. (3.19) is obtained from Eq. (3.6) after simplification of the λ factors and multiplying both sides by the common denominator $(1-CH_ac_a)(1-CH_bc_b)$. $\overline{D_0}(x_c,\omega_{0c})$ takes the well-known form of the characteristic equation for a simply supported beam

$$\bar{D}_0(x_c,\omega_{0c}) = \sin(L\lambda)\sinh(L\lambda)$$

$$\bar{D}_h(x_c,\omega_{0c}) = \sin(L\lambda)\,SH_aSH_b-\sinh(L\lambda)\,s_as_b$$

3.3.4 Clamped-free beam

The 7x7 global matrix Eq. (3.9) for a cantilever beam with a crack is reduced to a 5x5 matrix after eliminating the columns 1 and 2 relative to the restricted displacements at the left by the clamp. The actions from rows 1 and 2 are not considered in the final matrix

$$\mathbf{K}_c = EI\begin{bmatrix} S_a+\bar{k} & -Q_a & -\bar{k} & 0 & 0 \\ -Q_a & T_a+T_b & Q_b & Qq_b & -Tt_b \\ -\bar{k} & Q_b & S_b+\bar{k} & SC_b & -Qq_b \\ 0 & Qq_b & SC_b & S_b & -Q_b \\ 0 & -Tt_b & -Qq_b & -Q_b & T_b \end{bmatrix} \tag{3-30}$$

The terms multiplied by $\bar{k}$ in the resultant determinant are obtained from the determinant of the matrix in (3.30) when the intermediate rotations, those on the main diagonal affected by k, are treated as the same degree of freedom

$$\mathbf{K}_u = EI\begin{bmatrix} S_a+S_b & -Q_a+Q_b & SC_b & -Qq_b \\ -Q_a+Q_b & T_a+T_b & Qq_b & -Tt_b \\ SC_b & Qq_b & S_b & -Q_b \\ -Qq_b & -Tt_b & -Q_b & T_b \end{bmatrix} \tag{3-31}$$

and could be simplified as

$$D_0(x_c,\omega_{0c}) = \frac{2\lambda^4(1+\cos(L\lambda)\cosh(L\lambda))}{(1-CH_ac_a)(1-CH_bc_b)} \tag{3-32}$$

The remaining terms in the determinant of (3.30) are accommodated as

$$(S_a+S_b)(T_bS_b-Q_b^2)-(S_bQq_b^2+T_bSC_b^2-2Q_bSC_bQq_b)$$

and simplified from the expressions given in Equations (3.10) to (3.13) to reach the final form in Eq. (3.33)

$$S_a\frac{\lambda^4(2-\Delta_b)}{\Delta_b}+S_b\frac{\lambda^4(2-\Delta_b)}{\Delta_b}-\frac{2\lambda^4S_b}{\Delta_b}$$

$$D_h(x_c,\omega_{0c}) = \frac{\lambda^5(\sinh(L\lambda)\,c_ac_b-\sin(L\lambda)\,CH_aCH_b+CH_as_a+SH_bc_b-SH_ac_a-CH_bs_b)}{(1-CH_ac_a)(1-CH_bc_b)} \tag{3-33}$$

The form expressed by Eq. (3.19) is obtained from Eq. (3.6) after simplification of the λ factors and multiplying both sides by the common denominator $(1-CH_ac_a)(1-CH_bc_b)$. $\overline{D_0}(x_c,\omega_{0c})$ takes the well-known form of the characteristic equation for a cantilever beam

$$\bar{D}_0(x_c,\omega_{0c}) = 1+\cos(L\lambda)\cosh(L\lambda)$$

$$\bar{D}_h(x_c,\omega_{0c}) = \sinh(L\lambda)\,c_ac_b-\sin(L\lambda)\,CH_aCH_b+CH_as_a+SH_bc_b-SH_ac_a-CH_bs_b$$

The results for the cantilever beam could be compared with previous work based on the DSM, for example the papers by Banerjee and Guo [53] and Labib, et al. [67].

The procedure to find the natural frequencies of $\overline{D_c}(x_c,\omega_{0c})$ uses a Matlab® zero finding function on intervals where there is a sign change, with the interval size set to 0.001rad/s and the zero finding function tolerance set to $1\text{x}10^{-16}$. Natural frequency results from Labib, et al. [67] are presented in Table 3.2 next to those obtained using Eq. (3.18) for a beam of 200mm length with rectangular cross sectional area of 25mmx7.8mm, flexural rigidity 213.548 Nm^2 and linear density 1.5308 kgm^{-1} showing that the present method does compare well with these earlier approaches in both the

intact case and the damaged scenarios. It is important to mention that Eq. (3.19) does not have frequency dependent denominator and therefore there is no need to use the Wittrick-Williams algorithm [68]; the differences on the second frequency values could be related to the use of a very small tolerance in the Matlab® zero finding function.

Table 3.2. Natural frequencies of a cantilever cracked beam. L&K values from Labib, et al.

Crack location	Spring stiffness	Natural frequency, (rad/s)					
		First frequency		Second frequency		Third frequency	
(La/L)	k	Present	L&K	Present	L&K	Present	L&K
0.4	130	1034.6	1034.6	6469.76	6469.6	18152.32	18152
	28.8	1022.2	1022.2	6348.91	6348.9	17942.52	17942
	8.39	985.98	985.98	6035.94	6036.0	17446.88	17447
0.6	130	1037.31	1037.3	6457.02	6456.8	18137.10	18137
	28.8	1034.16	134.2	6292.26	6292.3	17879.45	17879
	8.39	1024.43	1024.4	5851.88	5852.0	17276.14	17276
Intact Beam		1038.21	1038.2	6506.37	6506.3	18218.04	18218

3.4 The behaviour of the determinantal functions

The obtained results from the previous section are compiled in the next table following the form of the equation (3.19),

Table 3.3. Closed form for cracked beams with common boundary conditions

Equivalent expression	
Clamped-clamped	
$\overline{D_0}(x_c, \omega_{0c})$	$1 - \cos(L\lambda)\cosh(L\lambda)$
$\overline{D_h}(x_c, \omega_{0c})$	$\sin(L\lambda)\, CH_a CH_b + \sinh(L\lambda)\, c_a c_b + s_a CH_a + s_b CH_b - c_a SH_a - c_b SH_b$
Clamped-pinned	
$\overline{D_0}(x_c, \omega_{0c})$	$\sin(L\lambda)\cosh(L\lambda) - sinh(L\lambda)cos(L\lambda)$
$\overline{D_h}(x_c, \omega_{0c})$	$\sin(L\lambda)\, CH_a SH_b + \sinh(L\lambda)\, c_a s_b + 2 s_b SH_b - SH_a SH_b c_a c_b - CH_a CH_b s_a s_b$
Pinned-pinned	
$\overline{D_0}(x_c, \omega_{0c})$	$\sin(L\lambda)\sinh(L\lambda)$
$\overline{D_h}(x_c, \omega_{0c})$	$\sin(L\lambda)\, SH_a SH_b - \sinh(L\lambda)\, s_a s_b$
Clamped-free	
$\overline{D_0}(x_c, \omega_{0c})$	$1 + \cos(L\lambda)\cosh(L\lambda)$
$\overline{D_h}(x_c, \omega_{0c})$	$\sinh(L\lambda)\, c_a c_b - \sin(L\lambda)\, CH_a CH_b + CH_a s_a + SH_b c_b - SH_a c_a - CH_b s_b$

and perfect agreement is found when comparing the obtained results with the closed-form solutions given by Khaji, et al. [66].

3.4.1 Frequency shift with location

As was stated in Section 3.3, for a very high value of stiffness, the term $2k\bar{D}_0(x_c, \omega_{0c})$ in Eq. (3.18) appears to be the dominant one, leading to the simplification $\bar{D}_0(x_c, \omega_{0c}) = 0$, which is actually the characteristic equation for a beam of length L. When the spring stiffness decrease, the influence of the term $\lambda\bar{D}_h(x_c, \omega_{0c})$ whose value depends of the crack position needs to be considered. To determine how important this effect is, an analysis of the values of the determinantal function $\bar{D}_h(x_c, \omega_{0c})$ will be performed below, starting from those at the natural frequencies of the un-cracked beam in different hinge positions. A plot of the obtained values for the function $\bar{D}_h(x_c, \omega_{0c})$ for constant ω_{0c}, for the first three eigenvalues for various hinge positions are given in Figure 3.3 to Figure 3.6.

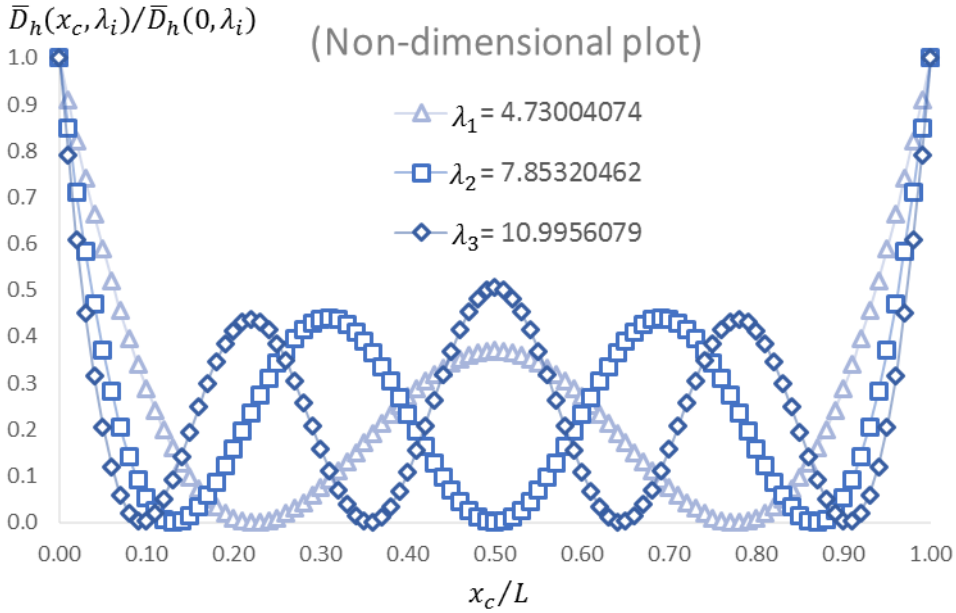

Figure 3.3. Non-dimensional plot of the function $\bar{D}_h$ evaluated at different locations for constant eigenvalues. Clamped-clamped beam case.

These plots could be interpreted as the effect of the discontinuity at the particular location. This effect is called the normalised frequency change in Labib, et al. [69] and to find it, it is necessary to use an approximate method known as delta method. In the present work it is only necessary to evaluate the determinantal function $\bar{D}_h(x_c, \omega_{0c})$ for the modal frequency values of the undamaged beam in each location.

The plot in Fig.3.3 indicates that the maximum effect of the crack will occur at the fixed ends. It was found numerically that when a severe crack is located very close to a clamped end the resulting eigenvalue is almost equal to the one for a pinned end. An indication of symmetry is observed when identical values are obtained for cracks located at the same distance on either side of the centre of the beam.

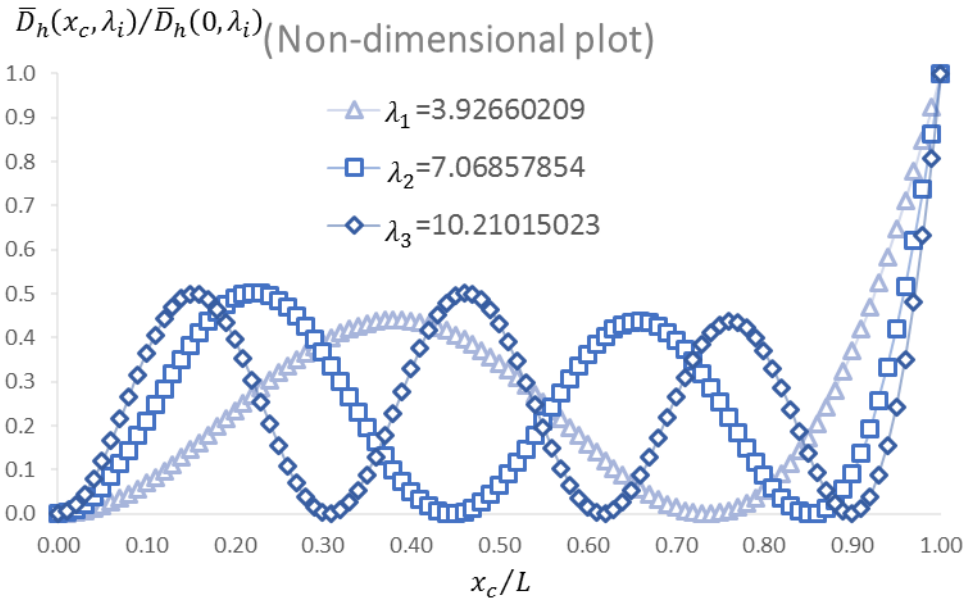

Figure 3.4. Non-dimensional plot of the function $\bar{D}_h$ evaluated at different locations for constant eigenvalues. Pinned-clamped beam case.

The plot in Fig.3.4 indicates that the symmetry is broken because of the un-symmetric boundary conditions. Additionally, the pinned end was always found to be insensitive implying that the value of the determinantal function is dependent onf the bending moment.

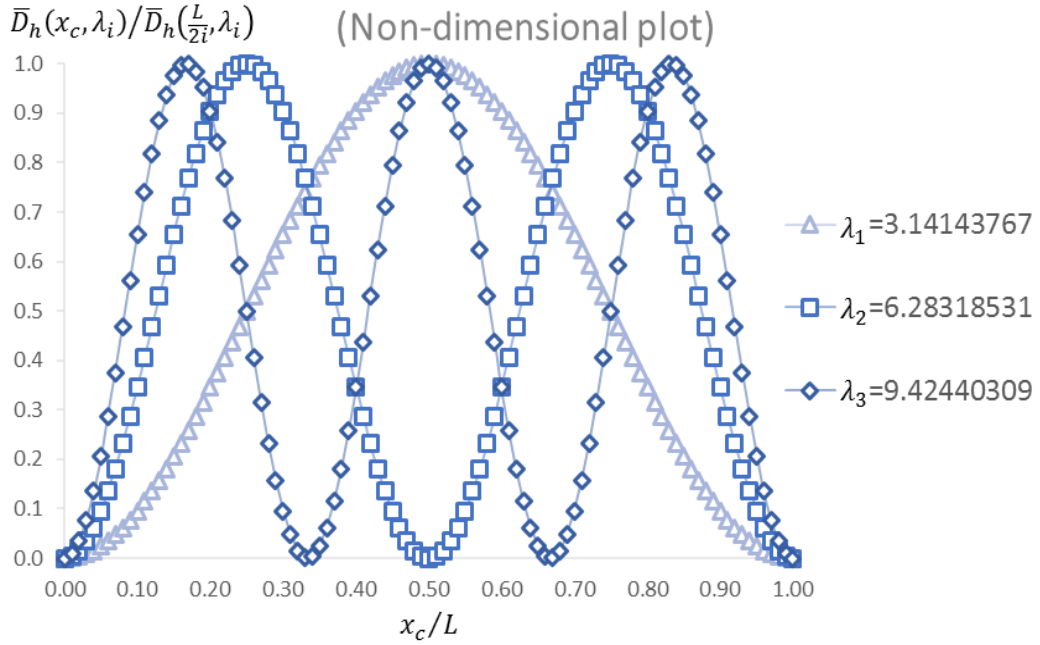

Figure 3.5. Non-dimensional plot of the function $\bar{D}_h$ evaluated at different locations for constant eigenvalues. Pinned-pinned beam case.

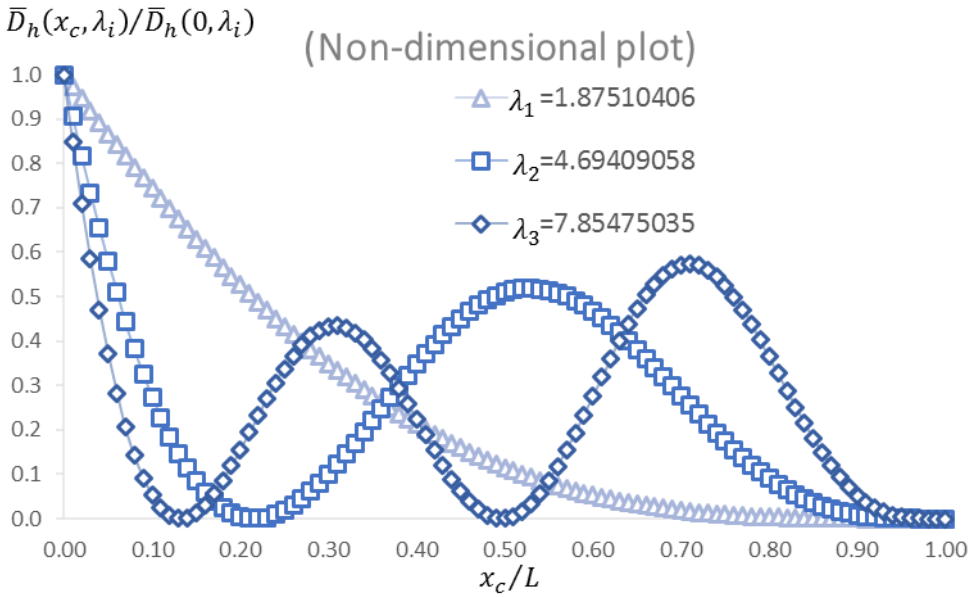

Figure 3.6. Non-dimensional plot of the function $\bar{D}_h$ evaluated at different locations for constant eigenvalues. Clamped-free beam case.

The plot in Fig.3.6 indicates that the maximum effect of the crack will occur at the fixed end and that the free end always will be insensitive giving strengthening the previous observation that the determinantal function may be related to the bending moment.

All the features mentioned for each plot for the determinant of the hinged structure are also found in the literature [65] for the normalised changes in frequency for a cracked beam with different severity. Therefore, bearing in mind that the determinant of the hinged structure is independent of the stiffness value for the spring modelling the crack, there is a possible implications that the relative frequency shift variations are dominated by the crack location rather than its severity.

3.4.2 Frequency shift with severity

There is a flaw on the crack literature mentioned by Dimarogonas [49] and implied by Labib, et al. [67] regarding the lack of accuracy in the derivation of the flexibility generated by a thickness reduction when the non-dimensional crack depth (d/h) is higher than 70% where the linearity of the stiffness model is lost. Eq. (3.6) however holds for any stiffness value, and it was decided to investigate the behaviour of the determinant for a wide range of stiffness using the present approach.

A numerical test in a non-dimensional stiffness range of 10^6 at the high end and 10 at the low end that cover crack-depth ratios (d/h) between 0% to 90% with a Matlab© code was developed to tabulate, for different values of stiffness and positions, the eigenvalue that made the determinant in Eq. (3.6) vanish. The data showed values of $\overline{D}_0(\omega_{0c})$ lower than one while the values for the function $\overline{D}_h(x_c, \omega_{0c})$ are moving in the order of hundreds for the first mode in the beam fixed in both ends.

These data are plotted as the ratio of the functions $\overline{D}_h(x_c, \omega_{0c})/\overline{D}_h(0, \omega_{0c})$ and shown in Figure 3.7 where ω_{0c} is the natural frequency when the crack is located at x_c found using the same procedure as the one for Table 3.2. The proximity between the results with (d/h) values lower than 73% shows that approximate methods based on the linearity between frequency and stiffness could be effective but now with an exact linear relationship in Eq. (3.6) which is valid for the whole range of crack depth, the approximate method is no longer needed.

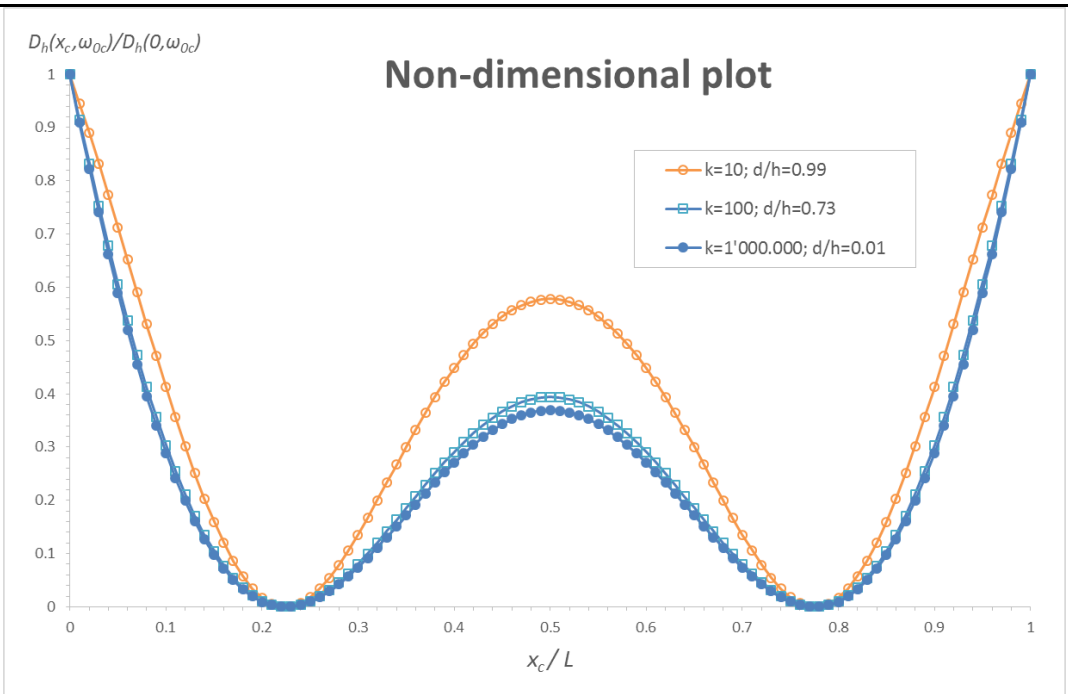

Figure 3.7. Functions ratio evaluated at eigenvalues. k=10:10^6.

For each vibration mode there are points where the eigenvalue is unchanged whether or not a rotational spring is located in them, this property generates insensitivity to damage for these locations in the specific mode, in Figure 3.7. Intuitively it may be said that the points at which the ratio is zero are not sensitive to the stiffness value. These are the locations at the natural frequency that makes the function $D_h(x,\omega)$ equals to zero.

These values are called points of contra-flexure and are located on the abscissa where at each mode the moment is zero. Khiem and Lien [65] refer to these as critical points at which cracks are unnoticed, and present their values for two boundary conditions. Taking a close look at Khiem and Lien [65] values it is noticed that the symmetry seen in Figs. 3.3 and 3.5 is not present; one reason for this is because the derivation of these points were made from a model of crack that cannot be accurate to higher flexibility values and therefore they have been updated in the present work and listed in Table 3.4.

Table 3.4. Contraflexion points location. K&L values from Khiem and Lien.

Boundary condition type	1st frequency		2nd frequency		3rd frequency	
	K&L	Present	K&L	Present	K&L	Present
Pinned-pinned	-	-	0.4	0.5	0.26672	0.257
					0.53328	0.5
Clamped-clamped	0.17928	0.225	0.10608	0.127	0.07632	0.0763
			0.4	0.5	0.28544	0.2854
	0.62072	0.775			0.51456	0.5146
			0.69392	0.675	0.72368	0.7237

3.5 Frequency shifts and squared moment an interesting moment-determinant relationship

Morassi [27] states that the effect of a crack on a frequency is proportional to the potential energy density of the corresponding undamaged mode shape evaluated at the cracked section implying that frequency sensitivity to damage position depends on the square of the curvature of the undamaged mode shape. The same principle was applied by Gillich and Praisach [35] finding a correlation between normalised frequency shifts and the normalised squared moment when using the expression for the strain energy stored in the elastic structure, dependent of the second derivative of the mode shape.

Gillich and Praisach [35] pointed out that for certain vibration modes the shift in the natural frequency depends on the position of the crack influenced by the mode shape. Additionally, they mention the existence of points of contra-flexure for each vibration mode as those where the energy is zero and therefore no frequency shift if the crack is located there.

A physical explanation could be obtained by considering the bending moment and the fact that a rotational spring produces an angular displacement when a moment is applied between its ends, so if there is no moment, the spring, even with a high flexibility remains inactive. A mathematical verification will be presented in the next paragraphs that stands for any structure which could be modelled by means of a frequency dependent dynamic stiffness matrix.

Without loss of generality, for illustrative purposes we consider the portal frame structure with a crack at the point $\mathbf{p} = (x_1, x_2)$ located within its length splitting the

structure in two parts. Let the internal bending moment at the crack position be *M* and *-M*.

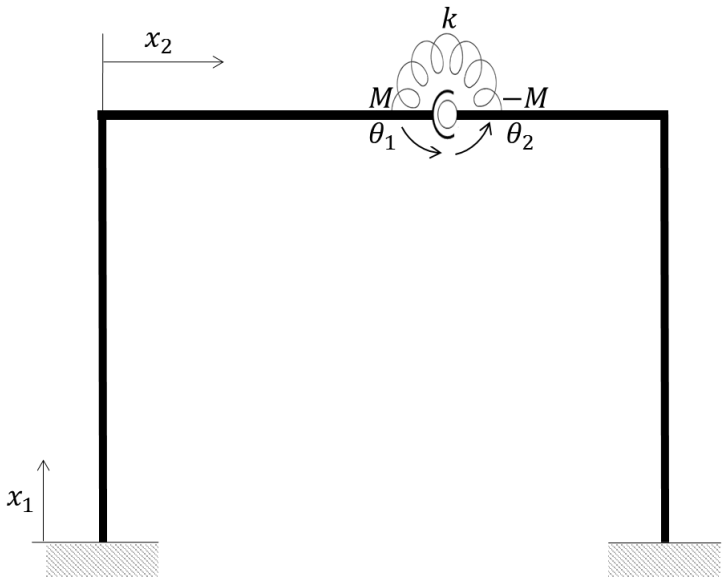

Figure 3.8. Cracked frame and internal moments

By Newton's third law, these actions will be equal and opposite as the crack effect represented by a rotational spring does not introduce a discontinuity in moment. Now separate the rotational spring from the structure resulting a combination of a hinged structure and the spring. Let the rotations of the structure at the two sides of crack location be $\theta_1$and θ_2. The internal moments will now act as external to the hinged structure. Then for the split structure the following DSM equation can be derived:

$$\begin{bmatrix} M \\ -M \end{bmatrix} = \begin{bmatrix} K_1 & K_2 \\ K_2 & K_3 \end{bmatrix} \begin{bmatrix} \theta_1 \\ \theta_2 \end{bmatrix} \tag{3-34}$$

where each K_i submatrix of dimension 1x1 could be obtained from the structural stiffness matrix through condensation, leading us to define the internal moments as

$$\begin{aligned} M &= K_1\theta_1 + K_2\theta_2 = 0 \\ -M &= K_2\theta_1 + K_3\theta_2 = 0 \end{aligned} \tag{3-35}$$

In the special case when there is no spring in the structure, $M = 0$ and Eqns. (3.35) lead to the determinantal equation for the hinged frame in the form,

$$D_h(\mathbf{p}, \omega) = K_1K_3 - K_2K_2 \tag{3-36}$$

On the other hand, when using the rotational spring model for a crack, $M = k(\theta_2 - \theta_1)$

$$\theta_2 = M/k + \theta_1 \tag{3-37}$$

allowing us through substituting Eq. (3.37) into Eqns. (3.35) to obtain the respective expressions

$$\frac{M}{\theta_1} = k\frac{K_1 + K_2}{k - K_2}$$
$$-\frac{M}{\theta_1} = k\frac{K_2 + K_3}{k + K_3} \quad (3\text{-}38)$$

Then using Eqns. (3.38) gives the determinantal equation for the cracked structure through $\frac{M}{\theta_1} - \frac{M}{\theta_1} = 0$

$$D_C(\mathbf{p}, \omega, k) = (K_1 + K_2)(k + K_3) + (K_2 + K_3)(k - K_2) = 0 \quad (3\text{-}39)$$

For the intact structure, the continuity in the slope must stand

$$\theta_2 = \theta_1 = \theta \quad (3\text{-}40)$$

Substituting Eqn. (3.40) into Eqns. (3.35) the moment over rotation ratio gives

$$\frac{M}{\theta} = (K_1 + K_2) = -(K_2 + K_3) \quad (3\text{-}41)$$

This leads us to the determinantal equation for the intact structure by subtracting one from the other

$$D_0(\mathbf{p}, \omega) = K_1 + 2K_2 + K_3 = 0 \quad (3\text{-}42)$$

From this, we have the determinant for the intact structure in terms of the frequency ω and the location of the potential crack **p**. Eqns. (3.36), (3.39) and (3.42) can be combined to state Eq. (3.6)

$$D_C(\mathbf{p}, \omega, k) = kD_0(\mathbf{p}, \omega) + D_h(\mathbf{p}, \omega) \quad (3\text{-}43)$$

Also, multiplying Eqns. (3.41) gives:

$$\left(\frac{M}{\theta}\right)^2 = -(K_1 + K_2)(K_2 + K_3) \quad (3\text{-}44)$$

whose expansion could be seen as

$$\left(\frac{M}{\theta}\right)^2 = -K_2(K_1 + 2K_2 + K_3) - K_1K_3 + K_2K_2 \quad (3\text{-}45)$$

Using Eqns. (3.36) and (3.42) in the Eq. (3.45),

$$\left(\frac{M}{\theta}\right)^2 = -K_2D_O(\mathbf{p}, \omega) - D_h(\mathbf{p}, \omega) \quad (3\text{-}46)$$

that at a natural mode of the intact structure, $D_o(\mathbf{p}, \omega) = 0$, leading us to the expression

$$\left(\frac{M^*}{\theta}\right)^2 = -D_h(\mathbf{p}, \omega) \quad (3\text{-}47)$$

where M^* is the bending moment in the uncracked structure at one of its natural modes. Equation (3.47) indicates the dependence of the value of the determinant of the hinged structure with the bending moment of the undamaged structure and more precisely, dependent on the square moment which is related with the curvature of the undamaged mode shape giving support to the observations by Caddemi and Morassi [70] and

Gillich, et al. [71]. Particular attention will be addressed to points where the bending moment is null at each natural mode, because at those points the determinant of the hinged structure is zero. Recalling Eq. (3.6), $D_C(\mathbf{p}, \omega, k)$ will be zero at the natural frequency irrespective of the values of k when the crack is at the point of contra-flexure. The last demonstration explains the insensitivity to cracks at the points where the moment is zero, contra-flexure point, for each particular mode.

3.6 Numerical validation for framework

Greco and Pau [72] presented the crack effect in Euler frames comparing the natural frequencies in free vibration by means of its dynamic stiffness matrices with and without a notch within the length of a one-storey frame depicted in Fig. 3.9.

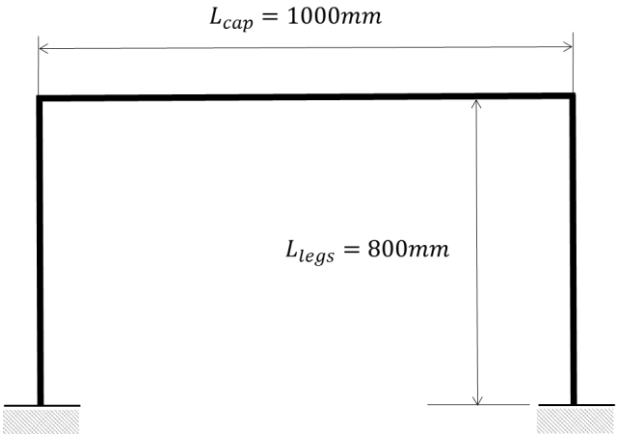

Figure 3.9. Greco and Pau frame

The frame is made of steel E=200GN/m^2 and ρ=7849kg/m^3 legs and cap lengths of 0.8m and 1.0m respectively and rectangular sectional area of 40x8mm^2.

3.6.1 Frequency variations due to cracks

The circular natural frequencies of the intact structure ω_{i0} are in the labels of Figures 3.10 to 3.12. Each figure depicts the frequency values when a crack modelled as a rotational spring of non-dimensional stiffness 100 is located along the frame. When the crack "travels" along the components of the frame, the first three natural frequencies take the values reported on the vertical axes of each figure. The sudden change in the plot occurs at the beam-column intersection, the domains labelled leg and cap refer to column and beam respectively.

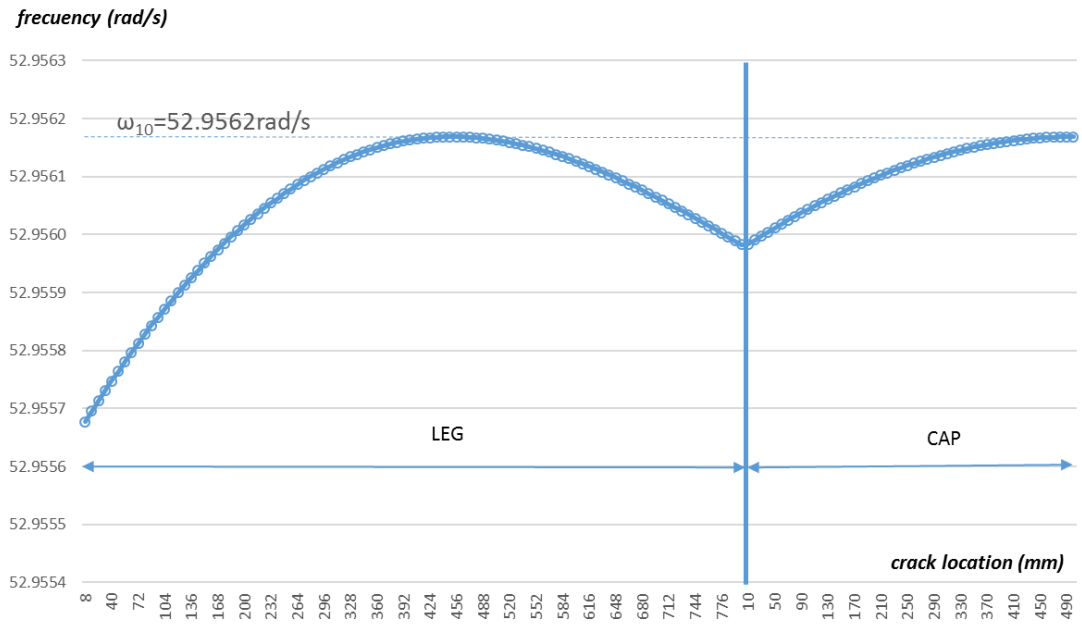

Figure 3.10. Greco and Pau frame, first frequency shift with crack location.

The shift in the first frequency, when the crack is located near the fixed end, is the highest on the frame in agreement with what was observed in Figs. 3.3 to 3.6; it is observed as well that there is no evidence of a crack at the midpoint of the cap, a well-known point of contra-flexure for the asymmetric mode. Also, there must be another point of contra-flexure somewhere in the leg near the coordinate 480mm from the fixed end as can be seen from Fig. 3.10.

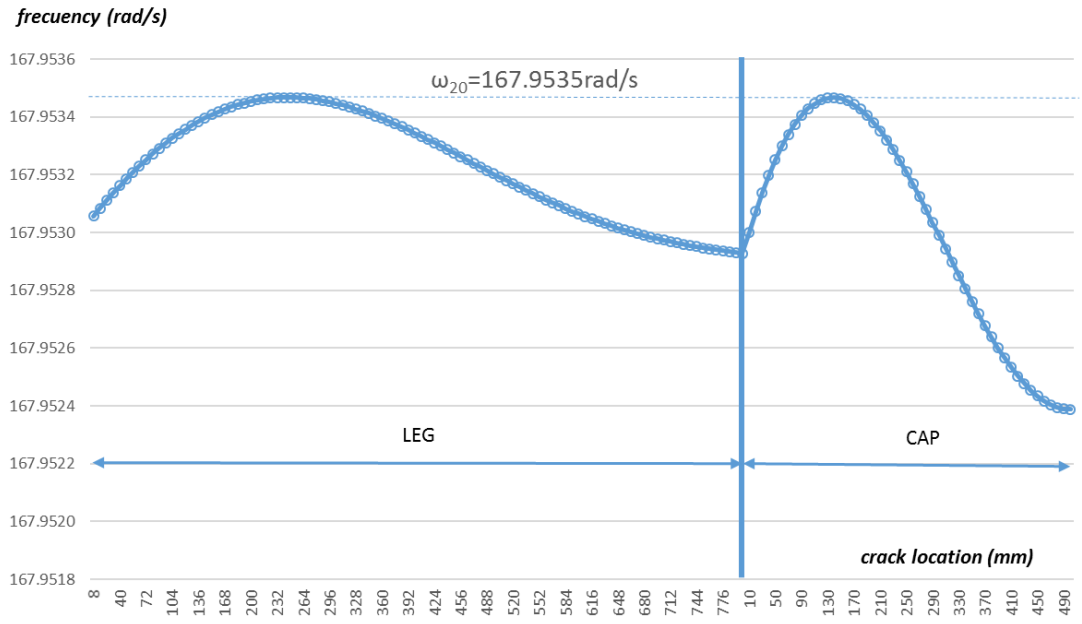

Figure 3.11. Greco and Pau frame, second frequency shift with crack location.

For the second frequency a high value of the frequency shift is noted at the leg-cap joint relative to the frequency shift of the fixed end indicating higher rotations on these points in the intact case that cannot be equalised because of the reduction in stiffness; the reason is the same for the midpoint in the cap but in this case the well-known curvature for a symmetric mode is such that the reduction in frequency is the higher but for this case is only 0.001 rad/s.

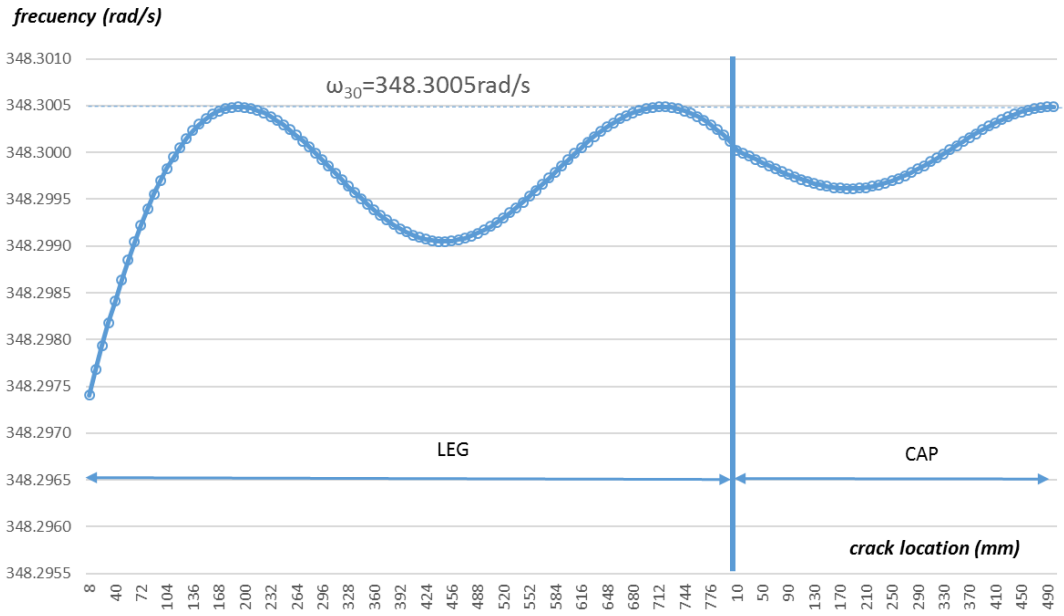

Figure 3.12. Greco and Pau frame, third frequency shift with crack location.

Figures 3.10 to 3.12 offer more evidence that the frequency shift is highly related to the mode shape of the intact structure, more specifically on its curvature, based on the fact that the points with high curvature are those with the higher frequency shift and those where the crack is ineffective turns out to be points of contra-flexure for the particular mode shape.

3.6.2 Determinantal equation from DSM

Initially we will present the validation of Equation (3.6) for the frequency values that produce $D_C(\mathbf{p}, \omega, k) = 0$, for a constant value of the spring stiffness in different assumed positions of damage, obtained when calculating the ratio

$$k = -\frac{D_h(\mathbf{p}, \omega)}{D_0(\mathbf{p}, \omega)} \tag{3-48}$$

The overall DSM for calculating each determinant is located right before to the graphical sketch of the structure (Figures 3.13-3.15) with the numbers indicating the degree of freedom and the labels for the different beams elements correspond to the

lengths of the frame components and the DSM elements collected in Table 3.1 as follow

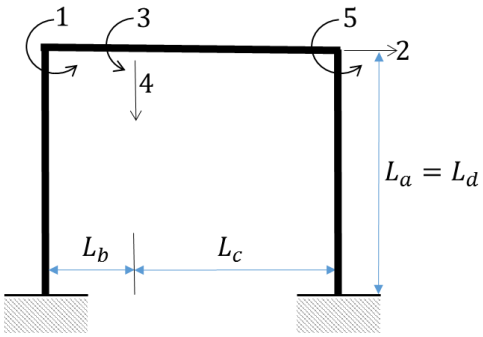

Figure 3.13. Intact frame model and DSM to calculate $D_0(\omega)$.

The second degree of freedom refers to the lateral displacement of the legs that is affected by the mass of the cap m_{cap} by $m = \frac{\omega^2}{EI} m_{cap}$.

$$\mathbf{K}_0\mathbf{d} = EI \begin{bmatrix} S_a + S_b & -Q_a & SC_b & -Qq_b & 0 \\ -Q_a & T_a + T_d - m & 0 & 0 & -Q_d \\ SC_b & 0 & S_b + S_c & Q_c - Q_b & SC_c \\ -Qq_b & 0 & Q_c - Q_b & T_b + T_c & Qq_c \\ 0 & -Q_d & SC_c & Qq_c & S_c + S_d \end{bmatrix} \begin{bmatrix} \theta_1 \\ \delta_2 \\ \theta_3 \\ \delta_4 \\ \theta_5 \end{bmatrix}$$

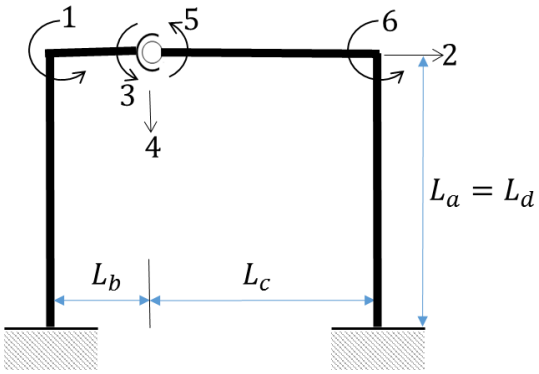

Figure 3.14. Hinged frame model and DSM to calculate $D_h(\mathbf{p}, \omega)$.

$$\mathbf{K}_h\mathbf{d} = EI \begin{bmatrix} S_a + S_b & -Q_a & SC_b & -Qq_b & 0 & 0 \\ -Q_a & T_a + T_d - m & 0 & 0 & 0 & -Q_d \\ SC_b & 0 & S_b & -Q_b & 0 & 0 \\ -Qq_b & 0 & -Q_b & T_b + T_c & Q_c & Qq_c \\ 0 & 0 & 0 & Q_c & S_c & SC_c \\ 0 & -Q_d & 0 & Qq_c & SC_c & S_c + S_d \end{bmatrix} \begin{bmatrix} \theta_1 \\ \delta_2 \\ \theta_3 \\ \delta_4 \\ \theta_5 \\ \theta_6 \end{bmatrix}$$

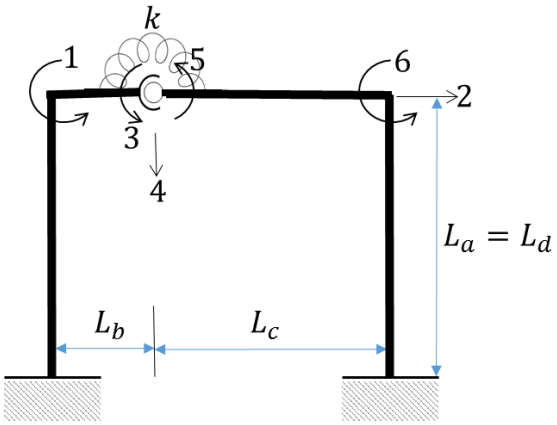

Figure 3.15. Cracked frame model and DSM to calculate $D_c(\mathbf{p},\omega)$.

$$\mathbf{K}_c\mathbf{d} = EI\begin{bmatrix} S_a+S_b & -Q_a & SC_b & -Qq_b & 0 & 0 \\ -Q_a & T_a+T_d-m & 0 & 0 & 0 & -Q_d \\ SC_b & 0 & S_b+\bar{k} & -Q_b & -\bar{k} & 0 \\ -Qq_b & 0 & -Q_b & T_b+T_c & Q_c & Qq_c \\ 0 & 0 & -\bar{k} & Q_c & S_c+\bar{k} & SC_c \\ 0 & -Q_d & 0 & Qq_c & SC_c & S_c+S_d \end{bmatrix}\begin{bmatrix} \theta_1 \\ \delta_2 \\ \theta_3 \\ \delta_4 \\ \theta_5 \\ \theta_6 \end{bmatrix}$$

The DSM for the hinged and cracked portal have the same DSM only that for the hinged frame $k = 0$.

Tables 3.5 and 3.6 show the values for the two first frequency values that nullify $D_c(\mathbf{p},\omega)$ for the cracked frame and the corresponding determinantal values of $D_0(\mathbf{p},\omega)$ and $D_h(\mathbf{p},\omega)$ for that particular frequency when the crack and hinge are located in different positions along the leg and cap demonstrating perfect agreement with Eq. (3.45) even for very low values of stiffness.

Table 3.5. Frequency and determinant values versus location. $k = 100$

Location		k =100		
(mm)		Frequency	Do	Dh
Legs	80	52.9558	1.303E-23	-1.303E-21
	160	52.9560	7.814E-25	-7.814E-23
	240	52.9561	1.339E-25	-1.339E-23
	320	52.9561	2.903E-26	-2.903E-24
	400	52.9562	3.558E-27	-3.558E-25
	480	52.9562	1.233E-27	-1.233E-25
	560	52.9561	2.742E-26	-2.742E-24
	640	52.9561	2.145E-25	-2.145E-23
	720	52.9560	3.328E-24	-3.328E-22
	800	52.9560	4.917E-20	-4.917E-18
Cap	100	52.9560	1.872E-24	-1.872E-22
	200	52.9561	1.056E-25	-1.056E-23
	300	52.9561	1.588E-26	-1.588E-24
	400	52.9562	2.336E-27	-2.336E-25
	500	52.9562	1.989E-29	-1.989E-27

Location		k =100		
(mm)		Frequency	Do	Dh
Legs	80	167.9533	-3.079E-23	3.079E-21
	160	167.9534	-7.407E-25	7.407E-23
	240	167.9535	-8.062E-28	8.062E-26
	320	167.9534	-8.963E-26	8.963E-24
	400	167.9533	-2.804E-25	2.804E-23
	480	167.9532	-6.354E-25	6.354E-23
	560	167.9531	-1.577E-24	1.577E-22
	640	167.9530	-5.693E-24	5.693E-22
	720	167.9530	-5.633E-23	5.633E-21
	800	167.9529	-6.259E-19	6.259E-17
Cap	100	167.9534	-2.071E-24	2.071E-22
	200	167.9534	-3.933E-25	3.933E-23
	300	167.9530	-6.672E-25	6.672E-23
	400	167.9526	-7.017E-25	7.017E-23
	500	167.9524	-7.025E-25	7.025E-23

In the case of $k = 100$, a small reduction in the frequency values is noticed while the determinantal values although very small, in terms of percentage present a high variability i.e. the smallest change is nearly 90% in the reported data for the first frequency.

Table 3.6. Frequency and determinant values versus location. $k = 0.01$

Location		k =0.01		
(mm)		Frequency	Do	Dh
Legs	80	50.3388	9.836E-20	-9.836E-22
	160	51.2808	6.278E-21	-6.278E-23
	240	52.0522	1.135E-21	-1.135E-23
	320	52.6047	2.566E-22	-2.566E-24
	400	52.9034	3.234E-23	-3.234E-25
	480	52.9401	1.134E-23	-1.134E-25
	560	52.7413	2.514E-22	-2.514E-24
	640	52.3631	1.933E-21	-1.933E-23
	720	51.8767	2.923E-20	-2.923E-22
	800	51.3526	4.184E-16	-4.184E-18
Cap	100	51.8546	1.636E-20	-1.636E-22
	200	52.3105	9.512E-22	-9.512E-24
	300	52.6586	1.468E-22	-1.468E-24
	400	52.8799	2.197E-23	-2.197E-25
	500	52.9554	1.883E-25	-1.883E-27

Location		k =0.01		
(mm)		Frequency	Do	Dh
Legs	80	166.4911	-2.236E-19	2.236E-21
	160	167.5584	-5.831E-21	5.831E-23
	240	167.9520	-6.854E-24	6.854E-26
	320	167.6578	-8.048E-22	8.048E-24
	400	166.8043	-2.561E-21	2.561E-23
	480	165.7119	-5.675E-21	5.675E-23
	560	164.7399	-1.342E-20	1.342E-22
	640	164.0826	-4.582E-20	4.582E-22
	720	163.7159	-4.334E-19	4.334E-21
	800	163.4638	-4.712E-15	4.712E-17
Cap	100	167.6065	-1.818E-20	1.818E-22
	200	167.1656	-3.533E-21	3.533E-23
	300	163.6550	-5.633E-21	5.633E-23
	400	160.0598	-5.491E-21	5.491E-23
	500	158.6349	-5.324E-21	5.324E-23

In the case of $k = 0.01$, the frequency values are bigger as is expected due to such a small stiffness but the most remarkable feature is appreciated when checking the variability of the determinantal values in terms of percentage. As is shown in Table 3.7

there have very similar values for the same positions even for changes in the stiffness that cover almost the whole range of crack lengths.

Table 3.7. Percentage determinant variations with different spring stiffness

Location (mm)		*k=100*	*k=0.01*
Legs	80	-	-
	160	1568%	1467%
	240	484%	453%
	320	361%	342%
	400	716%	694%
	480	188%	185%
	560	-96%	-95%
	640	-87%	-87%
	720	-94%	-93%
	800	-100%	-100%
Cap	100		-
	200	1673%	1620%
	300	565%	548%
	400	580%	568%
	500	11639%	11566%

a. First frequency

Location (mm)		*k=100*	*k=0.01*
Legs	80	-	-
	160	4056%	3734%
	240	91774%	84969%
	320	-99%	-99%
	400	-68%	-69%
	480	-56%	-55%
	560	-60%	-58%
	640	-72%	-71%
	720	-90%	-89%
	800	-100%	-100%
Cap	100		
	200	426%	415%
	300	-41%	-37%
	400	-5%	3%
	500	0%	3%

b. Second frequency

The last results give another indication that the severity of a crack acts as a scaling factor for the frequency sensitivity which is dominated mainly by the position of the crack in the structure.

3.6.3 Bending moment and the determinant relationship

Regarding the relationship between the bending moment and the determinant of the hinged structure at natural frequencies, Tables 3.7 and 3.8 present the determinant values of $D_h(\mathbf{p}, \omega)$ for the two first values of the natural frequency of the intact Greco and Pau frame in different locations of the hinge using the DSM (presented in Fig. 3.14 reproduced here).

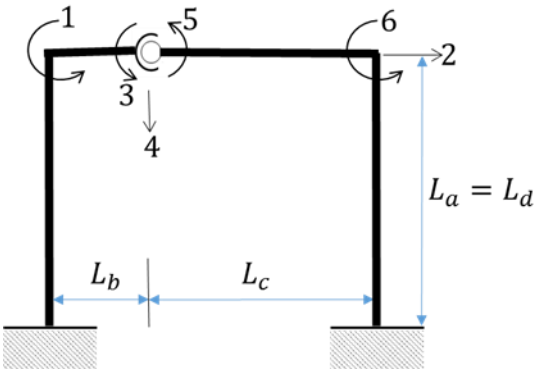

$$\mathbf{K}_h\mathbf{d} = EI\begin{bmatrix} S_a+S_b & -Q_a & SC_b & -Qq_b & 0 & 0 \\ -Q_a & T_a+T_d-m & 0 & 0 & 0 & -Q_d \\ SC_b & 0 & S_b & -Q_b & 0 & 0 \\ -Qq_b & 0 & -Q_b & T_b+T_c & Q_c & Qq_{\boldsymbol{c}} \\ 0 & 0 & 0 & Q_c & S_c & SC_c \\ 0 & -Q_d & 0 & Qq_c & SC_c & S_c+S_d \end{bmatrix}\begin{bmatrix} \theta_1 \\ \delta_2 \\ \theta_{\boldsymbol{3}} \\ \delta_{\boldsymbol{4}} \\ \theta_{\boldsymbol{5}} \\ \theta_6 \end{bmatrix}$$

According to Eq. (3.44), the determinantal value of the structure with a hinge at a point **p** is related with the squared moment $\left(\frac{M^*}{\theta}\right)^2$ obtained after multiplication of the moments per unit of rotation of each side of the hinge when the DSM is condensed in a 2x2 matrix that only possesses the rotations at each side of the hinge at the natural frequency of the intact structure.

The condensation technique sees the original system of equations, as the product's original factors in an arrangement of submatrices and sub-vectors.

$$\mathbf{Kd} = EI\begin{bmatrix} \mathbf{K}_1 & \mathbf{K}_2 \\ \mathbf{K}_3 & \mathbf{K}_4 \end{bmatrix}\begin{bmatrix} \mathbf{d}_1 \\ \mathbf{d}_2 \end{bmatrix}$$

The system is reduced to,

$$EI\left[\mathbf{K}_1 - \mathbf{K}_2\mathbf{K}_4{}^{-1}\mathbf{K}_3\right]\mathbf{q}_1 = \mathbf{K}_{Condensed}\mathbf{d}_1,\ \mathbf{d}_1 = \begin{bmatrix} \theta_{\boldsymbol{3}} \\ \theta_{\boldsymbol{5}} \end{bmatrix}$$

In this case the internal moments correspond to the degrees of freedom 3 and 5, and must be contained in the final sub-vector defining the submatrices,

$$\mathbf{K}_1 = EI\begin{bmatrix} S_b & 0 \\ 0 & S_c \end{bmatrix} \qquad \mathbf{K}_2 = EI\begin{bmatrix} SC_b & 0 & -Q_b & 0 \\ 0 & 0 & Q_{\boldsymbol{c}} & SC_c \end{bmatrix}$$

$$\mathbf{K}_3 = EI\begin{bmatrix} S_a+S_b & -Q_{\boldsymbol{a}} & -Qq_{\boldsymbol{b}} & 0 \\ -Q_{\boldsymbol{a}} & T_a+T_d-m & 0 & Qq_{\boldsymbol{d}} \\ -Qq_{\boldsymbol{b}} & 0 & T_b+T_c & Qq_{\boldsymbol{c}} \\ 0 & Qq_{\boldsymbol{d}} & Qq_{\boldsymbol{c}} & S_c+S_d \end{bmatrix} \qquad \mathbf{K}_4 = EI\begin{bmatrix} SC_b & 0 \\ 0 & 0 \\ -Q_b & Q_c \\ 0 & SC_{\boldsymbol{c}} \end{bmatrix}$$

the moments per unit of rotation of each side of the hinge are calculated as the product of the condensed matrix $\mathbf{K}_{Condensed}$ by the 2x1 vector of ones referring to the unit rotations presented in Tables 3.8 and 3.9 as well as their product $M^2 = M_L M_R$. Due to the fact that the moment was calculated using the 2x2 condensed form of the DSM of the hinged frame that only possess the rotations at each side of the hinge, there is a

"reduced" submatrix $\mathbf{B} = \mathbf{K}_3$, which possesses the condensed internal nodes and whose effect has to be taken into account by $\left(\frac{M^*}{\theta}\right)^2 = Det(\mathbf{B})M^2$ giving the determinantal value of $D_h(\mathbf{p}, \omega)$.

Table 3.8. Determinant and moment values versus location at first frequency.

Location (mm)		ω =	52.9561687278173				
		Dh(k=0)	Moment (M_L,M_R)		Det(B)	$M^2=M_L M_R$	Det(B)M^2
	80	-1.91E-21	1.26E-02	-1.26E-02	1.20E-17	-1.60E-04	-1.91E-21
	160	-9.28E-23	5.19E-03	-5.19E-03	3.45E-18	-2.69E-05	-9.28E-23
	240	-1.50E-23	2.75E-03	-2.75E-03	1.97E-18	-7.58E-06	-1.50E-23
L	320	-3.20E-24	1.44E-03	-1.44E-03	1.53E-18	-2.09E-06	-3.20E-24
E	400	-4.16E-25	5.32E-04	-5.32E-04	1.47E-18	-2.83E-07	-4.16E-25
G	480	-9.59E-26	-2.37E-04	2.37E-04	1.71E-18	-5.59E-08	-9.59E-26
S	560	-2.57E-24	-1.00E-03	1.00E-03	2.54E-18	-1.01E-06	-2.57E-24
	640	-2.05E-23	-1.91E-03	1.91E-03	5.60E-18	-3.66E-06	-2.05E-23
	720	-3.20E-22	-3.21E-03	3.21E-03	3.11E-17	-1.03E-05	-3.20E-22
	800	-4.73E-18	-5.58E-03	5.58E-03	1.52E-13	-3.12E-05	-4.73E-18
	100	-2.87E-22	-9.60E-03	9.60E-03	3.11E-18	-9.22E-05	-2.87E-22
C	200	-1.32E-23	-4.74E-02	4.74E-02	5.86E-21	-2.25E-03	-1.32E-23
A	300	-1.89E-24	1.08E-02	-1.08E-02	1.62E-20	-1.17E-04	-1.89E-24
P	400	-2.93E-25	3.12E-03	-3.12E-03	3.01E-20	-9.71E-06	-2.93E-25
	500	-1.99E-27	2.42E-04	-2.42E-04	3.38E-20	-5.88E-08	-1.99E-27

Looking at the column of the moments, it may be noted that there is a change in the sign between the coordinate 400mm and 480mm for the leg, with a minimum on the determinantal value at 480mm and it could be implied a contra-flexure point lies in between these points. While there is another change of sign in the moments column, the determinantal value does not reach a minimum therefore the zero value in the moment over rotation ratio reflects a curvature change in the mode shape.

Table 3.9. Determinant and moment values versus location at second frequency.

Location (mm)		ω =	167.9534673639100				
		Dh(k=0)	Moment (M_L,M_R)		Det(B)	$M^2=M_L M_R$	$Det(B)M^2$
LEGS	80	4.77E-21	1.14E-02	-1.14E-02	-3.66E-17	-1.30E-04	4.77E-21
	160	9.80E-23	3.51E-03	-3.51E-03	-7.96E-18	-1.23E-05	9.80E-23
	240	3.83E-25	3.46E-04	-3.46E-04	-3.20E-18	-1.20E-07	3.83E-25
	320	8.07E-24	-2.31E-03	2.31E-03	-1.51E-18	-5.35E-06	8.07E-24
	400	2.68E-23	-6.50E-03	6.50E-03	-6.34E-19	-4.23E-05	2.68E-23
	480	6.14E-23	-2.50E-02	2.50E-02	-9.82E-20	-6.26E-04	6.14E-23
	560	1.53E-22	2.47E-02	-2.47E-02	-2.50E-19	-6.12E-04	1.53E-22
	640	5.50E-22	8.93E-03	-8.93E-03	-6.90E-18	-7.98E-05	5.50E-22
	720	5.43E-21	5.47E-03	-5.47E-03	-1.81E-16	-2.99E-05	5.43E-21
	800	6.02E-17	3.92E-03	-3.92E-03	-3.92E-12	-1.54E-05	6.02E-17
CAP	100	4.93E-22	1.06E-03	-1.06E-03	-4.43E-16	-1.11E-06	4.93E-22
	200	3.32E-23	-1.05E-03	1.05E-03	-3.02E-17	-1.10E-06	3.32E-23
	300	6.57E-23	-3.44E-03	3.44E-03	-5.55E-18	-1.18E-05	6.57E-23
	400	7.01E-23	-8.44E-03	8.44E-03	-9.84E-19	-7.12E-05	7.01E-23
	500	7.03E-23	-9.99E-02	9.99E-02	-7.03E-21	-9.99E-03	7.03E-23

For the table of the second natural frequency and looking at the column of the moments, it may be noted that there is a change in the sign between the coordinate 100mm and 200mm for the cap, with a minimum on the determinantal value at 200mm therefore a contra-flexure point could be located in between these points which could be appreciated in Fig. 3.11.

3.7 Summary

The dynamic effect of a crack was studied using the DSM approach identifying two interesting properties of the determinantal expressions. The first is a relationship between the crack severity and the determinants of the cracked structure, undamaged structure and a structure with a hinge at the crack location. The above relationship permits to treat separately the two main properties of the crack namely the severity and the location of the crack. From the analytical results it seems that location rather than severity is the variable with great potential in the damage identification and therefore the equivalent structure with a hinge in the crack location and its determinant analysed at the natural frequencies will offer a means of extracting the features.

The second interesting finding is about a relationship between the square of the bending moment at the natural frequency of the undamaged structure at one location and the determinant of the structure with a hinge at the same location. The above relationship, which can also be inferred from the work by Morassi [27] shows that if

the hinge is located at a point of contra-flexure, where the bending moment is null in a particular mode, the natural frequency at that mode will not be affected. Therefore, the determinant of the hinged structure is null, and this clause is extended for a cracked structure. The next chapter will be devoted to devise uses for a point mass as a means of crack location.

Chapter 4

Point Mass Effects

The dynamic effect of discrete masses on continuous beams has been addressed since 1965 with different mathematical approaches as Naguleswaran [73] mentioned. What is clear from the literature is that as in the crack case, the changes in the natural frequencies due to an added mass occur not only by the size of the added mass but also by the position where it is located; probably that is why Shone [74] suggested that the non-dimensional parameters of crack and mass could be related and defined mathematically.

A paper titled "The effects of discrete masses and elastic supports on continuous beam natural frequencies" by Jacquot and Gibson [75] seems to cover all the questions that came out in the subject, but after that several authors had addressed the same subject with different approaches like De Rosa, et al. [76] who examined the dynamic behaviour of a slender beam carrying concentrated mass at an arbitrary abscissa giving approximated results for simply supported and clamped beams using an optimised version of the Rayleigh quotient.

Later on, a group headed by Philip D. Cha were focused on reducing the order of the characteristic determinant obtained from the assumed modes method or Lagrange's multipliers in conjunction with Lagrange's equations via algebraic manipulation. They initially applied the methodology to several spring-mass systems [77], extended it to damped elements [78] and to a miscellany of different discrete elements [79], all their findings among works from other authors are collected in Cha, et al. [80] providing good cross-references on the subject.

Many of the previous authors reach the exact frequency equation and solve it by approximate methods. Banerjee [81] presents a vast number of references on studies in free vibration behaviour of beams carrying spring-mass systems and in that context claims his work as the first time that the problem is proposed using DSM. His parametric study gives comparable results with those by Rossit and Laura [82] and avoids the use of the transcendental dynamic stability functions given by Ilanko [83].

4.1 DSM determinant with a crack and additional mass

As mentioned in Solís, et al. [84] only a significant damage would cause a measurable change when the damage detection is carried out by analysing the changes in the natural frequencies; they also noted that the damage effect could be veiled by environmental changes and experimental uncertainties. To overcome the problem of sensitivity of the changes in natural frequencies, Pandey, et al. [85] proposed to use the mode shapes to capture the discontinuity produced by the damage. However compared with the natural frequency measurements, the identification of mode shapes requires additional experimental and mathematical resources, but the effects of damage on the modes are only of the order of experimental noise and environmental effects, making the identification problem a complicated task [84].

In order to distinguish easily the changes induced by damage, Zhong and Oyadiji [86] used wavelet coefficients as an indicator of damage when they are applied to the differences in mode shapes between an undamaged beam and a damaged beam. It may be noted that Zhong and Oyadiji [86] and Bahador and Oyadiji [87] performed the modal analysis for different positions of a non-structural mass attached to the structure in order to make the damage detection method more robust and sensitive. The roving mass method proposed by Zhong and Oyadiji [36] involves locating the mass at different positions at each round of test, but during the vibration measurement the mass is not allowed to move axially, so its velocity effect such as Coriolis acceleration need not be considered.

As a demonstrative example of the use of the DSM the related mathematics of the procedure will be addressed for the general case as in Chapter 3. In using the DSM, the damaged structure with the attached mass $\bar{m}$ will be divided in three segments as shown in Figure 4.1.

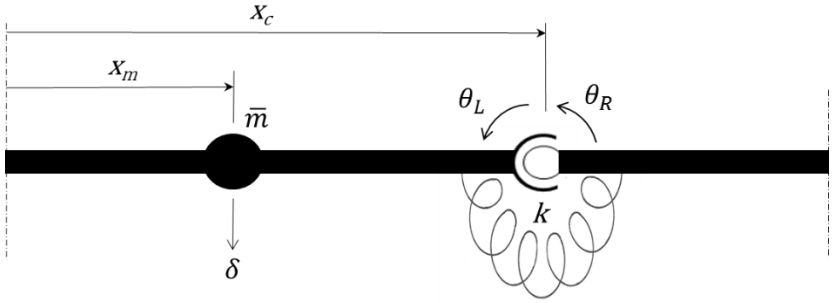

Figure 4.1. Beam segment with point mass and crack

The nodal actions are related with the nodal displacements in the modified structure through the global stiffness matrix $\mathbf{a}_{cm} = \mathbf{K}_{cm}\mathbf{d}_{cm}$,

$$\mathbf{a}_{cm} = \mathbf{K}_{cm}(x_c, x_m, \omega, k)\mathbf{d}_{cm},\ \mathbf{a}_{cm} = \begin{bmatrix} \mathbf{a}_0 \\ V \\ M_L \\ M_R \end{bmatrix},\ \mathbf{d}_{cm} = \begin{bmatrix} \mathbf{d}_0 \\ \delta \\ \theta_L \\ \theta_R \end{bmatrix}$$

For this demonstration let us allocate the extra degrees of freedom on the last three rows; therefore the first row represents the internal actions and displacements that are not pictured in Figure 4.1 collected with the vectors $\mathbf{a}_0$, $\mathbf{d}_0$. Three extra degrees of freedom are added, these being the transversal translation δ, at the point mass location x_m and; at each side of the crack located at x_c, two rotations θ_L and θ_R.

The global stiffness matrix of the damaged structure with the point mass is assembled again from the matrix of the undamaged structure. When a point mass m^* is located, its effect can be represented by a dynamic force associated with the translation at that location $V_d = -m\delta$, altering effectively the diagonal element of the corresponding dynamic stiffness matrix by $m = \bar{m}\omega^2$ in the second row. The dynamic stiffness matrix for the modified structure is written in the form

$$\mathbf{K}_{cm} = \begin{bmatrix} \mathbf{K}_0(x_c, x_m, \omega) & \mathbf{B}_1(x_c, x_m, \omega) & \mathbf{B}_2(x_c, x_m, \omega) & \mathbf{B}_3(x_c, x_m, \omega) \\ \mathbf{B}_1^{\mathrm{T}}(x_c, x_m, \omega) & k_{11}(\omega) - m & k_{12}(\omega) & 0 \\ \mathbf{B}_2^{\mathrm{T}}(x_c, x_m, \omega) & k_{21}(\omega) & k_{22}(\omega) + k & -k \\ \mathbf{B}_3^{\mathrm{T}}(x_c, x_m, \omega) & 0 & -k & k_{33}(\omega) + k \end{bmatrix} \quad (4\text{-}1)$$

where, as mentioned earlier, the last two columns relate to θ_L and θ_R, the rotational degrees of freedom on either side of the crack, and the first column relates to $\mathbf{d}_0$, all the other degrees of freedom of the structure. Thus $\mathbf{K}_0(x_c, x_m, \omega)$ is a square matrix, $\mathbf{B}_1(x_c, x_m, \omega)$, $\mathbf{B}_2(x_c, x_m, \omega)$ and $\mathbf{B}_3(x_c, x_m, \omega)$ are column vectors, k is the stiffness of the rotational spring representing the crack, and $k_{11}(\omega)$, $k_{12}(\omega) = k_{21}(\omega)$, $k_{13}(\omega) = k_{31}(\omega)$, $k_{22}(\omega)$ and $k_{33}(\omega)$ are scalars dependent of the crack and point mass locations. Performing partial Gaussian elimination on the matrix gives

$$\mathbf{K}_{cm}^{*} = \begin{bmatrix} \mathbf{K}_0^{\Delta}(\omega) & \mathbf{B}_1^*(\omega) & \mathbf{B}_2^*(\omega) & \mathbf{B}_3^*(\omega) \\ 0 & k_{11}^*(\omega) - m & k_{12}^*(\omega) & k_{13}^*(\omega) \\ 0 & k_{21}^*(\omega) & k_{\mathbf{22}}^*(\omega) + k & k_{\mathbf{23}}^*(\omega) - k \\ 0 & k_{31}^*(\omega) & k_{\mathbf{32}}^*(\omega) - k & k_{\mathbf{33}}^*(\omega) + k \end{bmatrix} \quad (4\text{-}2)$$

Where $\mathbf{K}_{\mathbf{0}}^{\mathbf{\Delta}}(\omega)$ is an upper triangular square matrix, $\mathbf{B}_{\mathbf{1}}^*(\omega)$, $\mathbf{B}_{\mathbf{2}}^*(\omega)$ and $\mathbf{B}_{\mathbf{3}}^*(\omega)$ are updated column vectors and $k_{ij}^*(\omega)$ updated scalars defined as follow,

$$k_{11}^*(\omega) = k_{11}(\omega) - \mathbf{B}_1^{\mathrm{T}}(x_c, x_m, \omega)\mathbf{K}_0^{-1}(x_c, x_m, \omega)\mathbf{B}_1(x_c, x_m, \omega)$$
$$k_{12}^*(\omega) = k_{21}^*(\omega) = k_{12}(\omega) - \mathbf{B}_1^{\mathrm{T}}(x_c, x_m, \omega)\mathbf{K}_0^{-1}(x_c, x_m, \omega)\mathbf{B}_2(x_c, x_m, \omega)$$
$$k_{13}^*(\omega) = k_{31}^*(\omega) = k_{13}(\omega) - \mathbf{B}_1^{\mathrm{T}}(x_c, x_m, \omega)\mathbf{K}_0^{-1}(x_c, x_m, \omega)\mathbf{B}_3(x_c, x_m, \omega)$$
$$k_{23}^*(\omega) = k_{23}^*(\omega) = k_{23}(\omega) - \mathbf{B}_2^{\mathrm{T}}(x_c, x_m, \omega)\mathbf{K}_0^{-1}(x_c, x_m, \omega)\mathbf{B}_3(x_c, x_m, \omega)$$
$$k_{22}^*(\omega) = k_{22}(\omega) - \mathbf{B}_2^{\mathrm{T}}(x_c, x_m, \omega)\mathbf{K}_0^{-1}(x_c, x_m, \omega)\mathbf{B}_2(x_c, x_m, \omega)$$
$$k_{\mathbf{33}}^*(\omega) = k_{\mathbf{33}}(\omega) - \mathbf{B}_3^{\mathrm{T}}(x_c, x_m, \omega)\mathbf{K}_0^{-1}(x_c, x_m, \omega)\mathbf{B}_3(x_c, x_m, \omega)$$

Before the expansion for the determinant of the matrix in Eq.4.2, the determinant of the hinged structure in the crack location $D_h(x_c, x_m, \omega)$ is obtained when the effects of the mass and the crack are nulled and expanded in the next way

$$D_h(x_c, x_m, \omega) = \left|\mathbf{K}_0^{\Delta}(x_c, x_m, \omega)\right| \left[k_{11}^*(\omega)\left(k_{22}^*(\omega)k_{33}^*(\omega) - \left(k_{23}^*(\omega)\right)^2\right) + 2k_{12}^*(\omega)k_{13}^*(\omega)k_{23}^*(\omega) - k_{12}^*(\omega)^2 k_{23}^*(\omega) - k_{13}^*(\omega)^2 k_{23}^*(\omega)\right] \quad (4\text{-}3)$$

Additionally the determinant for the unmodified structure will be obtained when the two rotations at the location of the crack are managed in a single degree of freedom, so that the dynamic stiffness matrix $\mathbf{K}_{um}$ becomes

$$\mathbf{K}_{um} = \begin{bmatrix} \mathbf{K}_0(x_c, x_m, \omega) & \mathbf{B}_1(x_c, x_m, \omega) & \mathbf{B}_2(x_c, x_m, \omega) + \mathbf{B}_3(x_c, x_m, \omega) \\ \mathbf{B}_1^{\mathrm{T}}(x_c, x_m, \omega) & k_{11}(\omega) & k_{12}(\omega) \\ \mathbf{B}_2^{\mathrm{T}}(x_c, x_m, \omega) + \mathbf{B}_3^{\mathrm{T}}(x_c, x_m, \omega) & k_{21}(\omega) & k_{22}(\omega) + k_{33}(\omega) \end{bmatrix} \quad (4\text{-}4)$$

Performing partial Gaussian elimination gives

$$\mathbf{K}_{um}^* = \begin{bmatrix} \mathbf{K}_0^{\Delta}(\omega) & \mathbf{B}_1^*(\omega) & \mathbf{B}_2^*(\omega) + \mathbf{B}_3^*(\omega) \\ 0 & k_{11}^*(\omega) & k_2^*(\omega) \\ 0 & k_2^*(\omega) & k^*(\omega) \end{bmatrix}$$

where,

$$k_2^*(\omega) = k_{12}(\omega) - \mathbf{B}_1^{\mathrm{T}}\mathbf{K}_0^{-1}(x_c, x_m, \omega)\left(\mathbf{B}_2^{\mathrm{T}} + \mathbf{B}_3^{\mathrm{T}}\right)$$
$$k_2^*(\omega) = k_{12}^*(\omega) + k_{13}^*(\omega)$$

and $k^*(\omega)$, the term accounting for the continuity in the point where the crack is located for the intact structure is

$$k^*(\omega) = k_{22}(\omega) + k_{33}(\omega) - \left(\mathbf{B}_2^{\mathrm{T}} + \mathbf{B}_3^{\mathrm{T}}\right)\mathbf{K}_0^{-1}(x_c, x_m, \omega)\left(\mathbf{B}_2^{\mathrm{T}} + \mathbf{B}_3^{\mathrm{T}}\right)$$
$$k^*(\omega) = k_{22}^*(\omega) + k_{33}^*(\omega) + 2k_{23}^*(\omega)$$

The above steps leads to the expansion for the determinant of the unmodified structure $D_0(x_c, x_m, \omega)$ as

$$D_0(x_c, x_m, \omega) = \left|\mathbf{K}_0^{\Delta}(\omega)\right| \left[k_{11}^*(\omega)k^*(\omega) - \left(k_2^*(\omega)\right)^2\right]$$
$$D_0(x_c, x_m, \omega) = \left|\mathbf{K}_0^{\Delta}(\omega)\right| \left[k_{11}^*(\omega)\left(k_{22}^*(\omega) + k_{33}^*(\omega) + 2k_{23}^*(\omega)\right) - \left(k_{12}^*(\omega) + k_{13}^*(\omega)\right)^2\right] \quad (4\text{-}5)$$

Using the expansions of Eqns. (4.3) and (4.5) in the expansion for the determinant of the dynamic stiffness matrix in Eq. (4.2) to the cracked structure in x_c with a point mass located in x_m $D_{cm}(x_m, x_c, \omega)$ will be seen as

$$D_{cm}(x_m, x_c, \omega) = kD_0(x_c, x_m, \omega) + D_h(x_c, x_m, \omega) - mkD_m(x_c, x_m, \omega) + mD_{mc}(x_c, x_m, \omega) \quad (4\text{-}6)$$

$$fD_{cm}(x_m, x_c, \omega) = D_0(x_c, x_m, \omega) + fD_h(x_c, x_m, \omega) - mD_m(x_c, x_m, \omega) + mfD_{mc}(x_c, x_m, \omega) \quad (4\text{-}7)$$

with $f = 1/k$ the local flexibility added for the crack, $D_m(x_c, x_m, \omega)$ the determinant accounting for the location of the point mass when there is no crack and $D_{mc}(x_c, x_m, \omega)$ accounting for the locations of the crack and mass simultaneously. Each of the previous named functions have the following expansion form

$$\begin{aligned} D_m(x_c, x_m, \omega) &= \left|\mathbf{K}_0^{\Delta}(\omega)\right| k^*(\omega) = \left|\mathbf{K}_0^{\Delta}(\omega)\right| \left[k_{22}^*(\omega) + k_{33}^*(\omega) + 2k_{23}^*(\omega)\right] \\ D_{mc}(x_c, x_m, \omega) &= \left|\mathbf{K}_0^{\Delta}(\omega)\right| \left[\left(k_{\mathbf{22}}^*(\omega) k_{\mathbf{33}}^*(\omega) - \left(k_{23}^*(\omega)\right)^2\right)\right] \end{aligned} \tag{4-8}$$

By closely observing the obtained terms from the different matrices, it is possible to notice that $D_m(x_c, x_m, \omega)$ could be obtained from the matrix in Eq. (4.4) when the row and column where the mass effect is included are taken off, as if in that location a pin is located. Following the previous manner, $D_{mc}(x_c, x_m, \omega)$ could be obtained by nullifying the stiffness value from the matrix in Eq. (4.2) and removing the row and column where the mass effect is included.

The next section deals with the closed form solutions that predict the dynamic behaviour of beams carrying a point mass within their length with four common boundary conditions.

4.2 Closed-form solutions for added mass in beams

Rossit and Laura [82] present different approaches to deal with the case of a beam with an attached mass in coordinate x_m along its length. The matrix will be obtained from Eq. (4.4), i.e. no crack, and the corresponding characteristic equation stated in Eq. (4.6) becomes,

$$0 = D_0(x_m, \omega) - mD_m(x_m, \omega) \tag{4-9}$$

From $\mathbf{K}_m$, the initial matrix for the free-free case defined by Eq. (4.10). The point mass located at x_c split the beam in two segments labelled according to Figure 4.2. The closed form solution of common boundary conditions rows and columns will be deleted according to the null actions and displacements as is explained for each case.

$$\mathbf{a}_m = \mathbf{K}_m(x_c, \omega, k)\mathbf{d}_m,\ \mathbf{a}_m = \begin{bmatrix} V_i \\ M_i \\ M_c \\ V_c \\ M_j \\ V_j \end{bmatrix},\ \mathbf{d}_m = \begin{bmatrix} \delta_i \\ \theta_i \\ \theta_c \\ \delta_c \\ \theta_j \\ \delta_j \end{bmatrix}$$

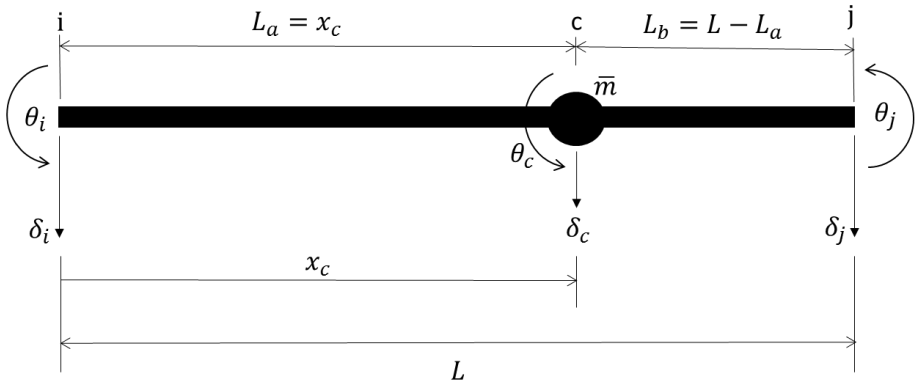

Figure 4.2. Free-free beam with point mass added

$$\mathbf{K}_m = EI\begin{bmatrix} T_a & Q_a & Qq_a & -Tt_a & 0 & 0 \\ Q_a & S_a & SC_a & -Qq_a & 0 & 0 \\ Qq_a & SC_a & S_a+S_b & Q_b-Q_a & SC_b & -Qq_b \\ -Tt_a & -Qq_a & Q_b-Q_a & T_a+T_b-m^* & Qq_b & -Tt_b \\ 0 & 0 & Qq_b & SC_b & S_b & -Q_b \\ 0 & 0 & -Tt_b & -Qq_b & -Q_b & T_b \end{bmatrix} \tag{4-10}$$

with $m^* = \frac{\omega^2}{EI}\overline{m}$

4.2.1 Clamped-clamped beam

For these boundary conditions, rows and columns for δ_i, δ_j, θ_i and θ_j are eliminated from Eq. (4.10) leading to the entities in Eq. (4.11).

$$\mathbf{K}_m = EI\begin{bmatrix} S_a+S_b & Q_b-Q_a \\ Q_b-Q_a & T_a+T_b-m \end{bmatrix} \tag{4-11}$$

The determinant $D_m(x_c,\omega)$ could be easily obtained as was established and seen in Eq. (4.12).

$$D_m(x_m,\omega) = (S_a+S_b) \tag{4-12}$$

When the determinant term from the additional mass is expanded using the functions from Table 3.1, we obtain the expression in Eq. (4.13).

$$D_m(x_c,\omega) = \frac{\lambda(\sinh(L\lambda)\,c_a c_b - \sin(L\lambda)\,CH_a CH_b + s_a CH_a + s_b CH_b - c_a SH_a - c_b SH_b)}{(1-CH_a c_a)(1-CH_b c_b)} \tag{4-13}$$

The common denominator corresponds to the product of the characteristic equation of the two fixed beams segments and could be eliminated by multiplying both sides of the equation by it, avoiding the poles of the determinant in frequencies close to their natural values and the characteristic equation for a beam with a lumped mass is obtained and collected in Table 4.1 as $\overline{D}_m(x_c,\omega)$ and the closed form solution for a point mass attached to a beam is seen as,

$$\overline{D}_0(x_c,\omega) - m\overline{D}_m(x_c,\omega) = 0 \tag{4-14}$$

Similarly as in the previous chapter, a plot of the obtained values for the function $\overline{D}_m(x_m, \omega)$ for constant eigenvalues along the beam are given in the next figures next to the obtained closed-form solution.

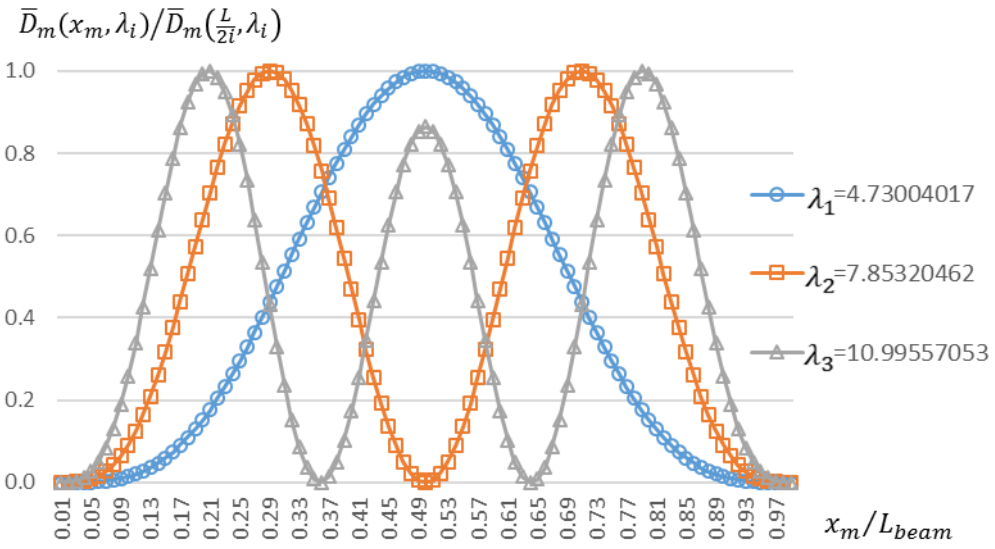

Figure 4.3. Non-dimensional plot of the function $\overline{D}_m$ evaluated at different locations for constant eigenvalues. Clamped-clamped beam case.

For the case of the clamped-clamped beam shown in Fig. 4.3, the symmetry of the boundary conditions is observed. That is why if attention is paid to the second eigenvalue, it is observed that when the mass is located in the middle of the beam $\overline{D}_m(x_c, \omega) = 0$.

4.2.2 Clamped-pinned beam

For a clamped-pinned beam where the end displacements plus one end rotation are limited, the rows and columns for δ_i, δ_j and θ_i are eliminated from Eq. (4.10) leading to the following simplified DSM.

$$\mathbf{K}_m = EI \begin{bmatrix} S_a + S_b & Q_b - Q_a & SC_b \\ Q_b - Q_a & T_a + T_b - m^* & Qq_b \\ SC_b & Qq_b & S_b \end{bmatrix} \tag{4-15}$$

$$D_m(x_c, \omega) = S_b(S_a + S_b) - SC_b^2 = S_a S_b + (S_b^2 - SC_b^2) = S_a S_b + 2Q_b \Delta_a$$

$$D_m(x_c, \omega) = \frac{\lambda(2s_b SH_b + SH_a SH_b c_a c_b + CH_a CH_b s_a s_b - \sin(L\lambda)\, CH_a SH_b - \sinh(L\lambda)\, c_a s_b)}{(1 - CH_a c_a)(1 - CH_b c_b)} \tag{4-16}$$

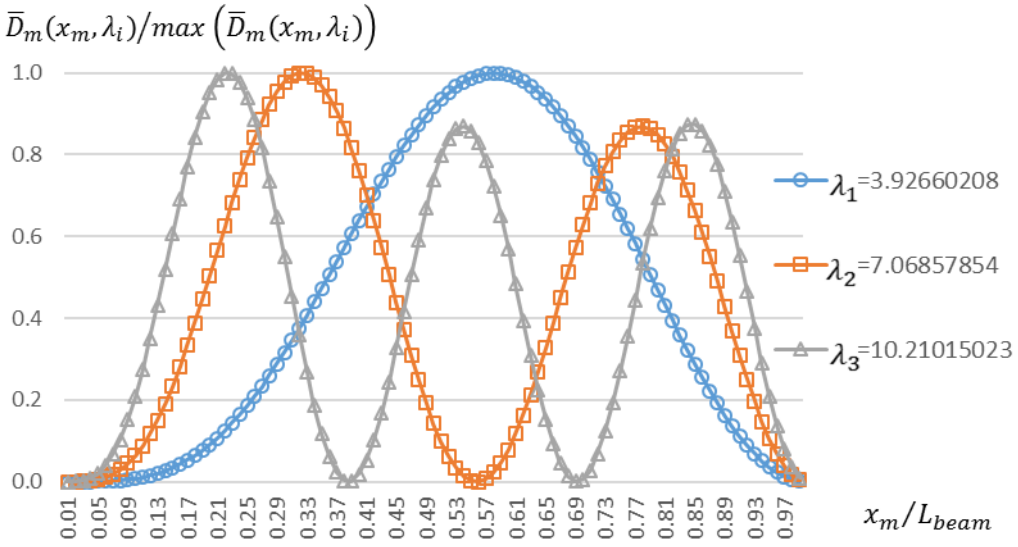

Figure 4.4. Non-dimensional plot of the function $\bar{D}_m$ evaluated at different locations for constant eigenvalues. Clamped-pinned beam case

The symmetry observed for the clamped-clamped case is broken and watching the graph one can assure that the pinned end is located in the right side of the beam because the effect of the mass is noticed very close to this end.

4.2.3 Pinned-pinned beam

For a simple supported beam the end displacements disappear, therefore rows and columns for δ_i and δ_j are eliminated from Eq. (4.10) leading to the entities in Eq. (4.17).

$$\mathbf{K}_m = EI\begin{bmatrix} S_a & SC_a & -Qq_a & 0 \\ SC_a & S_a+S_b & -Q_a+Q_b & SC_b \\ -Qq_a & -Q_a+Q_b & T_a+T_b-m^* & Qq_b \\ 0 & SC_b & Qq_b & S_b \end{bmatrix} \tag{4-17}$$

$$D_m(x_c,\omega) = \quad S_aS_b(S_a+S_b) - S_bSC_a^2 - S_aSC_b^2$$
$$D_m(x_c,\omega) = \quad S_a(S_b^2-SC_b^2) + S_b(S_a^2-SC_a^2) = 2\{S_aQ_b+S_bQ_a\}$$

$$D_m(x_c,\omega) = \frac{\lambda(\sin(L\lambda)\,SH_aSH_b - \sinh(L\lambda)\,s_as_b)}{(1-CH_ac_a)(1-CH_bc_b)} \tag{4-18}$$

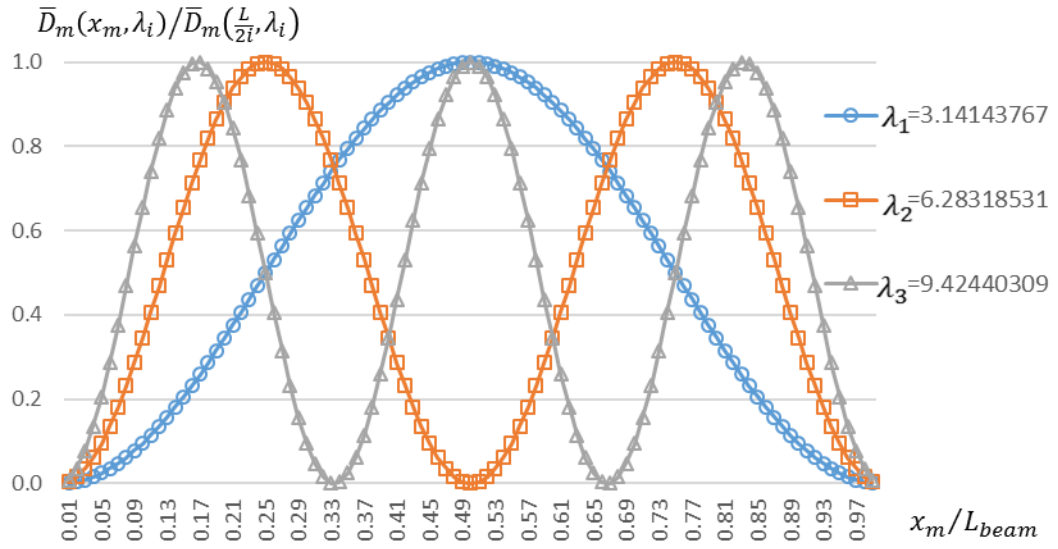

Figure 4.5. Non-dimensional plot of the function $\overline{D}_m$ evaluated at different locations for constant eigenvalues. Pinned-pinned case

The symmetry of the supported ends is clearly seen and the effect of the mass in the vicinity implies a pinned support.

4.2.4 Clamped-free beam

For a cantilever beam, the rotation and displacement of the clamped end δ_i and θ_i are eliminated from Eq. (4.10) leading to the entities in Eq. (4.19).

$$\mathbf{K}_m = EI\begin{bmatrix} S_a+S_b & -Q_a+Q_b & SC_b & -Qq_b \\ -Q_a+Q_b & T_a+T_b-m^* & Qq_b & -Tt_b \\ SC_b & Qq_b & S_b & -Q_b \\ -Qq_b & -Tt_b & -Q_b & T_b \end{bmatrix} \tag{4-19}$$

$$\begin{aligned} D_m(x_c,\omega) = & \; S_a(T_bS_b-Q_b^2)+S_b(T_bS_b-Q_b^2)-(S_bQq_b^2+T_bSC_b^2-2Q_bSC_bQq_b) \\ = & \; S_a\frac{\lambda^4(2-\Delta_b)}{\Delta_b}+S_b\frac{\lambda^4(2-\Delta_b)}{\Delta_b}-\frac{2\lambda^4S_b}{\Delta_b}=\lambda^4\left(S_a\frac{2}{\Delta_b}-S_b-S_a\right) \end{aligned}$$

$$D_m(x_c,\omega)=\frac{\lambda(\sin(L\lambda)CH_aCH_b-\sinh(L\lambda)\,c_ac_b+CH_as_a+SH_bc_b-SH_ac_a-CH_bs_b)}{(1-CH_ac_a)(1-CH_bc_b)} \tag{4-20}$$

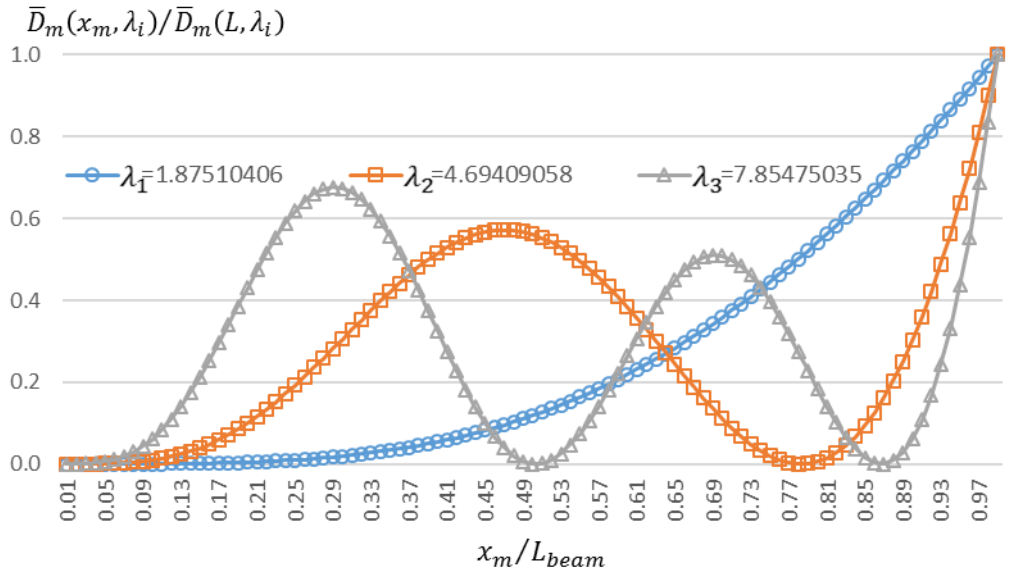

Figure 4.6. Non-dimensional plot of the function $\overline{D}_m$ evaluated at different locations for constant eigenvalues. Clamped-free beam case

The reason for the maximum effect of the mass at the right end in all the eigenvalues can be easily understood as it is a free end.

A compilation of the obtained closed form for the common boundary conditions is given in Table 4.1 and with it show that even though for the simply supported beam the functions $\overline{D}_h(x_c,\omega_0)$ and $\overline{D}_m(x_c,\omega_0)$ are the same, it does not stand for the other boundary conditions.

Table 4.1. Closed form determinants for crack and adding mass to common boundary conditions

Equivalent expression	
Clamped-clamped	
$\overline{D}_h(x_c, \omega_0)$	$\sin(L\lambda)\, CH_aCH_b + \sinh(L\lambda)\, c_ac_b + s_aCH_a + s_bCH_b\ - c_aSH_a - c_bSH_b$
$\overline{D}_m(x_c, \omega_0)$	$\sinh(L\lambda)\, c_ac_b - \sin(L\lambda)\, CH_aCH_b + s_aCH_a + s_bCH_b\ - c_aSH_a - c_bSH_b$
Clamped-pinned	
$\overline{D}_h(x_c, \omega_0)$	$\sin(L\lambda)\, CH_aSH_b + \sinh(L\lambda)\, c_as_b + 2s_bSH_b - SH_aSH_bc_ac_b - CH_aCH_bs_as_b$
$\overline{D}_m(x_c, \omega_0)$	$2s_bSH_b + SH_aSH_bc_ac_b + CH_aCH_bs_as_b - \sin(L\lambda)\, CH_aSH_b - \sinh(L\lambda)\, c_as_b$
Pinned-pinned	
$\overline{D}_h(x_c, \omega_0)$	$\sin(L\lambda)\, SH_aSH_b - \sinh(L\lambda)\, s_as_b$
$\overline{D}_m(x_c, \omega_0)$	$\sin(L\lambda)\, SH_aSH_b - \sinh(L\lambda)\, s_as_b$
Clamped-free	
$\overline{D}_h(x_c, \omega_0)$	$\sinh(L\lambda)\, c_ac_b - \sin(L\lambda)\, CH_aCH_b + CH_as_a + SH_bc_b - SH_ac_a - CH_bs_b$
$\overline{D}_m(x_c, \omega_0)$	$\sin(L\lambda) CH_aCH_b - \sinh(L\lambda)\, c_ac_b + CH_as_a + SH_bc_b - SH_ac_a - CH_bs_b$

An interesting situation occurs for the specific case of a simply supported beam, where a mass and a crack have similar effects. Therefore the dynamic effect of a crack could be simulated by adding a mass to validate through experimentation, the formulae of spring stiffness.

4.3 Point mass in a cracked beam data. Comparison with previous work. Zhong and Oyadiji [36]

As mentioned earlier, the use of a non-structural point mass located in several points along the length of the beam will present a discontinuity in the first derivative of the frequency plot in the crack location on the otherwise continuous graph of measured frequencies. Experimental results were published by Zhong and Oyadiji [36] for a simply supported beam of length 2400mm with a constant cross section 100x25mm^2 made of aluminium. The reported data correspond to the values of the two first natural frequencies measured when a cut saw at 400mm from the left end was infringed to the beam and a probing mass of 4kg was located in 25 different locations along the beam, with a probing interval of 100mm. Figures 4.7 and 4.8 show the frequency values reported by [36] and those obtained using DSM Eq. (4.1) in addition to the values of

the natural frequency when the point mass is added to a undamaged beam using DSM as benchmark to compare the frequency changes in both beam states.

To produce the data of the cracked beam, the present case demands the stiffness value that represents the flexibility introduced by the cut. Following the model develop by Chondros, et al. [20] for a saw cut of 5mm depth in a beam of 25mm thickness, the 20% non-dimensional crack length generates a 0.38 compliance leading to a non-dimensional spring stiffness $k = 255985$ for the 2.4m beam.

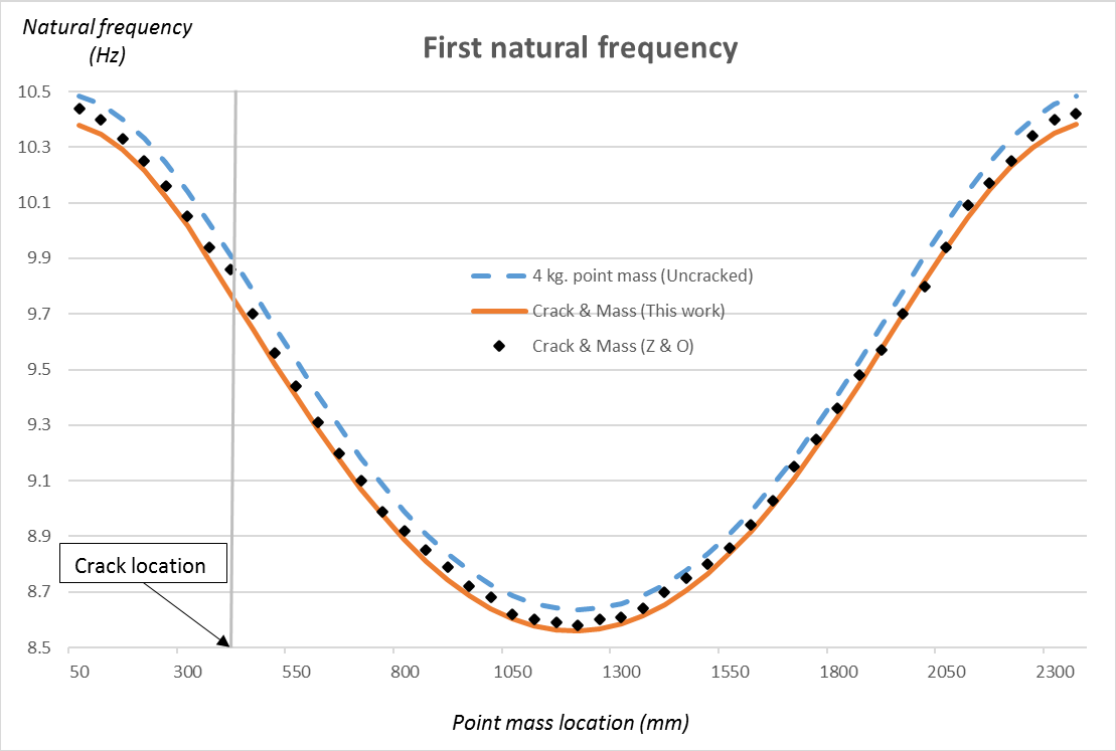

Figure 4.7. First natural frequency vs. added point mass location

With a first glance to the values measured and those obtained using DSM showed in Figure 4.7, one can observe a few matching points. Additionally but almost imperceptible it is possible to notice a change in the trend on the experimental data before and after the mass passes the crack.

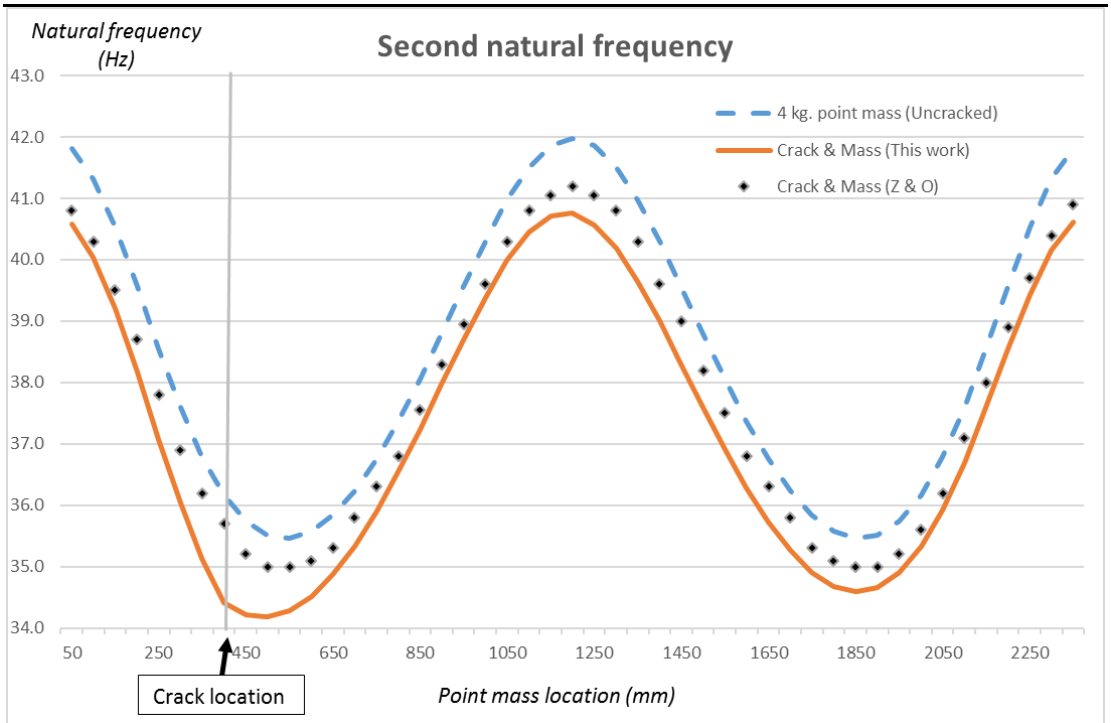

Figure 4.8. Second natural frequency vs. added point mass location

Figure 4.8 for the second frequency although there is not a single match between the values reported for the experiment and those obtained using DSM, it is noticed the asymmetry in the otherwise symmetric graph of the frequency when there is no crack with a more appreciable lean of the line for the cracked beam towards the side of the crack.

4.4 Summary

The use of dynamic effects of point masses on beams for crack identifications was analysed comparing data reported from one experiment and those obtained from dynamic stiffness matrices. An important remark regarding to the gap between the graphs is that the frequency shift remains constant in all the positions but in those locations near to the crack. Unfortunately, the last peculiarities were noticed because there is expected to be some change in the crack vicinity, and could pass unseen otherwise. That is probably why Zhong and Oyadiji [86], [88], [89] have been looking for a way to improve the readability of the changes caused by a crack through the use of wavelet transform. The next chapter proposes the use of another inertial property that could help to make the presence of a crack more noticeable.

Chapter 5

Inertial effects on cracks

The translational dynamic effect of discrete masses on continuous beams was addressed in the previous chapter as a tool that could help to identify the crack presence by simply looking at the plot of the frequency vs mass location. The obtained graphs indicate that there is a change in the slope of the frequency plot at the crack location that could be easily missed by the observer as there is no sudden change in the value of the frequency. In this chapter not only the translational effects of the added mass but the rotational inertia effect will also be considered, bearing in mind that the common crack model includes a discontinuity in the slope and the effect of the crack could therefore be noticed better by using a roving body possessing rotary inertia.

5.1 DSM determinant with a crack and a mass in the same position

In Section 4.2 the inertial effect of the roving mass due to a translational displacement and the obtained results show that although there is a change in the slope of the frequency plot, it needs to be magnified by a posterior procedure like wavelet transform to unveil the effect of the mass. A similar magnification of this effect could be achieved when the rotary inertia of the appended body is considered. The derivations presented here are limited to the case in which the body is appended immediately to one side or the other of the crack as this is sufficient for the purpose. As was done previously, to gain understanding of the effect of all the additional elements, the case for a beam clamped at both ends will be presented.

Figure 5.1 shows the elements involved in the case of a clamped-clamped cracked beam and Eq. (5.1) indicates the relationship between those elements in the dynamic equation in matrix form using the dynamic stability functions defined in Section 3.3.

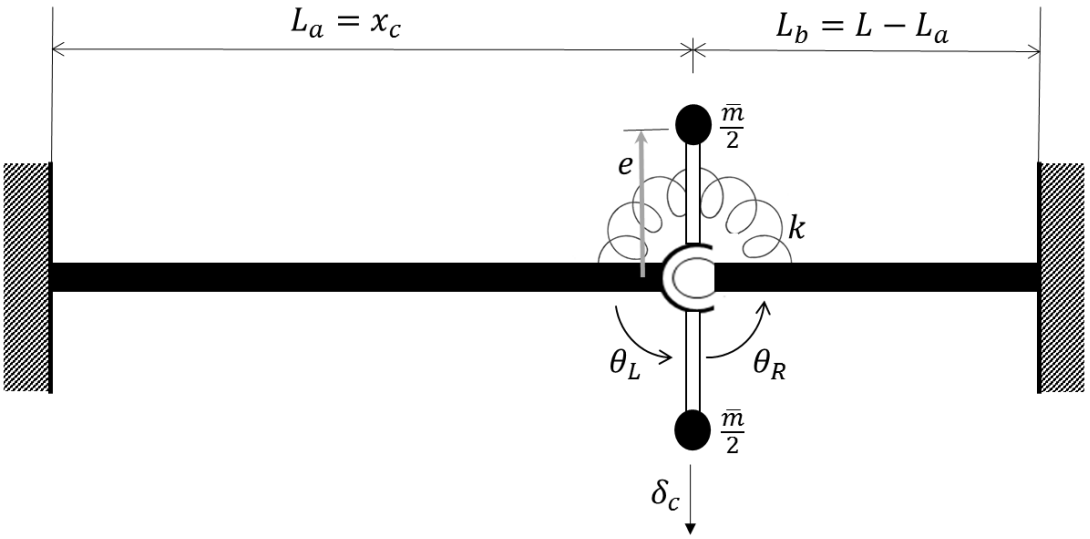

Figure 5.1. Fixed cracked beam with appended body

$$\begin{bmatrix} M_L \\ V_c \\ M_R \end{bmatrix} = EI \begin{bmatrix} S_a + \bar{k} & -Q_a & -\bar{k} \\ -Q_a & T_a + T_b & Q_b \\ -\bar{k} & Q_b & S_b + \bar{k} \end{bmatrix} \begin{bmatrix} \theta_L \\ \delta_c \\ \theta_R \end{bmatrix} \tag{5-1}$$

The added mass $\bar{m}$ at x_c, the crack location, produces a dynamic force associated with δ_c, the translation at the crack, altering effectively the diagonal element of the corresponding dynamics stiffness by $m^* = \frac{\omega^2}{EI}\bar{m}$ in the second row. When considering the rotational inertia of the added mass, there is a similar dynamic effect, this time in the moment associated with the rotational displacement $M_d = -I_0\theta_c$. The rotary inertia can be expressed in terms of the added mass as $I_0 = e^2\frac{\omega^2}{EI}\bar{m}$ where e is the effective eccentricity of the concentrated mass that will produce the same rotary inertia. Therefore the rotary inertia effect depends of the location of the mass relative to the crack and the global matrix takes the form of Eq. (5.2) when the added inertia is located at the left side of the spring or takes the form in Eq. (5.8) (which will be presented later) when it is located at the right side of the spring

$$\begin{bmatrix} M_L \\ V_c \\ M_R \end{bmatrix} = EI \begin{bmatrix} S_a + \bar{k} - I_0 & -Q_a & -\bar{k} \\ -Q_a & T_a + T_b - m^* & Q_b \\ -\bar{k} & Q_b & S_b + \bar{k} \end{bmatrix} \begin{bmatrix} \theta_L \\ \delta_c \\ \theta_R \end{bmatrix} \tag{5-2}$$

For the case shown in Equation (5.2) the determinant expression could be presented in the following form

$$\begin{gathered} \big(D_0(x_c,\omega) - mD_m(x_c,\omega) + D_{mr}(x_c,\omega) - D_r(x_c,\omega)\big)k + D_h(x_c,\omega) \\ + mD_{mc}(x_c,\omega) + D_{cmr}(x_c,\omega) + D_{cr}(x_c,\omega) = 0 \end{gathered} \tag{5-3}$$

with ω the natural frequency and x_c the crack location. It is important to mention that terms like D_0, D_h, D_m and D_{mc} maintain the same definition as in Eq. (4.6) when a

point mass is appended to the structure in the location of the crack. Some additional terms in Eq. (5.3) come from the expansion of

$$-I_0(T_a + T_b - m^*)\left(S_b + \bar{k}\right) - I_0 Q_b^2$$

which are defined as follows using the stability functions of Table 3.1.

$$D_{mr}(x_c, \omega) = m^* I_0$$
$$D_{mr}(x_c, \omega) = m^* I_0 \frac{(1 - CH_a c_a)(1 - CH_b c_b)}{(1 - CH_a c_a)(1 - CH_b c_b)} \tag{5-4}$$

$$D_r(x_c, \omega) = I_0(T_a + T_b)$$
$$D_r(x_c, \omega) = I_0 \frac{\lambda^3[(s_a\, CH_a + c_a\, SH_a)(1 - CH_b c_b) + (s_b\, CH_b + c_b\, SH_b)(1 - CH_a c_a)]}{(1 - CH_a c_a)(1 - CH_b c_b)} \tag{5-5}$$

$$D_{cmr}(x_c, \omega) = m^* I_0 S_b$$
$$D_{cmr}(x_c, \omega) = m^* I_0 \frac{\lambda(s_b\, CH_b - c_b\, SH_b)(1 - CH_a c_a)}{(1 - CH_a c_a)(1 - CH_b c_b)} \tag{5-6}$$

$$D_{cr}(x_c, \omega) = I_0\left(T_a S_b + T_b S_b - Q_b^2\right)$$
$$D_{cr}(x_c, \omega) = I_0 \frac{\lambda^4[(s_b\, CH_b - c_b\, SH_b)(s_a\, CH_a + c_a\, SH_a) + (1 + CH_b c_b)(1 - CH_a c_a)]}{(1 - CH_a c_a)(1 - CH_b c_b)} \tag{5-7}$$

On the other hand if the rotary inertia is on the right side of the crack, the DSM is of the form

$$\begin{bmatrix} M_L \\ V_c \\ M_R \end{bmatrix} = EI \begin{bmatrix} S_a + \bar{k} & -Q_a & -\bar{k} \\ -Q_a & T_a + T_b - m^* & Q_b \\ -\bar{k} & Q_b & S_b + \bar{k} - I_0 \end{bmatrix} \begin{bmatrix} \theta_L \\ \delta_c \\ \theta_R \end{bmatrix} \tag{5-8}$$

In the above equation the change in the coefficients from Eq. (5.2) is due to the location of I_0. The expansion of Eq. (5.2) is unchanged as well as the terms of Eqns. (5.4) and (5.5) and the terms that need to be changed due to the relocation of the mass are found from the expansion of

$$-I_0(T_a + T_b - m^*)\left(S_a + \bar{k}\right) - I_0 Q_a^2$$

$$D_{cmr}(x_c, \omega) = m^* I_0 S_a$$
$$D_{cmr}(x_c, \omega) = m^* I_0 \frac{\lambda(s_a\, CH_a - c_a\, SH_a)(1 - CH_b c_b)}{(1 - CH_a c_a)(1 - CH_b c_b)} \tag{5-9}$$

$$D_{cr}(x_c, \omega) = I_0\left(T_a S_a + T_b S_a - Q_a^2\right)$$
$$D_{cr}(x_c, \omega) = I_0 \frac{\lambda^4[(s_b\, CH_b + c_b\, SH_b)(s_a\, CH_a - c_a\, SH_a) + (1 - CH_b c_b)(1 + CH_a c_a)]}{(1 - CH_a c_a)(1 - CH_b c_b)} \tag{5-10}$$

Terms $D_{cmr}(x_c, \omega)$ and $D_{cr}(x_c, \omega)$ will be identical if the crack is located at a line of symmetry so that $T_a = T_b$, $S_a = S_b$ and $Q_a = Q_b$; otherwise the determinants will differ, and a frequency shift can be expected in general.

It can be noticed that $D_{cr}(x_c, \omega)$ and $D_{cmr}(x_c, \omega)$ have an effect on the determinant when the flexibility is different from zero, i.e. when there is a crack, and accommodates their values related to the opposite side, generating a jump in the frequency measurement when the crack is just passed.

Another important observation could be made by looking at the terms present when there is no crack. It was demonstrated that the term $D_0(x_c, \omega)$ has a very small change in the presence of cracks, while the inertial terms will have a noticeable change especially at higher frequencies, even with low values of the mass as these are affected by the square of the frequency, making it valuable for use in damage location if high frequency measurements can be used.

5.2 Roving mass in a single cracked cantilever beam

In the previous section, a clamped-clamped beam was used to demonstrate the dependence of the frequency equation on the location of the point mass, and Eq. (5.3) was derived as a general expression for any structure where each term, as was shown in chapters 3 and 4, is dependent not only on the boundary conditions but also on the location of both crack and point mass. To illustrate the inertial effects of the point mass roving in a beam, the numerical solution of the frequency equation using DSM approach will be presented in graphical form.

5.2.1 Single cracked beam, frequency parameter.

For a cantilever beam with a crack at x_c and a point mass with location x_m roving within its length L, the DSM equation involves three beam segments which lengths shown in Figure 5.2 correspond when the body is located between the fixed end and the crack making $L_a = x_m$, $L_b = x_c - x_m$ and $L_c = L - x_c$.

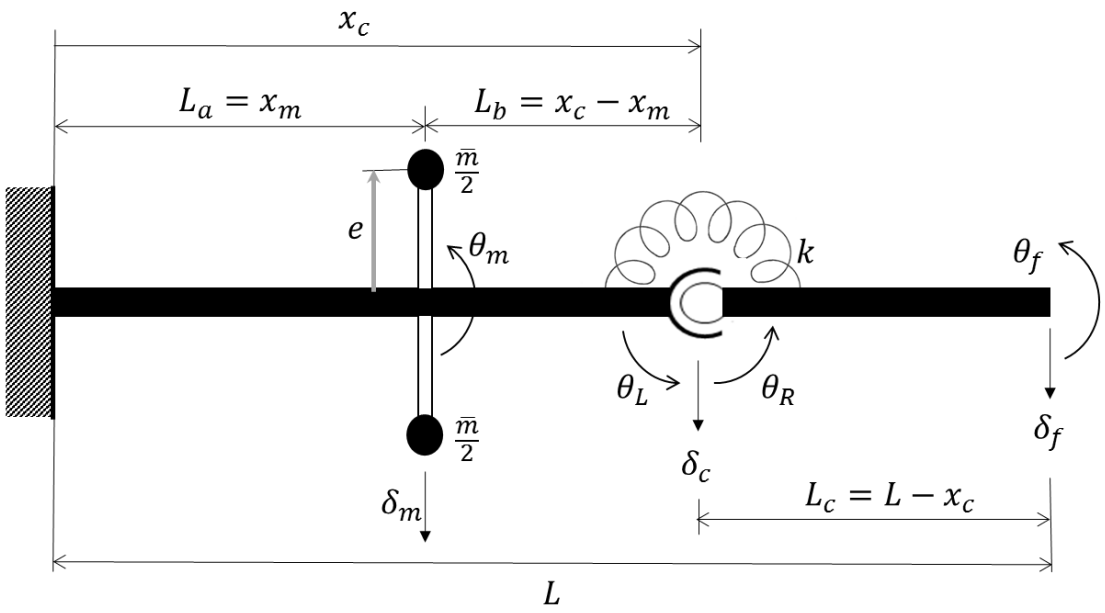

Figure 5.2. Cracked cantilever beam with appended body

The nodal actions and nodal displacements in the structure pictured in Fig.5.2 are related through $\mathbf{a}_c = \mathbf{K}_c\mathbf{d}_c$, where $\mathbf{K}_c$ is the DSM taking the form of Eq. (5.11) and

$$\mathbf{d}_c = \begin{bmatrix} \theta_m \\ \delta_m \\ \theta_L \\ \delta_c \\ \theta_R \\ \theta_f \\ \delta_f \end{bmatrix}$$

$$\mathbf{K}_c = EI \begin{bmatrix} S_a + S_b - I_0 & Q_b - Q_a & SC_b & -Qq_b & 0 & 0 & 0 \\ Q_b - Q_a & T_a + T_b - m^* & Qq_b & -Tt_b & 0 & 0 & 0 \\ SC_b & Qq_b & S_b + \bar{k} & -Q_b & -\bar{k} & 0 & 0 \\ -Qq_b & -Tt_b & -Q_b & T_b + T_c & Q_c & Qq_c & -Tt_c \\ 0 & 0 & -\bar{k} & Q_c & S_c + \bar{k} & SC_c & -Qq_c \\ 0 & 0 & 0 & Qq_c & SC_c & S_c & -Q_c \\ 0 & 0 & 0 & -Tt_c & -Qq_c & -Q_c & T_c \end{bmatrix} \quad (5\text{-}11)$$

In the numerical simulation, the mass and the crack will not be coincident to avoid null lengths. In a similar way, when the point mass is located between the free end and the crack the length of beam segments are defined as $L_a = x_c$, $L_b = x_m - x_c$ and $L_c = L - x_m$. The displacement vector and correspondent DSM have the form

$$\mathbf{d}_c = \begin{bmatrix} \theta_L \\ \delta_c \\ \theta_R \\ \theta_m \\ \delta_m \\ \theta_f \\ \delta_f \end{bmatrix}$$

$$\mathbf{K}_c = EI \begin{bmatrix} S_a + \bar{k} & -Q_a & -\bar{k} & 0 & 0 & 0 & 0 \\ -Q_a & T_a + T_b & Q_b & Qq_b & -Tt_b & 0 & 0 \\ -\bar{k} & Q_b & S_b + \bar{k} & SC_b & -Qq_b & 0 & 0 \\ 0 & Qq_b & SC_b & S_b + S_c - I_0 & Q_c - Q_b & SC_c & -Qq_c \\ 0 & -Tt_b & -Qq_b & Q_c - Q_b & T_b + T_c - m^* & Qq_c & -Tt_c \\ 0 & 0 & 0 & SC_c & Qq_c & S_c & -Q_c \\ 0 & 0 & 0 & -Qq_c & -Tt_c & -Q_c & T_c \end{bmatrix} \quad (5\text{-}12)$$

Numerical results for a clamped-clamped beam of unit length (with 10% of the total mass of the beam probing mass with no eccentricity) were generated using Eqns. (5.11) and (5.12). The crack is located near the middle span ($x_c = 0.495$) initially with a very high stiffness assuming near zero flexibility to verify results with Eq. (4.6) for the intact beam. Figures 5.3 and 5.4 show the results for second and third eigenvalues respectively where for both beam scenarios the graphs almost overlap.

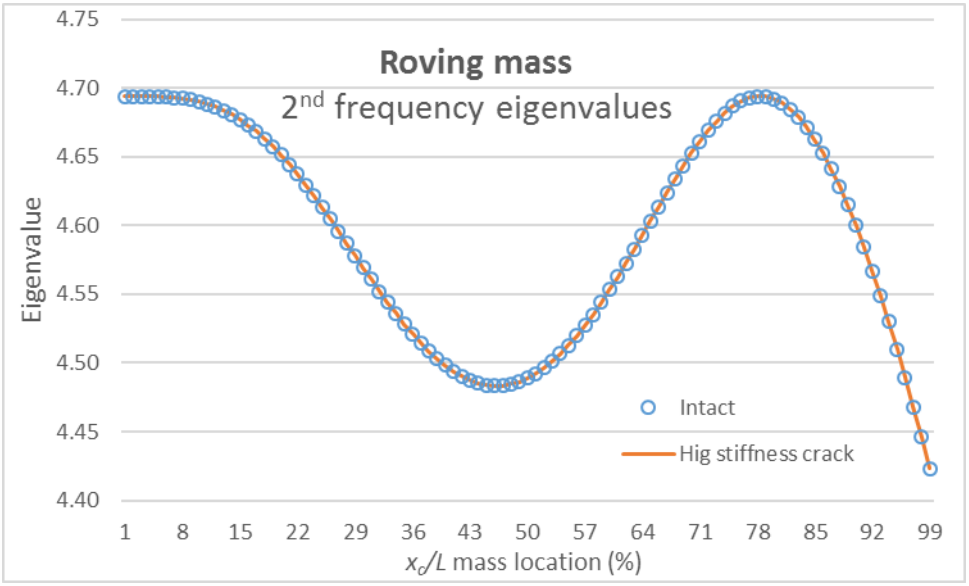

Figure 5.3. Roving mass on intact cantilever beam. Second eigenvalue shift, *e=0*

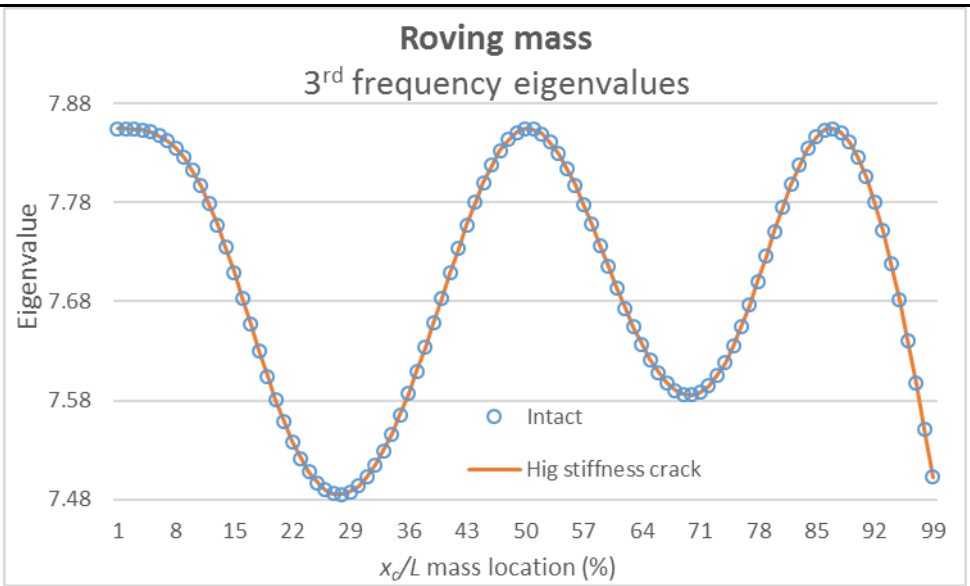

Figure 5.4. Roving mass on intact cantilever beam. Third eigenvalue shift, $e=0$

It may be noted that the use of high stiffness amounts to enforcing a constraint, the idea first proposed by Courant [90] which led to the now popular penalty method. The difference between the closed-form solution for an undamaged beam and the one obtained using the DSM with a high stiffness for the rotational spring remains small, the worst discrepancy being less than $2x10^{-6}$ percentage of the third eigenvalue for a cantilever beam. This shows that the stiffness values are high enough to effect a constraint and still reasonably small so as not to cause numerical problems [91]. Now moving towards the inclusion of the rotary inertia effect, meaning the use of a non-zero eccentricity; for this example eccentricity ($e = 0.01$) for the equivalent point mass was set to 1% of the length of the beam.

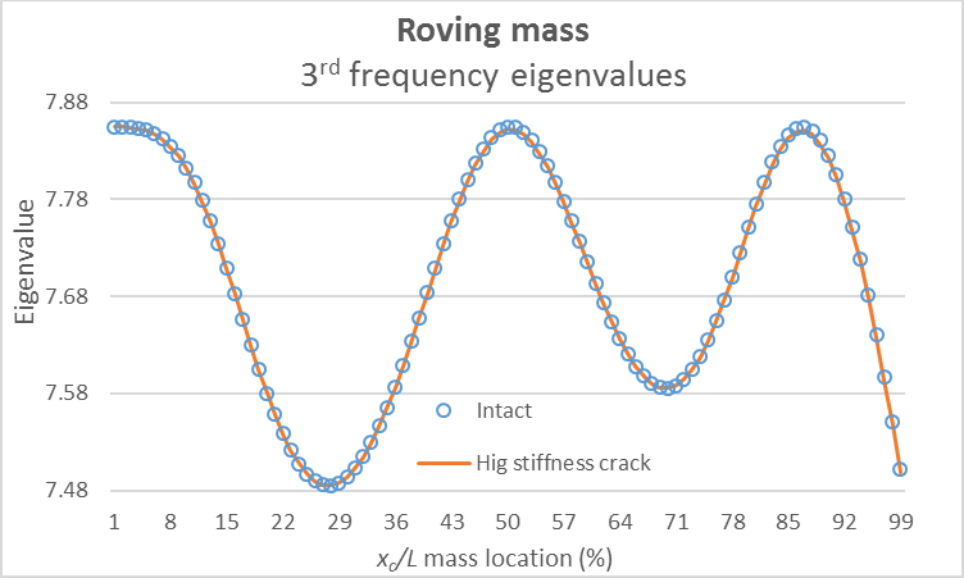

Figure 5.5. Roving mass on intact cantilever beam. Third eigenvalues shift, $e\neq0$

The resulting graphs, Figure 5.5, do not show any noticeable effect of the added rotary inertia, but the difference can be noted in the third decimal place. The maximum change in the frequency due to the rotary inertia effect was near to 0.05% of the third natural frequency.

Regarding the combined effect of the mass and the cracks with low stiffness, $k = 1$ equivalent to a non-dimensional crack length of over 30% (Figures 5.6 to 5.8), a reduction in the frequency at the first and second eigenvalues is noted and a sudden change in the continuity of the graph for the second one.

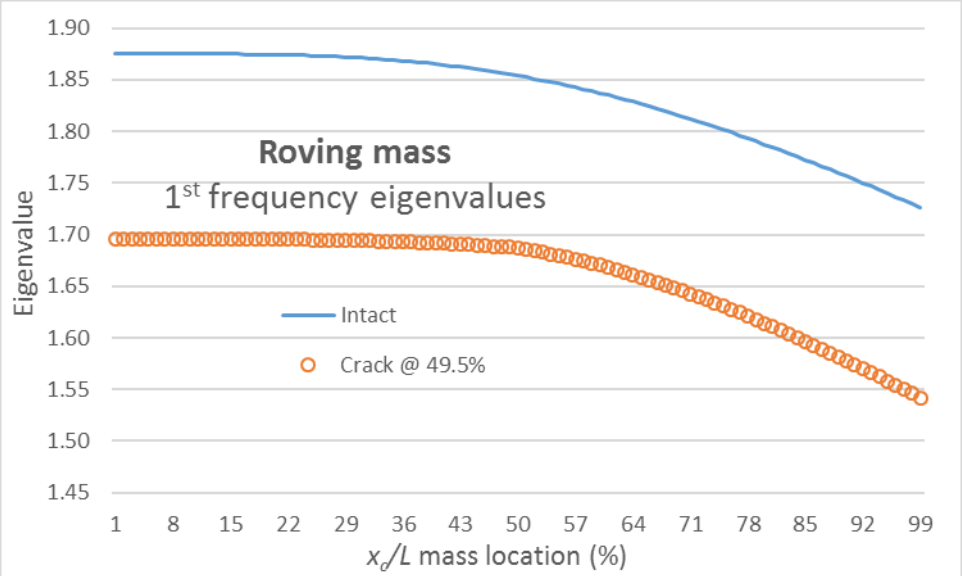

Figure 5.6. Roving mass on cantilever beam cracked @49.5%. First eigenvalues shift, $e \neq 0$

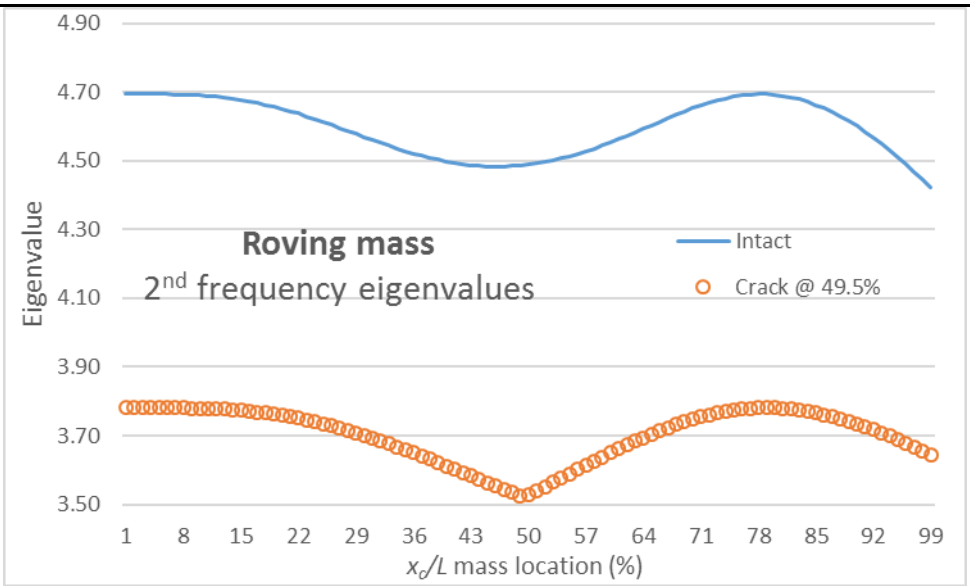

Figure 5.7. Roving mass on cantilever beam cracked @49.5%.

Second eigenvalues shift, $e \neq 0$

Figure 5.8 shows on the other hand that even with a low crack stiffness, there are no signs of a crack on the third eigenvalue, basically because the location of the crack lies on a contra-flexure point at this eigenvalue, as can be seen back in Fig. 3.6.

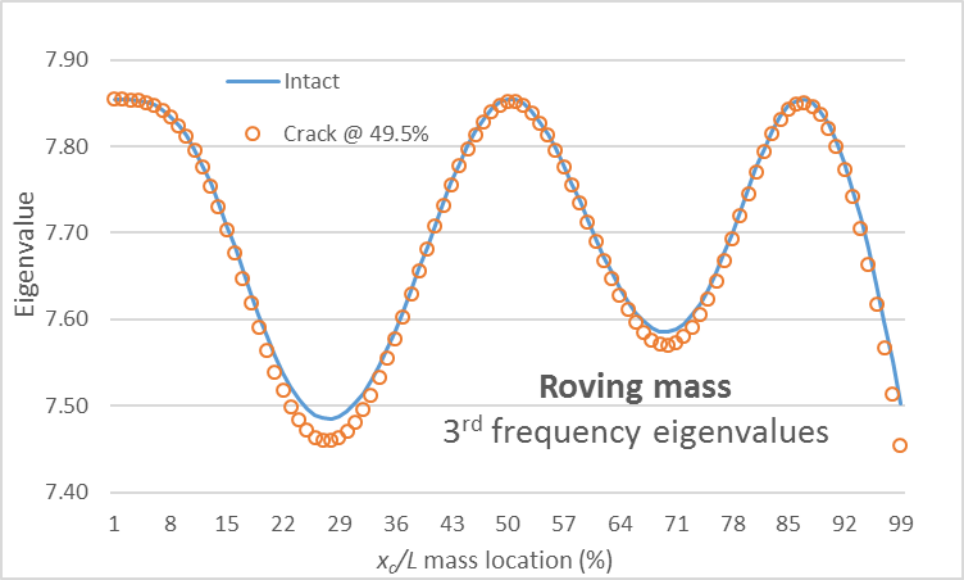

Figure 5.8. Roving mass on cantilever beam cracked @49.5%. Third eigenvalues shift, $e \neq 0$

From the last observation we can infer that the determinant factor on the frequency shifts due to cracks is the relative position of the crack with the contra-flexure points. Therefore, to gain readability in the graphs, the crack location is selected from Fig.3.6 and from it, the crack was now chosen in a location near the 40% of the length from the clamp where according to Fig. 3.6 there are no contra-flexure point for any of the first three eigenvalues.

Figures 5.9 to 5.11 show the behaviour of the frequency shift of a cantilever beam with a point mass roving within the length. In this occasion a reduction in the frequency at all the eigenvalues is seen.

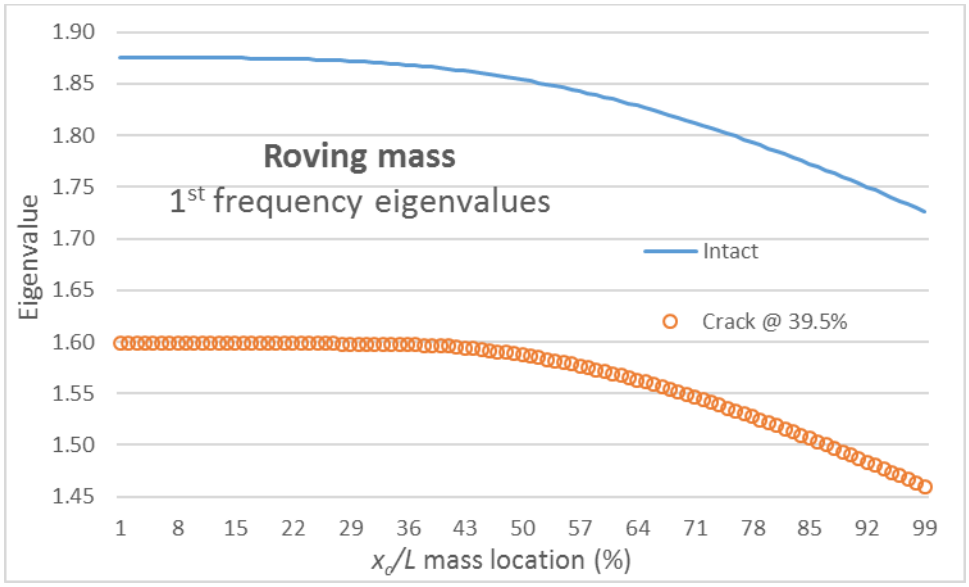

Figure 5.9. Roving mass on cantilever beam cracked @39.5%. First eigenvalues shift, $e \neq 0$

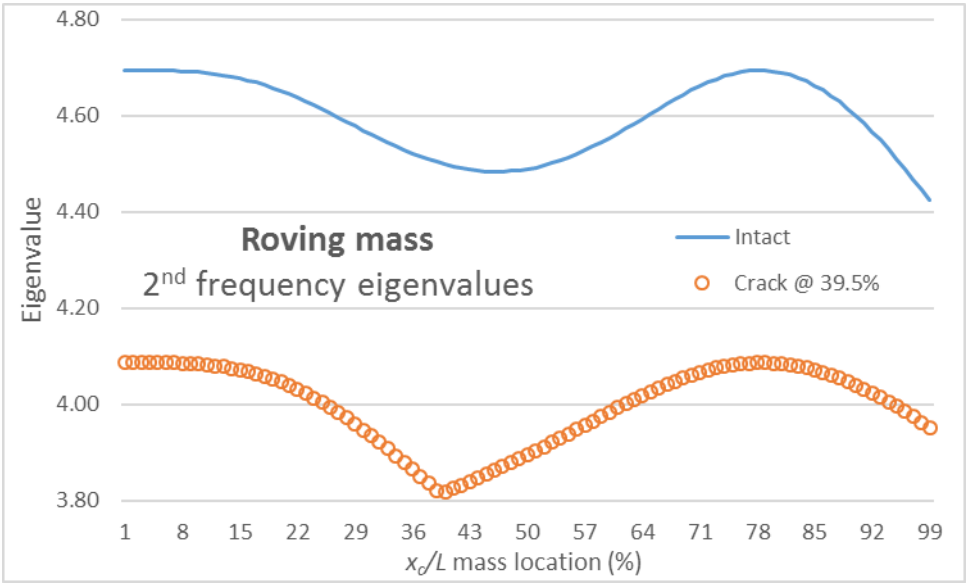

Figure 5.10. Roving mass on cantilever beam cracked @39.5%. Second eigenvalues shift, $e \neq 0$

It may be noted from Figures 5.10 and 5.11 that a jump in the slope of the graph occurs when the roving mass passes the crack. For the second frequency, as long the mass roves from the clamped end on the intact beam, the frequency decrease towards a minimum at its mid span; but in the beam cracked at its 40% length, the frequency starts to increase immediately after the mass passes the crack.

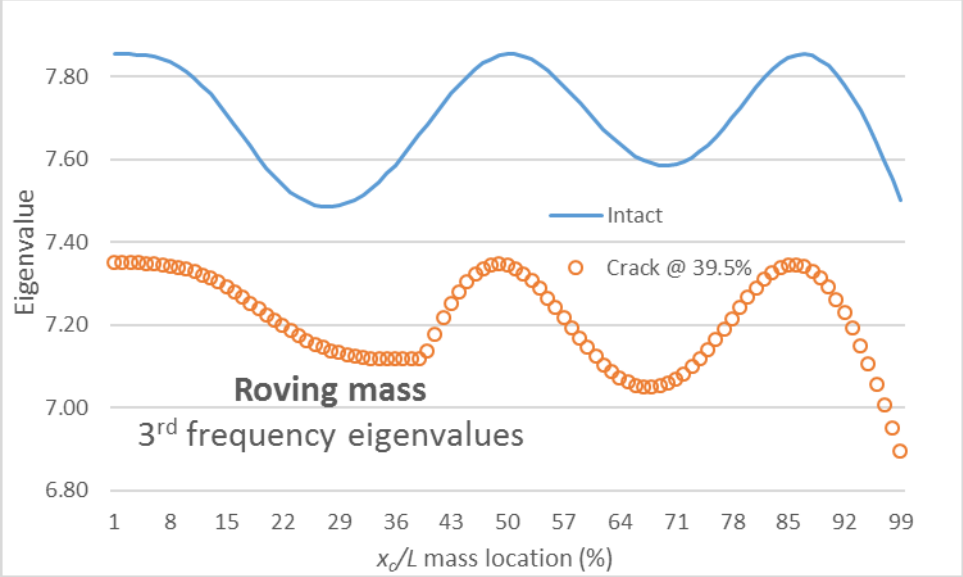

Figure 5.11. Roving mass on cantilever beam cracked @39.5%. Third eigenvalues shift, $e \neq 0$

In the case of the third frequency, the minimum frequency is reached farther than in the intact scenario exactly on the crack location. The previous results reveals a promising way of conducting damage identification based on the frequency shifts only.

Table 5.1 shows the values of the obtained eigenvalues in the roving mass locations when it is near the crack to give an idea of the different changes due to crack and roving mass location.

Table 5.1. First and third eigenvalues for cantilever beams using DSM.

Intact		1.875104			Intact		7.854756		
	@39%	@40%	@41%	@42%		@39%	@40%	@41%	@42%
mo	1.866112	1.865272	1.864383	1.863443	mo	7.658236	7.68354	7.708844	7.733666
mo + ecc	1.866093	1.865253	1.864363	1.863423	mo + ecc	7.657205	7.682342	7.707472	7.732119
Cracked @39.5%		1.598713			Cracked @39.5%		7.350299		
	@39%	@40%	@41%	@42%		@39%	@40%	@41%	@42%
mo	1.596602	1.596229	1.595632	1.594968	mo	7.116941	7.13927	7.181539	7.219826
mo + ecc	1.596597	1.596198	1.595600	1.594936	mo + ecc	7.116941	7.136037	7.178226	7.216438

The values in the table show that numerically speaking, identification of the jump in the frequency shift due to a crack could be a challenge due to the proximity of the order in those values even for crack locations far from points of contra-flexure, especially in lower frequencies. There is a property that could emerge from the characteristic equation developed in Section 5.2: that is the higher the frequency the higher the jump, which means it is easier to identify. This is because the resisting moment due to rotary inertia is proportional to the square of the frequency.

Therefore a point mass may help to identify a damage when looking at the frequency shift graph of higher frequencies where the crack locations is between points of contra-flexure using a device with enough eccentricity from the neutral axis of the beam so as to generate a sufficiently large local moment that could be perceived by the measuring equipment.

5.2.2 Single cracked beam: Frequency values.

For a final verification of the obtained results and the effectiveness of roving a point mass to identify the crack location on a beam, a simple experiment was performed using available equipment at the University of Waikato (UoW) and simple enough to understand the effect of the variables considered as well as to be reproduced anywhere. The heart of this work is to capture the effect of cracks mainly through the use of frequency measurements. Therefore the experiment relies on the capture of the natural frequencies in a structure on the basis of the Frequency Response Function (FRF) between an input and an output.

The UoW possesses the CoCo-80, a commercial vibration analyser developed for Cristal Instruments with built-in hardware and software ready to use for vibration measurements. The input was generated by an impact hammer developed by Brüel & Kjær with interchangeable head tips for low, medium and high frequencies while the output was sensed by a triaxial and multipurpose accelerometer developed by the same Nordic company.

The analyser parameter in this case is the defining point for the experiment. Frequency resolution in the CoCo-80 is dependent on the frequency range and the resolution of the scale. For this reason the best frequency resolution had to be limited to the lower band of the spectrum.

Regarding the specimen, a metallic beam was selected because of the homogeneity of the mechanical properties. The experiment was performed with two identical beams made of flat aluminium bar of 25mm width and 3mm thickness. The cantilever condition was achieved by clamping one end to a supposedly rigid desk (Fig. 5.12) and to avoid rotations two bolted steel plates were used to clamp the beam.

Figure 5.12. Cantilever fixed end detail

The clear span of the beams (final length of the beam discounting the bolted plates) is 480mm and the expected natural frequencies for the three first eigenvalues are $f_1 = 10.71\text{Hz}$, $f_2 = 67.12\text{Hz}$ and $f_3 = 187.93\text{Hz}$ supposing an elastic modulus $E = 70\text{GPa}$ and a mass density $\mu = 202.5\text{g/m}$.

The CoCo-80 frequency range is set to a maximum of 180Hz making the frequency resolution equal to 0.5Hz on the display. The accelerometer is located on the free end and the impacting point is marked near the fixed end, after 40s the analyser shows three differentiable peaks in the FRF graph (Fig 5.13) at $f_1 = 7.74\text{Hz}$, $f_2 = 54.16\text{Hz}$ and $f_3 = 158.98\text{Hz}$, corresponding to the first three natural frequencies of the cantilever beam.

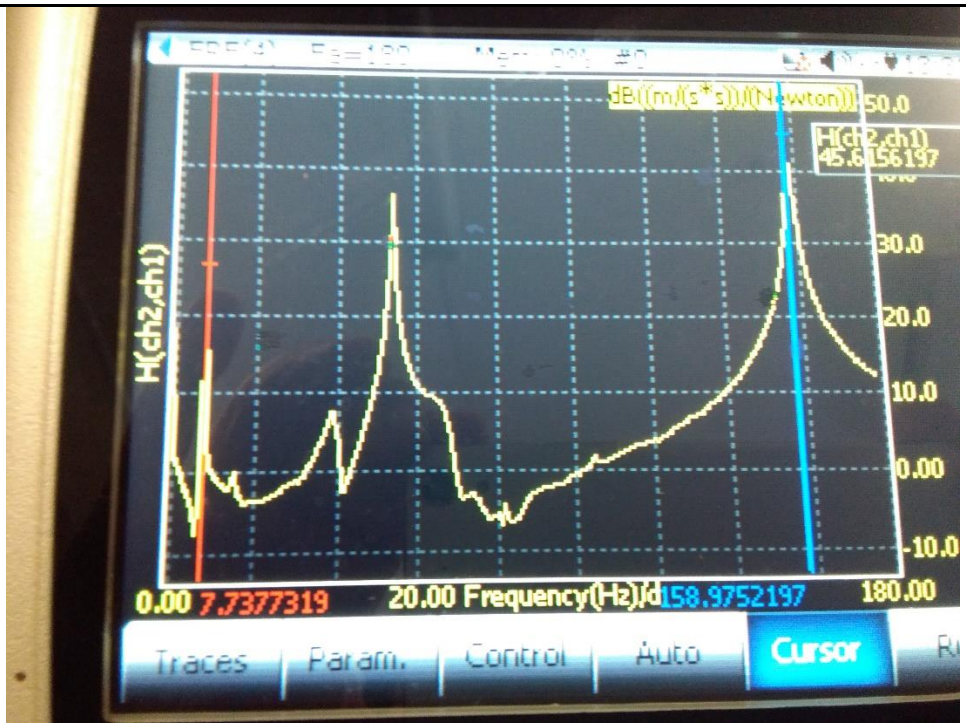

Figure 5.13. Measured FRF peaks for intact aluminium cantilever beam

The difference between theoretical and experimental frequency values may have many causes. Error analysis on the translation from non-dimensional parameters to measured dimensions may help to identify the variables with the major impact. Equation (A.1) in the appendix indicates that eigenvalues, length and height variations are the most influential in the final frequency value.

The mass of the accelerometer and its connector are 10% of the mass of the beam affecting eigenvalues, additionally, material properties ($\mu = 2677\text{kg/m}^3$ and $E = 61\text{GPa}$) were characterised in the Large Scale Laboratory of UoW.

Table 5.2. Updated frequencies.

frequency	λ_i		f_i (Hz)
	theory	$+m_{acc}$	updated
1st.	1.875	1.726	8.51
2nd.	4.694	4.423	55.87
3rd.	7.855	7.502	160.73

As realising fully clamped conditions is difficult, the clamped end may have had some flexibility. The lack of rigidity in the support will be disregarded because the aim is not to validate the frequency equation but to see if there is any sudden shift in the frequency as the rowing body passes the crack. This will be addressed in the next chapter.

The same experimental set-up is made for the second beam specimen with a reduction of almost 50% in its sectional area at 40% of the length measured from the fixed end that was found to produce noticeable effect due to the crack in the third natural frequency. The FRF peaks (Figure 5.14) are now located at $f_1 = 7.74Hz$ $f_2 = 53.46Hz$ and $f_3 = 158.27Hz$, giving an indication of rigidity loss somewhere along the beam.

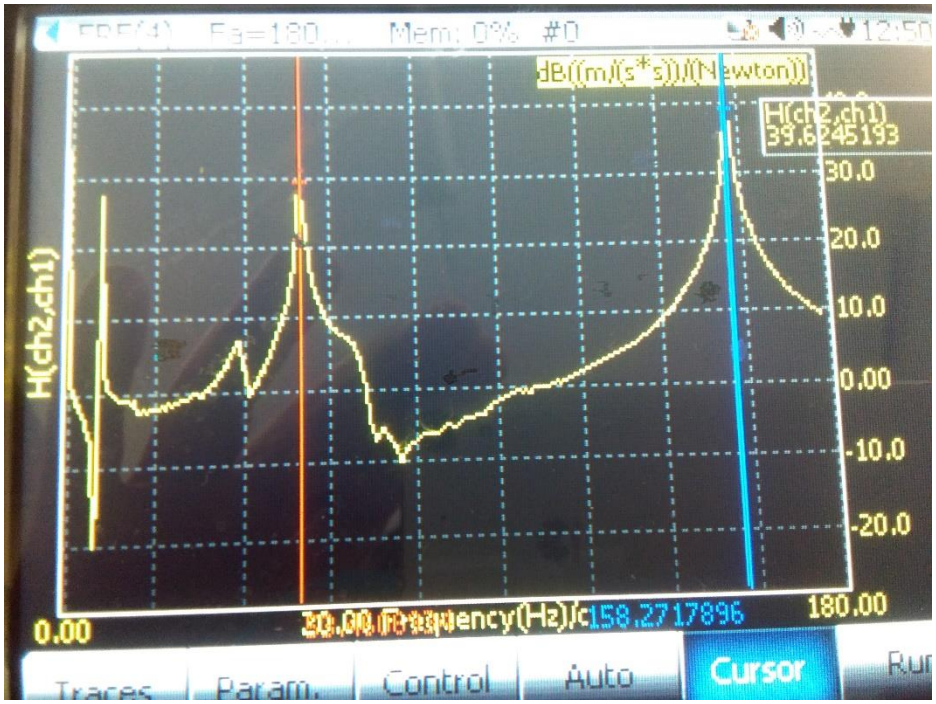

Figure 5.14. Measured FRF peaks for cracked aluminium cantilever beam

The same clamp used to avoid rotations on the fixed end will be used as a point mass with rotary inertia. For the purpose of this experiment the clamp will be secured for both the intact and cracked beam only in four positions labelled as shown in Figure 5.15 covering two places before the crack and two places after the crack.

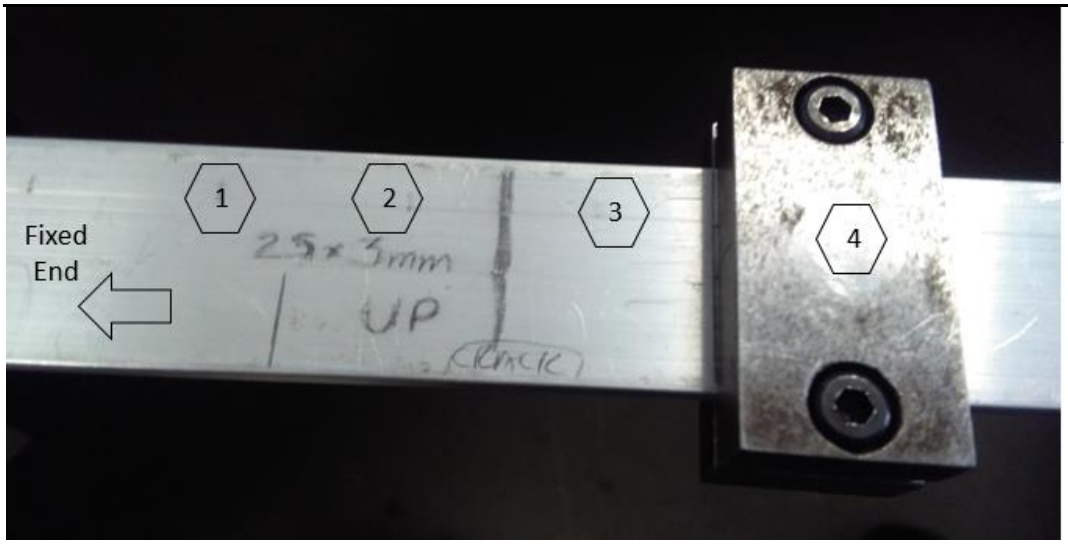

Figure 5.15. Mass attaching points relative to crack location

It is important to remember that the third frequency will be chosen because the crack effect is expected to be higher in this case compared to the first two. The plots of Figure 3.6 are now separated for each frequency (Figures 5.16 and 5.17) in order to present the intervals where the damage has the highest effect in addition with a line called sensitivity threshold indicating what will be the crack positions that will be detected in the particular frequency.

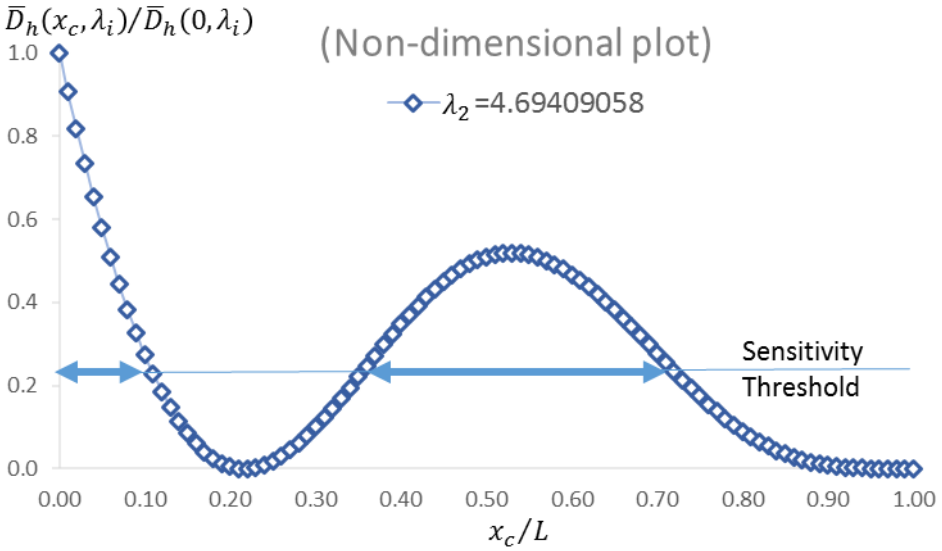

Figure 5.16. Intervals with high crack effect selection. Second natural frequency

The threshold line can be designed by modifying the eccentricity of the point mass according to the frequency resolution of the equipment and the minimal crack severity that is expected to be identified.

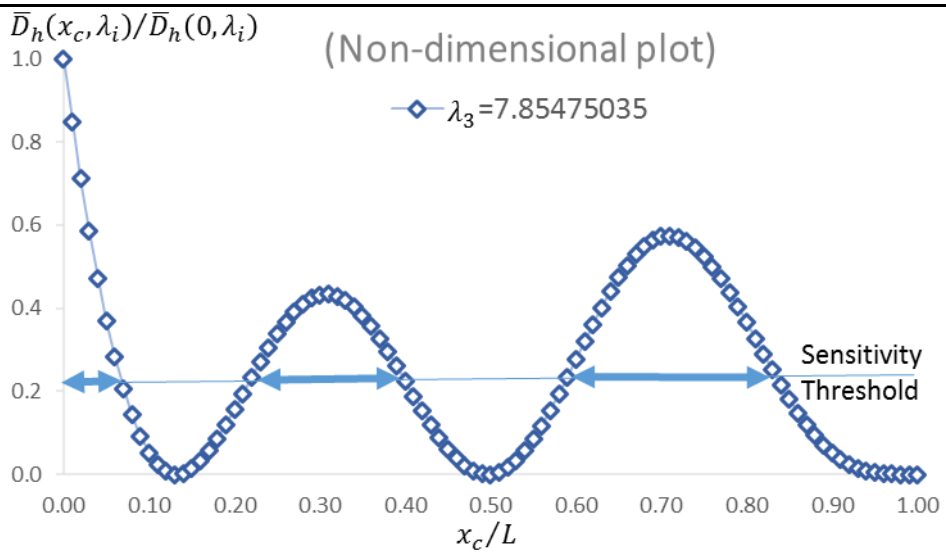

Figure 5.17. Intervals with high crack effect selection. Third natural frequency

According to Figure 5.11, on the interval near to 40% of the length, the frequency shift increases monotonically when the body is roved towards the free end for the intact beam but a sudden increase must be appreciated if there is a crack on that section.

The point mass location and the measured frequency values for the third frequency are presented in Fig. 5.18 as a schematic representation of Fig. 5.15. On the upper half there are presented for the intact beam the frequency values in Hertz at each point mass location and their relative change respective with the values at the previous location. Similar fashion is followed on the lower half now in the presence of a crack at the end between sections two and three.

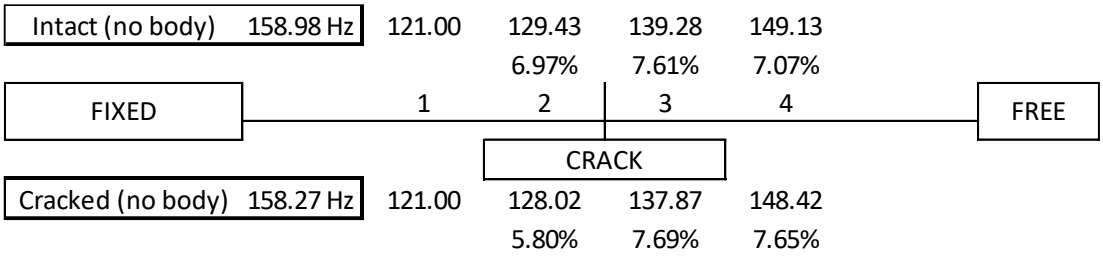

Figure 5.18. Measured third frequency with added mass

The relative changes obtained between the different locations of the body for the undamaged beam remain relatively constant (in the range 6.97% to 7.61%) for this frequency in this beam segment. For the cracked beam with the roving body, there is a relatively higher change as the body passes the crack (5.8% to 7.69%). This indicates that the flexibility due to the crack is amplified in the presence of the roving body, although the values obtained do not make a conclusive case for the reasons mentioned later.

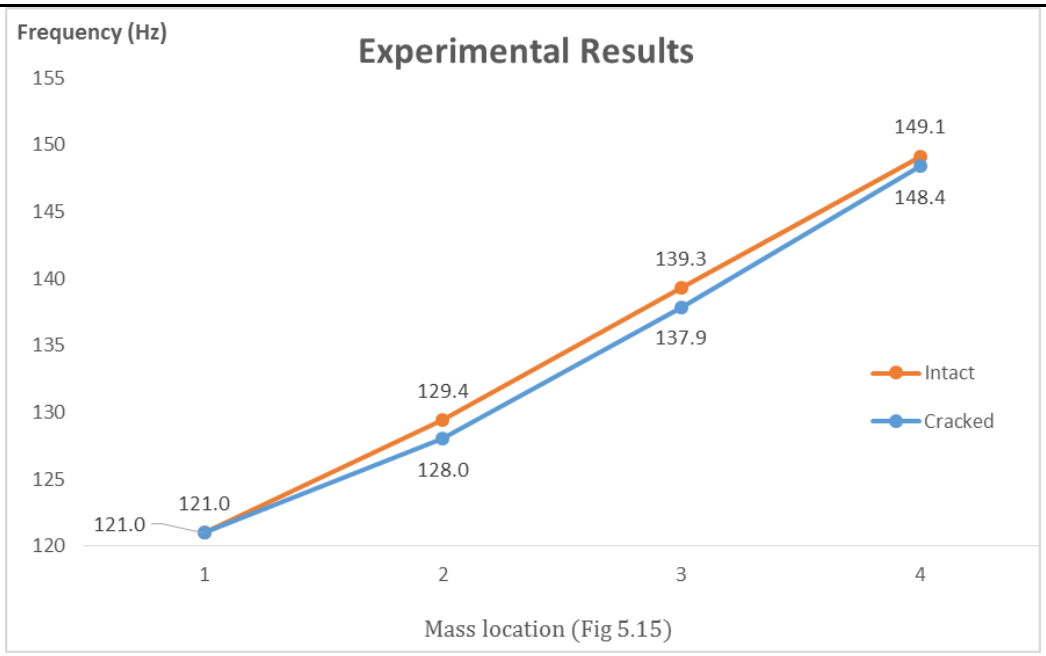

Figure 5.19. Experimental results for the third frequency with added mass

Figure 5.19 shows that the gap between frequencies in the measured section increase only between points 2 and 3; on the other hand in position one, there is no change between intact and cracked beam while in position four it is possible to appreciate a reduction on the measured frequencies for the two states.

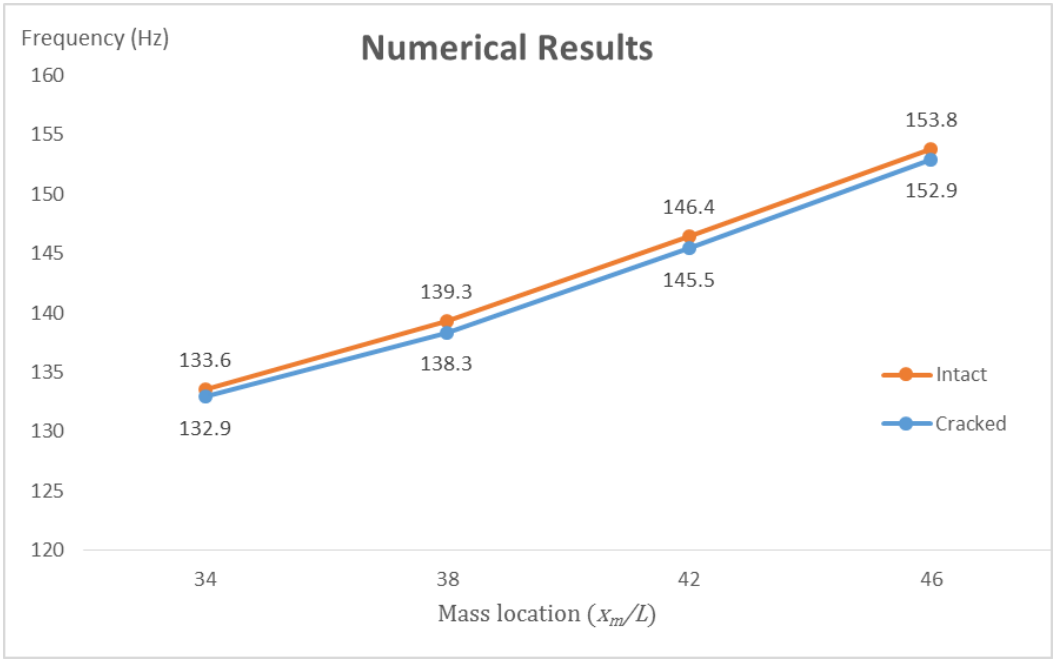

Figure 5.20. Numerical results for the third frequency with added mass

Numerical simulation using DSM were performed assuming a non-dimensional stiffness $k = 100$, considering the point mass with rotation on the geometrical centre and the mass of the accelerometer on the free end. Figure 5.20 shows the plot of the

numerical simulation results which hold the same particulars mentioned for the experimental ones. The lower frequency values in the experiment may indicate a flexibility not considered in the simulation. One probable cause is the clamp rigidity assumed perfect that could allow rotations in reality.

A lesson learnt from this is that the fixed boundary conditions are harder to realise and free-free beam may be offer a better choice. In practice this means suspending it on very flexible supports.

Another lesson learnt from the experiment is the influence of the size of the body on the axial coordinate. The roving body has to be as thin as possible as otherwise it limits the number of measuring points along the beam. For this case, a 25mm width in a 480mm beam length allows only 19 measuring points and Fig. 4.11 will become a discrete plot as is shown in Fig. 5.21 where a closer look of the cracked case reveals two trends on the plot with the crack as their limit. This needs to be born in mind in future experimental planning.

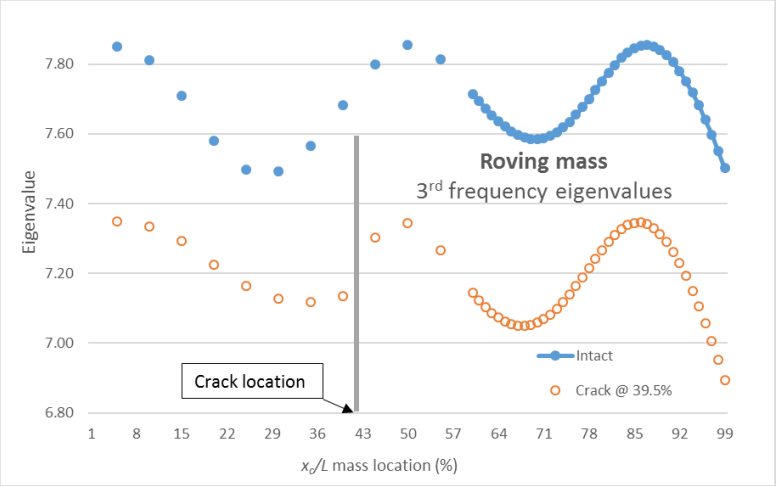

Figure 5.21. Discrete values for the third frequency with added mass

5.3 Summary

This chapter demonstrates that the concept of roving a mass within the length of a beam promises to be a powerful tool for damage identification particularly in the location of local flexibilities. The theory and numerical simulation indicated that when the mass is designed in such a way that its rotary inertia affects the structure, the section with the local flexibility (crack) could be discerned accurately leading to a new crack location methodology if measurement techniques are improved and experimentally

verified. Regarding to the experimental application of the theory, difficulties in securing a perfect clamp end, uncertainty of the inertial effect of the attached accelerometer and physical limitations on the location of the probe mass demand a higher level of sophistication to claim success with the proposed location methodology. In the next chapter, the inverse problem will be addressed using frequency shifts only; initially to identify location and severity of a structure with one crack, and afterwards offers an example to determine the local flexibility when the location is known.

Chapter 6

Inverse Problem

The previous chapters were devoted to presenting the characteristic equations of structures in the presence of elements which impact their dynamic response. Additionally the numerical simulations offer an understanding of the effect of each of these factors on the natural frequencies. Furthermore, it was proven that the determinant of a structure could be decoupled as many times as needed, as additional non-structural elements with dynamic effect are attached to the system. In this chapter, a method to identify the location and amplitude of a flexibility element using only natural frequency measurements is presented. System identification will be achieved by controlled changes to the system, through the use of an attached mass and the decoupling of the determinant of the new system.

6.1 Identifying local flexibility

The procedure for identifying a damage starts with a crack being seen as an agent of local flexibility which changes the natural frequencies. For this procedure, then the natural frequency measurements are needed. Based on the fact that the determinantal equation Eq. (3.6) for a single cracked structure is valid for all the natural frequencies of the structure and, the first two natural frequencies $\omega = \omega_1$ and $\omega = \omega_2$ this relationship will take the following forms:

$$D_c(x_c, \omega_1) = kD_0(x_c, \omega_1) + D_h(x_c, \omega_1) = 0 \tag{6-1}$$

$$D_c(x_c, \omega_2) = kD_0(x_c, \omega_2) + D_h(x_c, \omega_2) = 0 \tag{6-2}$$

Equating k from the above equations gives

$$k = \frac{-D_h(x_c, \omega_1)}{D_0(x_c, \omega_1)} = \frac{-D_h(x_c, \omega_2)}{D_0(x_c, \omega_2)} = \frac{-D_h(x_c, \omega_3)}{D_0(x_c, \omega_3)} \tag{6-3}$$

This is because the spring stiffness is a constant for all the natural frequencies. Therefore, evaluating the determinant ratio at the measured frequencies at different locations will provide us with the values of k that nullifies the characteristic equation. Those locations where the stiffness value is a constant may be the more likely crack positions. If there is more than one possible location, then the search can be narrowed down by bringing in further natural frequencies $\omega = \omega_3, \ldots$ etc.

The previous paradigm of damage detection demands a statistical treatment to get rid of the severity variable and needs a model for the stiffness of the spring, related to the crack geometry and structure load [48]. One of the main features of the proposed methodology is the use of functions that are independent of the severity of the damage. Therefore using only vibrational measurements, the location of the crack will be defined without knowing the severity.

Labib, et al. [69] developed a similar procedure by means of a difference parameter dependent only on the location of the crack after normalising the shifts in the assumed natural frequencies using the DSM. In his procedure the parameter of the assumed and measured natural frequencies are assessed at all the possible locations of the structure and those where there are no differences indicate the most probable location of damage. To evaluate the procedure Labib [92] worked with a two bay, two storey steel frame with clamped bases as shown in Fig. 6.1.

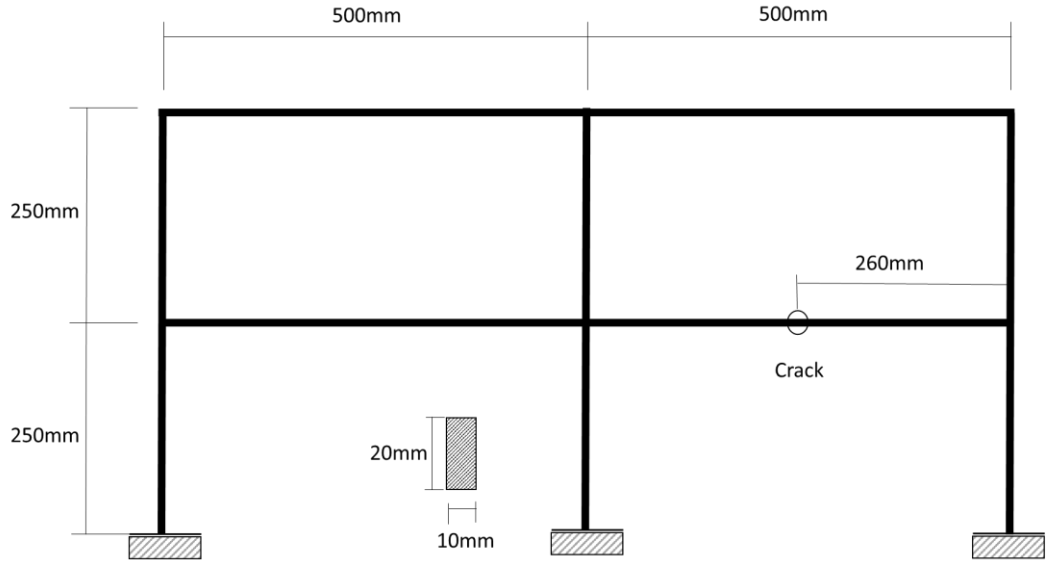

Figure 6.1. Two bay, two storey frame used by Labib (2015).

The analytical and experimental natural frequencies for the intact structure reported by Labib are presented in Table 6.1 as well as those calculated for this report.

Table 6.1. First six frequencies for 2B2S intact frame

	f_1 (Hz)	f_2 (Hz)	f_3 (Hz)	f_4 (Hz)	f_5 (Hz)	f_6 (Hz)
Labid (DSM)	38.54	128.01	142.54	168.92	176.86	193.83
Labid (Exp)	-	-	140.93	168.46	177.12	194.21
This work (DSM)	38.547	128.039	142.635	169.112	177.238	194.562

The calculations based on the DSM were repeated because it was noticed that the measured frequencies were higher for the fifth and sixth modes while the third and fourth values were lower. These calculations perform a Matlab® zero finding function on the DSM of the structure discarding by means of the W-W algorithm those corresponding to determinant poles.

To illustrate the application of the methodology and its effectiveness in a simple search, the two bay two storey damaged frame was used in a numerical experiment. Its frequencies are calculated in the same fashion as for the undamaged frame but with the DSM updated with the crack severity and location established by Labib. These frequencies, obtained numerically from the defined crack, are assumed as acquired from an experiment ("pseudo-experimental" data using the same terminilogy as in [72]) and listed in Table 6.2.

Table 6.2. Pseudo-experimental data for intact and cracked frame

	f_3 (Hz)	f_4 (Hz)	f_5 (Hz)	f_6 (Hz)
Intact	142.635	169.112	177.238	194.562
Crack @52%, k=100	142.625	169.082	177.212	194.495

Using the expression stated in Eq. (6.3) the respective values for $D_0(x_c, \omega_i)$ and $D_h(x_c, \omega_i)$ for a set of ninety nine equally spaced locations were calculated and the stiffness values that nullify Eq. (3.6) are obtained for each measured frequency and plotted in Figure 6.2. All the obtained curves are located on the positive side of the stiffness, and intercept in a unique crossover point at 52% of the cap and in the stiffness value of 0.29EI. The positive value of stiffness is consistent with the reduction in the natural frequencies for the intact beam and the crossing point indicates that, for this particular member, from all the possible stiffness values there is one and only one possible crack location.

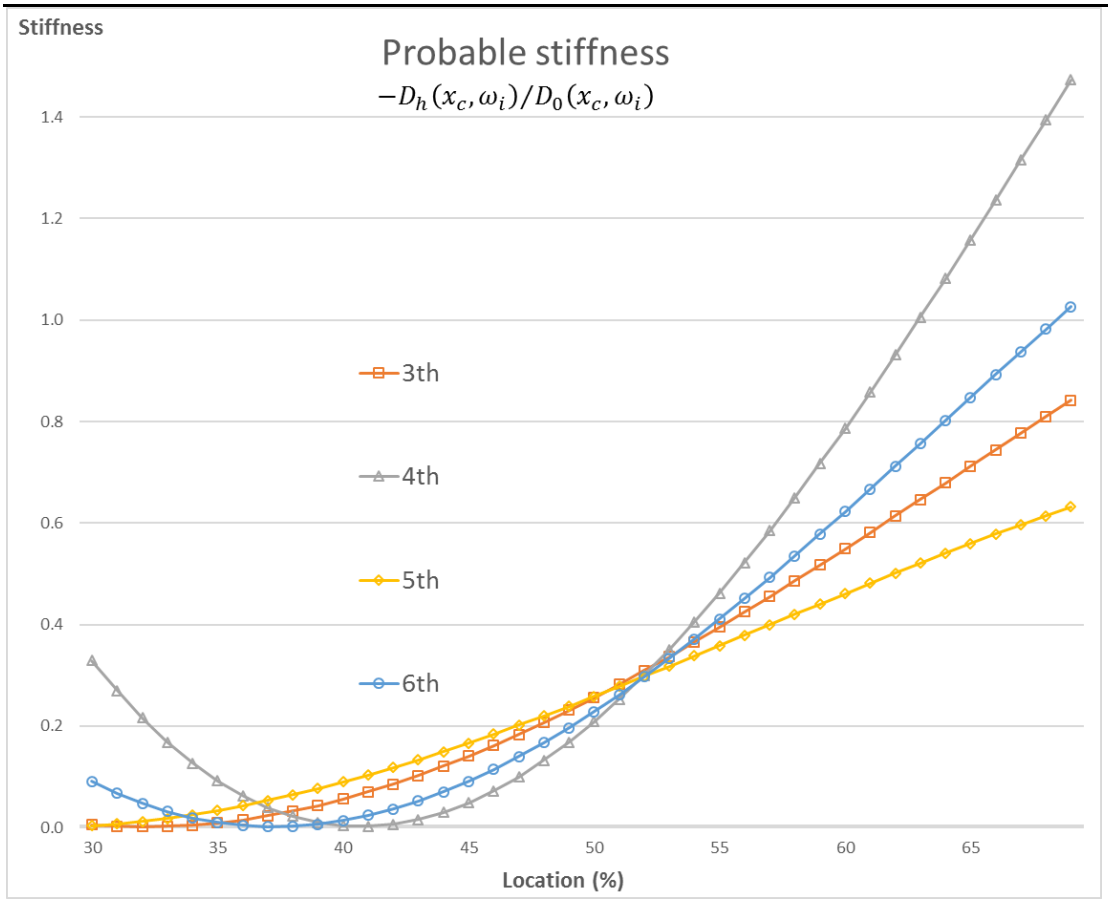

Figure 6.2. Numerical search from pseudo-experimental data on Labib frame

The previous graph was achieved because of the use of values obtained from the numerical simulation, which could only be obtained in a perfect world where the measurement equipment is not affected by external sources. In real life, there is no such a thing as precise measurements and there will be always many factors of uncertainty that need to be considered. As an example of the effect of a small deviation in the measurements, Figure 6.3 shows the obtained plot for $f = 176.94Hz$, the fifth frequency measured by Labib using his equipment frequency resolution of 0.6Hz.

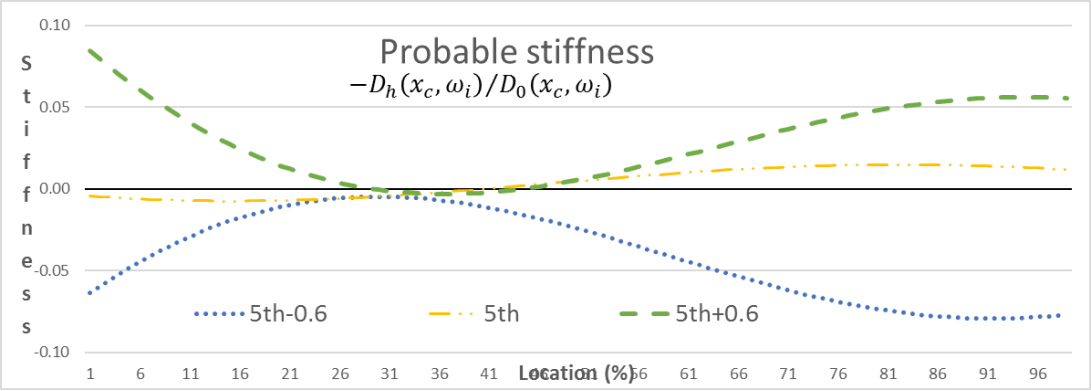

Figure 6.3. Probable stiffness changes on 0.6Hz frequency resolution.

Figure 6.3 shows that the frequency resolution for this particular structure matters. The negative stiffness value refers to an increment whether in the local stiffness or flexibility creating uncertainty about the actual situation and reducing confidence on the experimental values

A detailed picture of this issue is presented in Figure 6.4 using Labib measurements listed in Table 6.3 with two choices for the 5th frequency, a dashed and dotted line for Labid measurement and a dashed line for the one with an increment equal to the equipment resolution.

Table 6.3. Experimental frequencies for intact and cracked frame. Labib (2015)

	f_3 (Hz)	f_4 (Hz)	f_5 (Hz)	f_6 (Hz)
Intact	140.93	168.46	177.12	194.21
Crack @52%	140.69	167.24	176.94	192.81

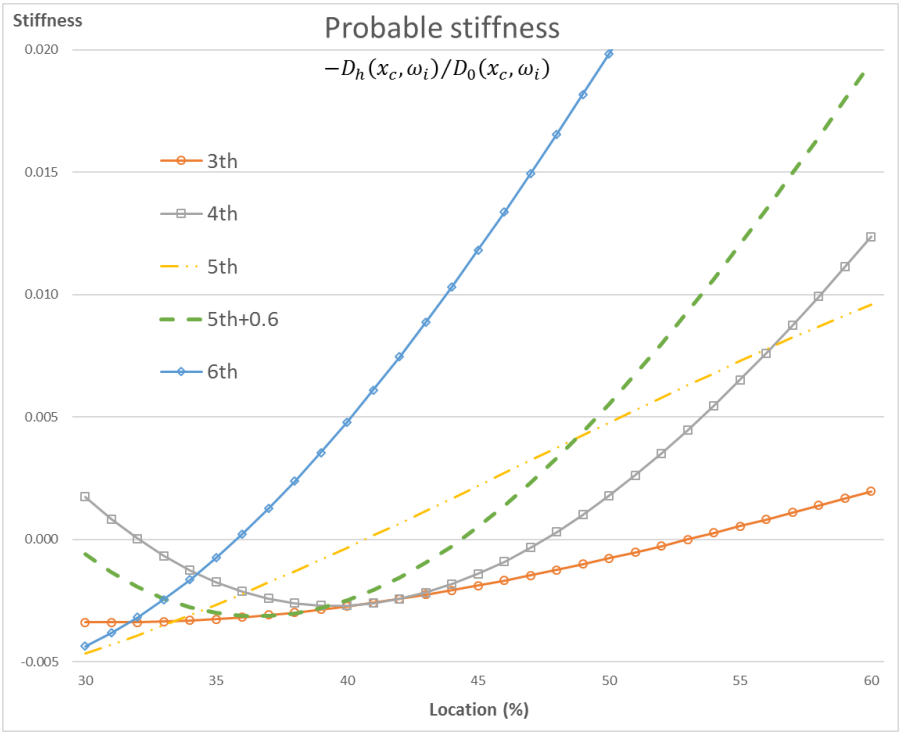

Figure 6.4. Numerical search from Labib measured values on frame

The real crack location could be captured checking one of the two crossing points between the fourth and fifth frequency near to the 35% and 55% of the length. Using the third frequency will help to discard one of those probable locations, but instead another crossing point between the third and fourth lines occurs near to the 40% of the beam element that becomes a triple crossing when the increased fifth frequency is used instead of the one reported by Labib breaching the confidence of the experiment.

The use of the DSM method in the characteristic equation leads to an exact solution, allowing the formulation of more accurate models with less computational burden. However, when using the DSM, small changes in the frequency produce high variations in the determinant values. Although this high sensitivity approach generates good precision in computer simulation, it becomes a big issue in damage identification because most of the damage scenarios produce a frequency spectrum that lies in the noise intervals generating a lack of reliability as in the present example.

6.2 System identification

Identification of parameters in modelled systems was the initial application of vibration measurements to validate mathematical and computational models. The necessity to maintain an updated model is due to the acceptance that a good initial model guarantee a better prediction of the real world. Experiments performed by Narkis and Elmalah [93] and Alfano and Pagnotta [94] Türker and Bayraktar [95] are just few research publications of parameter identification. This section develop procedures to identify the actual values of fixed supports using measured frequencies and determinantal equations derived in previous chapters.

The classical boundary conditions are a combination of three supports free, pinned and clamped according with or without the restriction of translational and rotational displacements. As mentioned in Chapter 3, for a beam with clamped ends when a severe crack is located immediately next to the ends, the expected natural frequency will be similar to a beam with a pinned end because the crack may allow rotational displacement, therefore a clamp allowing rotational displacements could be updated using the model proposed in the next paragraph.

The inverse problem is defined to determine the actual rigidity of the fixed end modelled as a combination of a pinned support and a rotational spring of stiffness k. The problem is to find the k value that solves the characteristic equation for the system of Fig 6.5, which may be seen as the special case for the problem posed in Fig 4.1 with a known crack location.

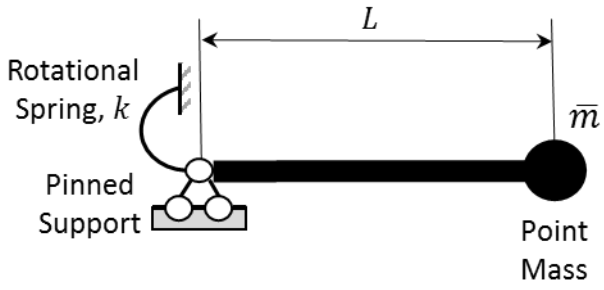

Figure 6.5. Model for a loose clamp with a probe mass

The dynamic equation of the system nodal values is defined by

$$\begin{bmatrix} M_L \\ M_R \\ V_R \end{bmatrix} = EI \begin{bmatrix} S+\bar{k} & SC & -Qq \\ SC & S & -Q \\ -Qq & -Q & T-m^* \end{bmatrix} \begin{bmatrix} \theta_L \\ \theta_R \\ \delta_R \end{bmatrix} \tag{6-4}$$

where the subscripts in the stability functions listed in Table 3.1 have been removed because the segment length is equal to the beam length $L_e = L$.

$$S = \frac{\lambda[\sin(L\lambda)\cosh(L\lambda) - \cos(L\lambda)\sinh(L\lambda)]}{1-\cosh(\lambda L)\cos(\lambda L)}$$

$$SC = \frac{\lambda[\sinh(\lambda L) - \sin(\lambda l)]}{1-\cosh(\lambda l)\cos(\lambda l)}$$

$$Q = \frac{\lambda^2[\sin(\lambda L)\sinh(\lambda L)]}{1-\cosh(\lambda L)\cos(\lambda L)}$$

$$Qq = \frac{\lambda^2[\cosh(\lambda L) - \cos(\lambda L)]}{1-\cosh(\lambda L)\cos(\lambda L)}$$

$$T = \frac{\lambda^3[\sin(L\lambda)\cosh(L\lambda) + \cos(L\lambda)\sinh(L\lambda)]}{1-\cosh(\lambda L)\cos(\lambda L)}$$

With k the rotational stiffness, and m the frequency parameter dependent on the added mass defined as $m^* = \frac{\omega^2}{EI}\bar{m}$ with ω the circular natural frequency.

Expansion of Eq. (6.4) leads to the closed form stated in Eq. (4.6) and rewritten in Eq. (6.5), for this case is simpler because the position of the crack in known $x_c = 0$, and the position of the mass is set at the free end, $x_m = L$.

$$D_{cm}(\omega) = kD_0(\omega) + D_h(\omega) - mkD_{hm}(\omega) - mD_{mc}(\omega) = 0 \tag{6-5}$$

Here,

$$D_0(\omega) = \lambda^4(1+\cos(L\lambda)\cosh(L\lambda))$$
$$D_h(\omega) = \lambda^5\big(\cos(L\lambda)\sinh(L\lambda) - \sin(L\lambda)\cosh(L\lambda)\big)$$
$$D_{hm}(\omega) = \lambda\big(\sin(L\lambda)\cosh(L\lambda) - \cos(L\lambda)\sinh(L\lambda)\big)$$
$$D_{mc}(\omega) = 2\lambda^2(\sin(L\lambda)\sinh(L\lambda))$$

Knowing the inertial effect of the mass and with the measured frequency the equivalent spring stiffness of the not so rigid clamped end is calculated with

$$k = \frac{D_{hc}(\omega) - mD_{mc}(\omega)}{mD_{hm}(\omega) - D_0(\omega)} \tag{6-6}$$

The stiffness value is found for each measured frequency and the average value may be set as the one to be used in the updated model.

Table 6.4. Experimental frequencies for cantilever beam with loose clamp.

		Probe mass (g)	
		19	14.3
		Stiffness (MN.m)	
Frequency (Hz)	7.24	10.76	10.34
	7.74	15.07	14.33
	8.24	22.53	21.05
	54.66	29.21	26.04
	54.16	25.85	23.18
	53.66	22.99	20.69
	158.48	41.39	35.27
	158.98	44.25	37.58
	159.48	47.39	40.08

If the additional mass is considered as unknown, a homogeneous system of equations may be created considering any set of frequencies. For the developing example, each of the first three natural frequencies ω_1, ω_2, and ω_3 null $D_{cm}(\omega)$ in Equation (6.5) giving the equations

$$\begin{aligned} D_{cm}(\omega_1) &= kD_0(\omega_1) + D_{hc}(\omega_1) - mkD_{hm}(\omega_1) - mD_{mc}(\omega_1) = 0 \\ D_{cm}(\omega_2) &= kD_0(\omega_2) + D_{hc}(\omega_2) - mkD_{hm}(\omega_2) - mD_{mc}(\omega_2) = 0 \\ D_{cm}(\omega_3) &= kD_0(\omega_3) + D_{hc}(\omega_3) - mkD_{hm}(\omega_3) - mD_{mc}(\omega_3) = 0 \end{aligned}$$

or, in matrix form

$$\begin{bmatrix} D_{mc}(\omega_1) & D_{hm}(\omega_1) & D_0(\omega_1) \\ D_{mc}(\omega_2) & D_{hm}(\omega_2) & D_0(\omega_2) \\ D_{mc}(\omega_3) & D_{hm}(\omega_3) & D_0(\omega_3) \end{bmatrix} \begin{bmatrix} m \\ mk \\ -k \end{bmatrix} = \begin{bmatrix} D_{hc}(\omega_1) \\ D_{hc}(\omega_2) \\ D_{hc}(\omega_3) \end{bmatrix} \tag{6-7}$$

the eigenvector give us the unknown value for m and k and an additional term to check the solution. Unfortunately, the system loaded with the experimental data from Table 6.4 leads to unrealistic results. The obtained results for m differs from those obtained from the known inertial probe properties; and the product of m and k does not agree with those obtained individually.

6.3 Summary

This chapter proposed the use of the linear relationship of the determinantal equations derived from the DSM method for inverse problem applications. The failure in the identification of crack location and clamp flexibility indicates the need for more controlled experiments that will be addressed in the future work section at the end of the conclusions in the next chapter.

Chapter 7

Conclusions

7.1 Direct Problem: Properties of the determinantal equations

Two interesting properties of the determinantal expressions have been discovered through numerical experimentation, symbolic manipulation and mathematical proofs. The first is the relationship at any frequency ω, stated as $D_c(\omega) = kD_0(\omega) + D_h(x,\omega)$; between the crack severity k and the determinants of the cracked structure $D_c(\omega)$, undamaged structure $D_0(\omega)$ and a structure with a hinge $D_h(x,\omega)$ at the crack location x.

The above relationship permits to treat separately the two main properties of the crack, namely the severity and the location of the crack allowing a simplification to solve the inverse problem.

Regarding to the second interesting finding, it is stated as the relationship $\left(\frac{M^*}{\theta}\right)^2 = -D_h(x,\omega_0)$ between the square of M^*, the bending moment at the natural frequency of the undamaged structure ω_0 at any location x and the determinant of the structure with a hinge at the same location $D_h(x,\omega_0)$.

The above relationship, which can also be inferred from the work by Morassi [27] shows that if the hinge is located at a point of contra-flexure, where the bending moment is null in a particular mode, and therefore, $D_h(x,\omega_0) = 0$, the natural frequency at that mode will not be affected by a crack no matter how severe it is.

Using the stiffness matrix approach for the multi-cracked problem, the effect of each of the rotational springs along the length of an Euler-Bernoulli beam could be introduced into the required determinant in a recursive way by summing the characteristic equations of two beams, one where the beam is continuous in the crack location multiplied by the spring stiffness and the other where the crack is replaced by a hinge. This is repeated until all crack stiffnesses are included.

7.2 Inverse problem: Crack location

Using the DSM and numerical simulations it was proven that the roving of a body possessing rotary inertia introduces a sudden change in the frequency as the body passes through the crack location. It has been shown that the frequency shift due to

roving rotary inertia could lead to a simple procedure to identify the number of cracks and crack location without the need for any calculations.

Experiments were performed in an attempt to verify the applicability of simple tools and using a roving mass possessing rotary inertia to assess the location of a single crack in a cantilever beam. The expected sudden change in the frequency vs mass location was not easily discerned because the relatively low resolution of frequency measurement in the equipment used and uncertainties in the acceleration sensor and the fixity of the roving mass at the clamped end.

7.3 Future Work

There is an open window to explore the possibility of using the determinant of the hinged structure as the only tool for crack location and the use of the parameter identification to improve the crack model for high severities.

Determinantal properties which hold for any structure modelled with the DSM, could be extended to axially loaded beams and skeletal structures.

Experiments on simple structures need to be performed to validate analytical predictions of adding local inertias and/or boundary restrictions for parameter identifications and their summation effects. In addition, it will be necessary to develop mechanical devices that effectively transmit rotary inertia in real-life structures in order to validate the presented identification procedure.

Appendix

Error analysis

A non-dimensional frequency parameters are used during the calculations of eigenvalues for each DSM. To establish the influence on the final value of the measured frequency, an error analysis is performed starting from the parameter definition

$$\lambda^4 = \frac{\beta^4}{L^4} = \frac{\mu}{EI}\omega^2 = \frac{\rho A}{EI}\omega^2$$

$$\omega = \left(\frac{\beta}{L}\right)^2 \left(\frac{EI}{\rho A}\right)^{0.5}$$

For a rectangular section area is $A = bh$, and second moment of area $I = \frac{bh^3}{12}$ gives

$$\frac{EI}{\rho A} = \frac{Eh^2}{12\rho}$$

$$\omega = \left(\frac{\beta}{L}\right)^2 \left(\frac{Eh^2}{12\rho}\right)^{0.5}$$

Applying chain rule to the rate of change of the frequency

$$\frac{\delta\omega}{\omega} = \frac{\partial\omega}{\partial\beta}\frac{\delta\beta}{\omega} + \frac{\partial\omega}{\partial E}\frac{\delta E}{\omega} + \frac{\partial\omega}{\partial h}\frac{\delta h}{\omega} + \frac{\partial\omega}{\partial\rho}\frac{\delta\rho}{\omega} + \frac{\partial\omega}{\partial L}\frac{\delta L}{\omega}$$

And partial derivatives as is indicated

$$\frac{\delta\omega}{\omega} = 2\frac{\delta\beta}{\beta} + \frac{1}{2}\frac{\delta E}{E} + \frac{\delta h}{h} + \frac{1}{2}\frac{\delta\rho}{\rho} + 2\frac{\delta L}{L} \qquad \text{(A.1)}$$

The error in the eigenvalue values is highly dependent of the boundary conditions and the inertial effect of the accelerometer. The errors in the input parameters are as listed below

Elastic Modulus	δE= 10GPa	E= 70GPa
Section thickness	δh = 0.00005m	h = 0.003m
Volumetric density	$\delta\rho$ = 1kg/m^3	ρ = 2700kg/m^3
Specimen Length	δL =0.0005m	L =0.480m

Assuming that the determination of the eigenvalue is carried out without any error, the change in the frequency for the theoretical values of an aluminium bar is 9%. Using this error, the theoretical frequency lay in the intervals: $f_1 = 10.71 \pm 0.97Hz$, $f_2 = 67.12 \pm 6.07Hz$ and $f_3 = 187.93 \pm 16.98Hz$ none of them covering the

measured values $f_1 = 7.74Hz$, $f_2 = 54.16Hz$ and $f_3 = 158.98Hz$ therefore the assumption of correctness in the eigenvalue must be discarded.

Experimental determination of the elastic modulus was obtained from the tensile test machine (Figure A.1) located in the Large Scale Laboratory of the University of Waikato. The elastic modulus was defined as the average slope of the stress-strain plot of five bars (Table A.1) with data. The stress values are calculated from the specimen sectional area 12.1x3.05mm2 and the strain from the calibrated initial length of 50.000mm in the machine built-in routine.

Figure A.1. Tensile test machine to determine aluminium elastic modulus.

Table A.1. Elastic modulus measured

	Bar #1	Bar #2	Bar #3	Bar #4	Bar #5
Elastic Modulus	61.843GPa	58.408GPa	61.889GPa	60.820GPa	60.277GPa
Average					60.648GPa

The updated input parameters to calculate the error are

Elastic Modulus	δE= 10GPa	E= 60.648GPa
Section thickness	δh = 0.00005m	h = 0.003m
Volumetric density	$\delta \rho$ = 1kg/m^3	ρ = 2677kg/m^3
Specimen Length	δL =0.0005m	L =0.480m

Leading to an increment in the error percentage of only 1% which support the supposition of flexibility of the clamp.

References

[1] S. W. Doebling, C. R. Farrar, M. B. Prime, and D. W. Shevitz, "Damage identification and health monitoring of structural and mechanical systems from changes in their vibration characteristics: a literature review," Los Alamos National Laboratory, Los Alamos, NM1996.

[2] H. Sohn, C. R. Farrar, F. M. Hemez, J. J. Czarnecki, D. D. Shunk, D. W. Stinemates, *et al.*, "A Review of Structural Health Monitoring Literature: 1996-2001," Los Alamos National Laboratory, Los Alamos, NM2003.

[3] J.-J. Sinou, "A review of damage detection and health monitoring of mechanical systems from changes in the measurement of linear and non-linear vibrations," ed: Nova Science Publishers, Inc., 2009.

[4] D. An, N. H. Kim, and J.-H. Choi, "Practical options for selecting data-driven or physics-based prognostics algorithms with reviews," *Reliability Engineering & System Safety*, vol. 133, pp. 223-236, 2015.

[5] S. W. Doebling, C. R. Farrar, and M. B. Prime, "A summary review of vibration-based damage identification methods," *Shock and vibration digest*, vol. 30, pp. 91-105, 1998.

[6] C. R. Farrar, P. J. Cornwell, S. W. Doebling, and M. B. Prime, "Structural health monitoring studies of the Alamosa Canyon and I-40 Bridges," Los Alamos National Laboratory, Los Alamos, NMJuly 2000 2000.

[7] M. M. Alamdari, T. Rakotoarivelo, and N. L. D. Khoa, "A spectral-based clustering for structural health monitoring of the Sydney Harbour Bridge," *Mechanical Systems and Signal Processing*, vol. 87, pp. 384-400, 2017.

[8] J.-C. Golinval, "Damage Detection in Structures Based on Principal Component Analysis of Forced Harmonic Responses," *Procedia Engineering*, 2017.

[9] M. Silva, A. Santos, E. Figueiredo, R. Santos, C. Sales, and J. C. Costa, "A novel unsupervised approach based on a genetic algorithm for structural damage detection in bridges," *Engineering Applications of Artificial Intelligence*, vol. 52, pp. 168-180, 2016.

[10] Z. Tan, D. Thambiratnam, T. Chan, and H. A. Razak, "Detecting damage in steel beams using modal strain energy based damage index and Artificial Neural Network," *Engineering Failure Analysis*, vol. 79, pp. 253-262, 2017.

[11] Y. Yang and S. Nagarajaiah, "Blind identification of damage in time-varying systems using independent component analysis with wavelet transform," *mechanical systems and signal processing*, vol. 47, pp. 3-20, 2014.

[12] A. C. Altunışık, F. Y. Okur, and V. Kahya, "Modal parameter identification and vibration based damage detection of a multiple cracked cantilever beam," *Engineering Failure Analysis*, vol. 79, pp. 154-170, 2017.

[13] M. Reda Taha, A. Noureldin, J. Lucero, and T. Baca, "Wavelet transform for structural health monitoring: a compendium of uses and features," *Structural Health Monitoring*, vol. 5, pp. 267-295, 2006.

[14] H. Hao and Y. Xia, "Vibration-based damage detection of structures by genetic algorithm," *Journal of computing in civil engineering*, vol. 16, pp. 222-229, 2002.

[15] M. Stache, M. Guettler, and S. Marburg, "A precise non-destructive damage identification technique of long and slender structures based on modal data," *Journal of Sound and Vibration*, vol. 365, pp. 89-101, 2016/03/17/ 2016.

[16] M. S. Hossain, Z. C. Ong, Z. Ismail, S. Noroozi, and S. Y. Khoo, "Artificial neural networks for vibration based inverse parametric identifications: A review," *Applied Soft Computing,* vol. 52, pp. 203-219, 2017.

[17] D. A. Tibaduiza, L. E. Mujica, J. Rodellar, and A. Güemes, "Structural damage detection using principal component analysis and damage indices," *Journal of Intelligent Material Systems and Structures,* vol. 27, pp. 233-248, 2016.

[18] S. Caddemi and I. Caliò, "Exact closed-form solution for the vibration modes of the Euler–Bernoulli beam with multiple open cracks," *Journal of Sound and Vibration,* vol. 327, pp. 473-489, 2009.

[19] N. Khiem and L. Toan, "A novel method for crack detection in beam-like structures by measurements of natural frequencies," *Journal of Sound and Vibration,* vol. 333, pp. 4084-4103, 2014.

[20] T. Chondros, A. Dimarogonas, and J. Yao, "A continuous cracked beam vibration theory," *Journal of Sound and Vibration,* vol. 215, pp. 17-34, 1998.

[21] D. Zheng and N. Kessissoglou, "Free vibration analysis of a cracked beam by finite element method," *Journal of Sound and vibration,* vol. 273, pp. 457-475, 2004.

[22] C. Bilello, L. A. Bergman, and D. Kuchma, "Experimental investigation of a small-scale bridge model under a moving mass," *Journal of Structural Engineering,* vol. 130, pp. 799-804, 2004.

[23] P. Ricci and E. Viola, "Stress intensity factors for cracked T-sections and dynamic behaviour of T-beams," *Engineering fracture mechanics,* vol. 73, pp. 91-111, 2006.

[24] G. R. Irwin, "Analysis of stresses and strains near the end of a crack traversing a plate," *Journal of Applied Mechanics,* vol. 24, pp. 361-364, 1957.

[25] P. Cawley and R. D. Adams, "A vibration technique for non-destructive testing of fibre composite structures," *Journal of Composite Materials,* vol. 13, pp. 161-175, 1979.

[26] C. Huang and A. Leissa, "Vibration analysis of rectangular plates with side cracks via the Ritz method," *Journal of Sound and Vibration,* vol. 323, pp. 974-988, 2009.

[27] A. Morassi, "Crack-induced changes in eigenparameters of beam structures," *Journal of Engineering Mechanics,* vol. 119, pp. 1798-1803, 1993.

[28] P. Nikolakopoulos, D. Katsareas, and C. Papadopoulos, "Crack identification in frame structures," *Computers & structures,* vol. 64, pp. 389-406, 1997.

[29] C. P. Fritzen, "Vibration-based structural health monitoring–concepts and applications," in *Key Engineering Materials*, 2005, pp. 3-20.

[30] G. L. Qian, S. N. Gu, and J. S. Jiang, "The dynamic behaviour and crack detection of a beam with a crack," *Journal of Sound and Vibration,* vol. 138, pp. 233-243, 1990/04/22/ 1990.

[31] S. Caddemi, I. Caliò, and M. Marletta, "The dynamic non-linear behaviour of beams with closing cracks," in *AIMETA 2009 XIX Congresso di Meccanica Teorica ed Applicata*, 2009, pp. 1-10.

[32] M. G. Wood, "Damage analysis of bridge structures using vibrational techniques," PhD, Aston University, 1992.

[33] M. I. Friswell, "Damage identification using inverse methods," *Philosophical Transactions of the Royal Society of London A: Mathematical, Physical and Engineering Sciences,* vol. 365, pp. 393-410, 2007.

[34] J. Banerjee, "Dynamic stiffness formulation for structural elements: a general approach," *Computers & structures,* vol. 63, pp. 101-103, 1997.

[35] G.-R. Gillich and Z.-I. Praisach, "Modal identification and damage detection in beam-like structures using the power spectrum and time–frequency analysis," *Signal Processing*, vol. 96, pp. 29-44, 2014.

[36] S. Zhong and S. O. Oyadiji, "Analytical predictions of natural frequencies of cracked simply supported beams with a stationary roving mass," *Journal of Sound and Vibration*, vol. 311, pp. 328-352, 2008.

[37] P. H. Kulla, "The continuous elements method," *N97-717Z*, p. 347, 1991.

[38] C.-P. Yu and J. M. Roesset, "Dynamic stiffness matrices for linear members with distributed mass," *Tamkang journal of science and engineering*, vol. 4, pp. 253-264, 2001.

[39] V. Koloušek and R. F. McLean, *Dynamics in engineering structures*: Butterworths, 1973.

[40] F. Williams and J. Banerjee, "Free vibration of composite beams-an exact method using symbolic computation," *Journal of Aircraft*, vol. 32, pp. 636-642, 1995.

[41] X. Liu and J. Banerjee, "Free vibration analysis for plates with arbitrary boundary conditions using a novel spectral-dynamic stiffness method," *Computers & Structures*, vol. 164, pp. 108-126, 2016.

[42] J. Banerjee, S. Papkov, X. Liu, and D. Kennedy, "Dynamic stiffness matrix of a rectangular plate for the general case," *Journal of Sound and Vibration*, vol. 342, pp. 177-199, 2015.

[43] M. Boscolo and J. Banerjee, "Layer-wise dynamic stiffness solution for free vibration analysis of laminated composite plates," *Journal of Sound and Vibration*, vol. 333, pp. 200-227, 2014.

[44] R. W. Clough and J. Penzien, "Dynamics of structures," 1975.

[45] G. Rebecchi, "Beam axial load identification using one vibration mode shape," PhD, Università degli Studi di Ferrara, 2011.

[46] M. Mohsin and E. Sadek, "The distributed mass-stiffness technique for the dynamical analysis of complex frameworks," *The Structural Engineer*, vol. 46, pp. 345-351, 1968.

[47] K. Worden and J. Dulieu-Barton, "An overview of intelligent fault detection in systems and structures," *Structural Health Monitoring*, vol. 3, pp. 85-98, 2004.

[48] K. Worden, C. R. Farrar, G. Manson, and G. Park, "The fundamental axioms of structural health monitoring," *Proceedings of the Royal Society a-Mathematical Physical and Engineering Sciences*, vol. 463, pp. 1639-1664, Jun 8 2007.

[49] A. D. Dimarogonas, "Vibration of cracked structures: a state of the art review," *Engineering Fracture Mechanics*, vol. 55, pp. 831-857, 1996.

[50] P. G. Kirmser, "The effects of discontinuities on the natural frequency of beams," in *Proc. American Society of Testing and Materials*. vol. 44, ed, 1944, pp. 897-904.

[51] W. Thomson, "Vibration of slender bars with discontinuities in stiffness," *Journal of Applied Mechanics-Transactions of the Asme*, vol. 17, pp. 203-208, 1943.

[52] M. Shirazizadeh, H. Shahverdi, and A. Imam, "A Simple Finite Element Procedure for Free Vibration and Buckling Analysis of Cracked Beam-Like Structures," *Journal of Solid Mechanics*, vol. 8, pp. 93-103, 2016.

[53] J. R. Banerjee and S. Guo, "On the Dynamics of a Cracked Beam," in *Proceedings of 50 th AIAA/ASME/ASCE/AJS/ASC Structures, Structural dynamics, and Materials Conference*, 2009.

[54] Y. Li, "Fracture Mechanics Investigation of Structures with Defects," alma, 2013.

[55] U. Andreaus and P. Casini, "Identification of multiple open and fatigue cracks in beam-like structures using wavelets on deflection signals," *Continuum Mechanics and Thermodynamics,* vol. 28, pp. 361-378, 2016.

[56] M. Diaferio and V. Sepe, "Modal identification of damaged frames," *Structural Control and Health Monitoring,* vol. 23, pp. 82-102, 2016.

[57] T. Bose and A. Mohanty, "Vibration analysis of a rectangular thin isotropic plate with a part-through surface crack of arbitrary orientation and position," *Journal of Sound and Vibration,* vol. 332, pp. 7123-7141, 2013.

[58] C. Huang, A. Leissa, and C. Chan, "Vibrations of rectangular plates with internal cracks or slits," *International Journal of Mechanical Sciences,* vol. 53, pp. 436-445, 2011.

[59] S. Christides and A. Barr, "One-dimensional theory of cracked Bernoulli-Euler beams," *International Journal of Mechanical Sciences,* vol. 26, pp. 639-648, 1984.

[60] J. Brandon, "Some insights into the dynamics of defective structures," *Proceedings of the Institution of Mechanical Engineers, Part C: Journal of Mechanical Engineering Science,* vol. 212, pp. 441-454, 1998.

[61] S. Cheng, A. Swamidas, X. Wu, and W. Wallace, "Vibrational response of a beam with a breathing crack," *Journal of Sound and vibration,* vol. 225, pp. 201-208, 1999.

[62] R. Ruotolo and C. Surace, "Damage assessment of multiple cracked beams: numerical results and experimental validation," *Journal of sound and vibration,* vol. 206, pp. 567-588, 1997.

[63] E. Shifrin and R. Ruotolo, "Natural frequencies of a beam with an arbitrary number of cracks," *Journal of Sound and Vibration,* vol. 222, pp. 409-423, 1999.

[64] D. Zheng and S. Fan, "Natural frequency changes of a cracked Timoshenko beam by modified Fourier series," *Journal of sound and vibration,* vol. 246, pp. 297-317, 2001.

[65] N. Khiem and T. Lien, "A simplified method for natural frequency analysis of a multiple cracked beam," *Journal of Sound and Vibration,* vol. 245, pp. 737-751, 2001.

[66] N. Khaji, M. Shafiei, and M. Jalalpour, "Closed-form solutions for crack detection problem of Timoshenko beams with various boundary conditions," *International Journal of Mechanical Sciences,* vol. 51, pp. 667-681, 2009.

[67] A. Labib, D. Kennedy, and C. Featherston, "Free vibration analysis of beams and frames with multiple cracks for damage detection," *Journal of Sound and Vibration,* 2014.

[68] W. H. Wittrick and F. Williams, "A general algorithm for computing natural frequencies of elastic structures," *The Quarterly Journal of Mechanics and Applied Mathematics,* vol. 24, pp. 263-284, 1971.

[69] A. Labib, D. Kennedy, and C. Featherston, "Crack localisation in frames using natural frequency degradations," *Computers & Structures,* vol. 157, pp. 51-59, 2015.

[70] S. Caddemi and A. Morassi, "Multi-cracked Euler–Bernoulli beams: Mathematical modeling and exact solutions," *International Journal of Solids and Structures,* vol. 50, pp. 944-956, 2013.

[71] G.-R. Gillich, Z.-I. Praisach, V. Iancu, and E. Stanciu, "Diagnosis of a Portal Frame Using Frequency Shift Analysis," *Romanian Journal of Acoustics and Vibration,* vol. 12, p. 139, 2015.

[72] A. Greco and A. Pau, "Damage identification in Euler frames," *Computers & Structures,* vol. 92, pp. 328-336, 2012.

[73] S. Naguleswaran, "Transverse vibrations of an Euler–Bernoulli uniform beam carrying several particles," *International journal of mechanical sciences,* vol. 44, pp. 2463-2478, 2002.

[74] S. P. Shone, "A flexural wave scattering method for damage detection in beams," PhD, University of Southampton, 2006.

[75] R. Jacquot and J. Gibson, "The effects of discrete masses and elastic supports on continuous beam natural frequencies," *Journal of Sound and Vibration,* vol. 23, pp. 237-244, 1972.

[76] M. De Rosa, C. Franciosi, and M. Maurizi, "On the dynamic behaviour of slender beams with elastic ends carrying a concentrated mass," *Computers & Structures,* vol. 58, pp. 1145-1159, 1996.

[77] P. Cha and W. Wong, "A novel approach to determine the frequency equations of combined dynamical systems," *Journal of Sound and Vibration,* vol. 219, pp. 689-706, 1999.

[78] P. Cha, "Eigenvalues of a linear elastica carrying lumped masses, springs and viscous dampers," *Journal of sound and vibration,* vol. 257, pp. 798-808, 2002.

[79] P. D. Cha, "A general approach to formulating the frequency equation for a beam carrying miscellaneous attachments," *Journal of Sound and Vibration,* vol. 286, pp. 921-939, 2005.

[80] P. D. Cha, M. Chan, and G. Nielsen, "Eigenfrequencies of an arbitrarily supported beam carrying multiple in-span elastic rod-mass systems," *Journal of Vibration and Acoustics,* vol. 130, p. 061008, 2008.

[81] J. Banerjee, "Free vibration of beams carrying spring-mass systems− A dynamic stiffness approach," *Computers & Structures,* vol. 104, pp. 21-26, 2012.

[82] C. Rossit and P. Laura, "Free vibrations of a cantilever beam with a spring–mass system attached to the free end," *Ocean Engineering,* vol. 28, pp. 933-939, 2001.

[83] S. Ilanko, "Transcendental dynamic stability functions for beams carrying rigid bodies," *Journal of sound and vibration,* vol. 279, pp. 1195-1202, 2005.

[84] M. Solís, A. J. Benjumea, M. Algaba, and P. Galvín, "Analysis of stationary roving mass effect for damage detection in beams using wavelet analysis of mode shapes," in *Journal of Physics: Conference Series*, 2015, p. 012014.

[85] A. Pandey, M. Biswas, and M. Samman, "Damage detection from changes in curvature mode shapes," *Journal of sound and vibration,* vol. 145, pp. 321-332, 1991.

[86] S. Zhong and S. O. Oyadiji, "Identification of cracks in beams with auxiliary mass spatial probing by stationary wavelet transform," *Journal of Vibration and Acoustics,* vol. 130, p. 041001, 2008.

[87] A. Bahador and S. O. Oyadiji, "Use of the Roving Mass Technique and SWT to Identify and Locate Multiple Cracks in Simply-Supported Beams," in *Vibration Engineering and Technology of Machinery*, ed: Springer, 2015, pp. 253-263.

[88] S. Zhong and S. O. Oyadiji, "Detection of cracks in simply-supported beams by continuous wavelet transform of reconstructed modal data," *Computers & structures,* vol. 89, pp. 127-148, 2011.

[89] S. Zhong and S. O. Oyadiji, "Sampling interval sensitivity analysis for crack detection by stationary wavelet transform," *Structural Control and Health Monitoring,* vol. 20, pp. 45-69, 2013.

[90] R. Courant, "Variational methods for the solution of problems of equilibrium and vibrations," *Bull. Amer. Math. Soc,* vol. 49, pp. 1-23, 1943.

[91] S. Ilanko and L. E. Monterrubio, "Bipenalty method from a frequency domain perspective," *International Journal for Numerical Methods in Engineering,* vol. 90, pp. 1278-1291, 2012.

[92] A. Labib, "Crack detection in frames using natural frequency degradations," PhD, School of Engineering, Cardiff University, Cardiff, United Kingdom, 2015.

[93] Y. Narkis and E. Elmalah, "Crack identification in a cantilever beam under uncertain end conditions," *International journal of mechanical sciences,* vol. 38, pp. 499-507, 1996.

[94] M. Alfano and L. Pagnotta, "Determining the elastic constants of isotropic materials by modal vibration testing of rectangular thin plates," *Journal of sound and vibration,* vol. 293, pp. 426-439, 2006.

[95] T. Türker and A. Bayraktar, "Structural parameter identification of fixed end beams by inverse method using measured natural frequencies," *Shock and Vibration,* vol. 15, pp. 505-515, 2008.